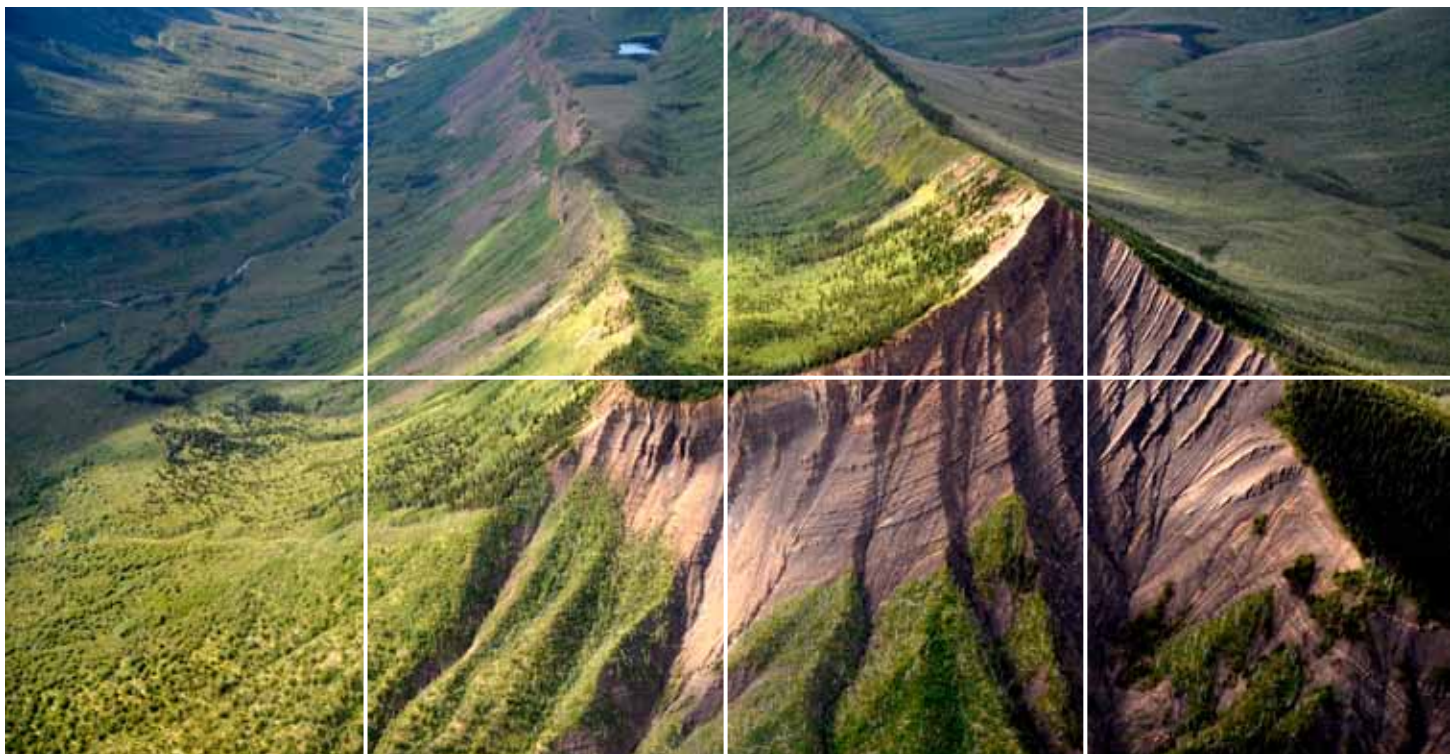


Oil And Gas Geoscience Reports 2013



BC Ministry of Natural Gas Development
Geoscience and Strategic Initiatives Branch



© British Columbia Ministry of Natural Gas Development
Geoscience and Strategic Initiatives Branch
Victoria, British Columbia, May 2013

Please use the following citation format when quoting or reproducing parts of this document:

Ferri, F., Hickin, A.S. and Reyes, J. (2012): Horn River basin-equivalent strata in Besa River Formation shale, northeastern British Columbia (NTS 094K/15); in Geoscience Reports 2012, *British Columbia Ministry of Natural Gas Development*, pages 1–15.

Colour digital copies of this publication in Adobe Acrobat PDF format are available, free of charge, from the British Columbian Oil and Gas Division's website at:

<http://www.empr.gov.bc.ca/OG/OILANDGAS/Pages/default.aspx>

Front cover photo by F. Ferri. Looking north at a syncline located approximately 15 km south of Hells Gate on the Liard. The exposed section consists of Toad Formation turbidite deposits (Montney - Doig equivalents). A section of Liard Formation (Halfway equivalent) sandstone marks the resistive rim. Shales of the lowermost Buckinghorse Formation sit unconformably above the Liard Formation.

Page iii photo by F. Ferri. Looking north at the Alaska Highway, several kilometres south of Liard River. The bridge over the Liard River can be seen in the distance.

Back cover photo by F. Ferri. Kindle Formation sandstone and siltstone exposed on a mountain near the headwaters of Vizer Creek.

FOREWORD

Geoscience Reports, together with its precursor the Summary of Activities, is in its ninth year of publication. This report is an annual publication of the Petroleum Geoscience Section of the Geoscience and Strategic Initiatives Branch, Oil and Gas Division, BC Ministry of Natural Gas Development. The annual Geoscience Reports summarizes petroleum-related projects undertaken by branch staff and their collaborators within the province of British Columbia. This public geoscience information provides baseline regional data that can be utilized by those embarking on petroleum exploration and development within the province. These reports promote the petroleum resources of the province, and will also support responsible development and the formulation of related policy and regulation.

The 2013 volume of Geoscience Reports contains five articles related to oil and gas research which include:

1. A summary of field activities in the western Liard Basin by Filippo Ferri, which describes two field-related projects in 2012. The first an ongoing regional mapping program within the Toad River map area in conjunction with Margot McMechan of the Geological Survey of Canada and the second an examination of Besa River lithologies in western and northern Liard Basin. Collaborators on this project included Tiffani Fraser of the Yukon Geological Survey, Kathryn Fiess and Leanne Pyle representing the Northwest Territories Geoscience Office and Fabrice Cordey of the University of Lyon.
2. A paper by Ed Janicki, Conventional Oil Pools of British Columbia, describes an upcoming publication which will provide updated information on major oil pools in the province. This has not been made available in a concise format since the mid-1990's
3. An examination of porosity development within Horn River shales by Nick Harris and Tiang Dong of the University of Alberta.
4. A snapshot of the helium potential within natural gas pools of northeast British Columbia by Elizabeth Johnson.
5. A determination of the gas, liquids and oil windows of the Montney Formation based on thermal maturity and well production data by Filippo Ferri, Aaron Nelson, Royalty Branch, Oil and Gas Division, and Mark Hayes of the BC Oil and Gas Commission.

Readers are encouraged to view the British Columbian Oil and Gas Division's website at <http://www.empr.gov.bc.ca/OG/OILANDGAS/Pages/default.aspx> for upcoming publications by the Geoscience and Strategic Initiatives Branch.

Filippo Ferri

Director, Petroleum Geoscience
Geoscience and Strategic Initiatives Branch
Oil and Gas Division
BC Ministry of Natural Gas Development

TABLE OF CONTENTS

GEOSCIENCE REPORTS 2012

LIQUIDS POTENTIAL OF THE LOWER TO MIDDLE TRIASSIC MONTNEY AND DOIG FORMATIONS, BRITISH COLUMBIA	1
<i>by Filippo Ferri, Mark Hayes and Aaron Nelson</i>	
SUMMARY OF FIELD ACTIVITIES IN THE WESTERN LIARD BASIN, BRITISH COLUMBIA	13
<i>by Filippo Ferri, Margot McMechan, Tiffani Fraser, Kathryn Fiess, Leanne Pyle and Fabrice Cordey</i>	
CHARACTERIZING POROSITY IN THE HORN RIVER SHALE, NORTHEASTERN BRITISH COLUMBIA.....	33
<i>by Nicholas B. Harris and Tian Dong</i>	
CONVENTIONAL OIL POOLS OF BRITISH COLUMBIA	41
<i>by Ed Janicki</i>	
HELIUM IN NORTHEASTERN BRITISH COLUMBIA	45
<i>by Elizabeth G. Johnson</i>	



LIQUIDS POTENTIAL OF THE LOWER TO MIDDLE TRIASSIC MONTNEY AND DOIG FORMATIONS, BRITISH COLUMBIA

Filippo Ferri¹, Mark Hayes² and Aaron Nelson³

ABSTRACT

Zones of dry gas, wet gas and oil potential within the Montney Formation were outlined using T_{max} values from Rock Eval™ analysis of core and cuttings, and from raw gas production and allocated gas plant sales data.

Results from both techniques are, for the most part, in general agreement, but discrepancies are present in the southern part of the Montney play trend. These departures may be either due to the suppression of the T_{max} value by migrated oil/bitumen or contamination by oil-based drilling fluids. Alternatively, low production of liquids in the southern Montney trend may be the result of a higher percentage of type III kerogen, which produces considerably less liquid hydrocarbons.

Ferri, F., Hayes, M. and Nelson, A. (2013): Liquids potential of the Lower to Middle Triassic Montney and Doig formations, British Columbia; *in Geoscience Reports 2013, British Columbia Ministry of Natural Gas Development*, pages 1–11.

¹Geoscience and Strategic Initiatives Branch, Oil and Gas Division, British Columbia Ministry of Natural Gas Development, Victoria, British Columbia, Fil.Ferri@gov.bc.ca

²Operations Division, Resource Development and Geology, British Columbia Oil and Gas Commission, Victoria, British Columbia

³Royalty Policy Branch, Oil and Gas Division, British Columbia Ministry of Natural Gas Development, Victoria, British Columbia

Key Words: Montney, Doig, natural gas liquids, condensate, oil, Rock Eval, thermal maturity, natural gas processing, production, plant sales

INTRODUCTION

The production of natural gas in British Columbia is now primarily from tight and shale gas reservoirs, the bulk originating from the Montney Formation (Figs. 1, 2). The current rate of development within the Montney Formation is not only an indication of the more favourable reservoir characteristics (porosity, organic carbon content, pressures), but also a reflection of the higher natural gas liquid (C2–C4) and condensate (C5–C12) concentrations of the formation, the latter of which adds considerable value to well production during this period of low natural gas prices.

Considering the increased level of Montney liquids¹ production in the province (Fig. 3), understanding the spatial distribution (i.e., mapping) of this potential will be critical. This is true not only from an economic standpoint, but also from a developmental and royalty perspective. The mapping of the liquids potential within the Montney Formation was attempted through compilation and contouring of 1) thermal maturity data (Rock Eval, reflectance microscopy) found within published reports, papers and well data

submission and 2) liquids production per unit volume of gas produced.

An outcome of this exercise has been a more readily available dataset of well-head liquids production. The well-head production of liquids is calculated at the gas plant based on well-head gross gas production and gas analysis. Historically, this information has been kept by the British Columbia Ministry of Finance, but it has now been supplied to the British Columbia Oil and Gas Commission and procedures are being implemented to publically distribute this dataset.

THERMAL MATURITY

Thermal maturity data for the Montney and Doig formations were obtained from several sources, including 1) regional Rock Eval analysis of cuttings across northeastern British Columbia and Alberta carried out by the Geological Survey of Canada (Riediger, 1990; Snowdon, 2000; Fowler and Snowdon, 2001, 2007a, b); 2) compilation of core and cutting analysis produced by the British Columbia Ministry

¹In this paper, the term 'liquids' is used in reference to natural gas liquids (C2–C4) and condensate (C5 and higher) production.

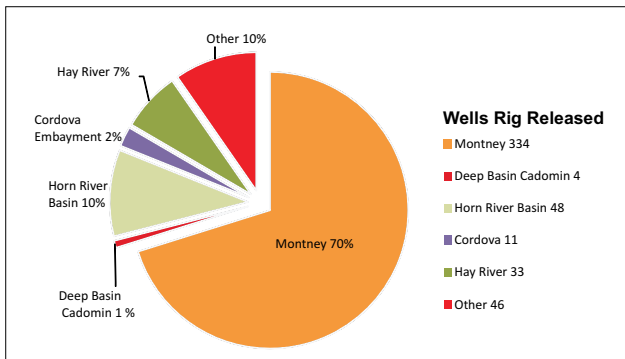


Figure 1. The percentages of production from formations in north-eastern British Columbia in 2012. Also shown are the number of wells drilled during 2012, based on rig release data.

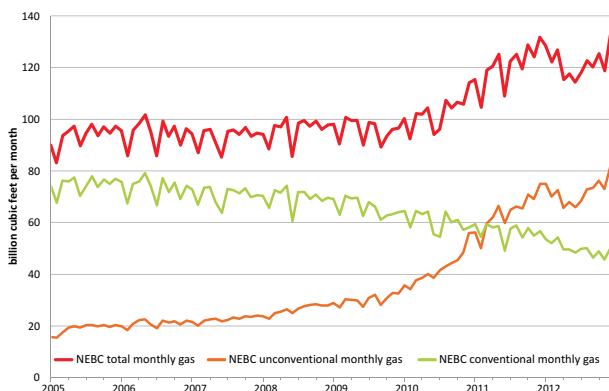


Figure 2. Overall production from conventional and unconventional reservoirs, northeastern British Columbia (NEBC: northeastern British Columbia).

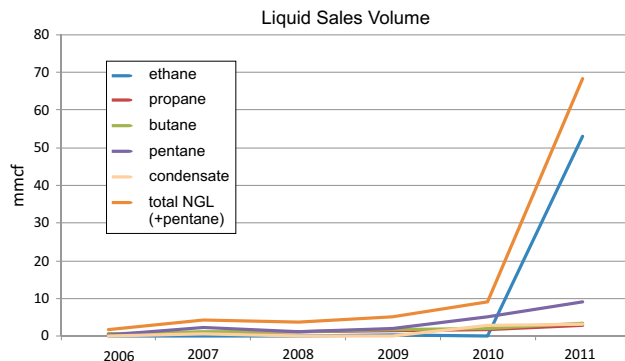


Figure 3. Liquids (natural gas liquids [NGL] and condensate) sales volume in British Columbia from 2006 to 2011, in million cubic feet (mmcf).

of Energy, Mines and Natural Gas (Walsh et al., 2007; Ferri et al., 2013); and 3) published papers (Ibrahimbash and Riediger, 2004).

The majority of thermal maturity data used in this report was part of Rock Eval/total organic carbon (TOC) datasets. In Rock Eval analysis, the T_{max} value is used as a measure of the thermal maturity of the kerogen within an organic-rich sample. During Rock Eval pyrolysis, T_{max} is

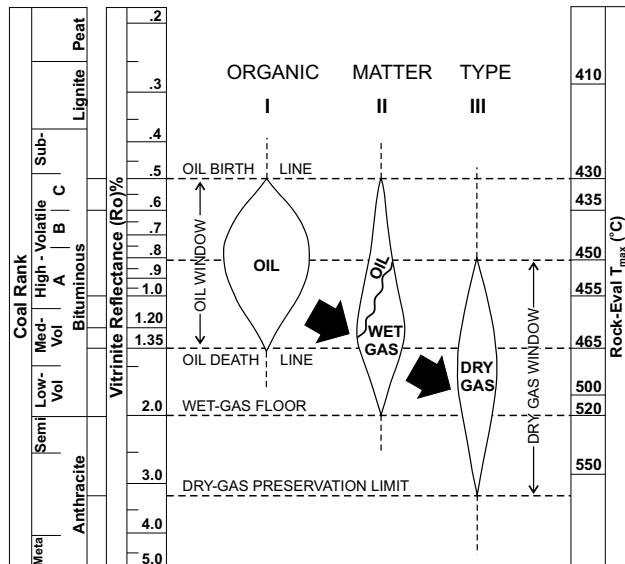


Figure 4. Zones of petroleum generation and destruction.

the temperature recorded at the S2 peak; i.e., the temperature at the maximum production of hydrocarbons during stepwise heating of a sample (Fig. 5). Experimental data has shown that this temperature increases in conjunction with the maximum paleotemperatures recorded by the rock (Peters, 1986; Fig. 4). This temperature is also sensitive to the type of kerogen present in the rock (Fig. 5). Empirical data has shown a direct correlation between specific T_{max} values and the production and preservation of petroleum in the rock column (Fig. 4; Peters, 1986).

Reflectance microscopy of organic matter, primarily of coal macerals (i.e., vitrinite) is the most common and robust method for determining the level of thermal maturation in an organic-rich sedimentary rock (Dow, 1977). There is a positive linear relationship between the amount of light reflected from a polished maceral immersed in oil (%Ro) and the degree of thermal maturation the maceral has attained, i.e., the amount of reflected light increases with maturation. In the long history of coal exploration, thermal maturity based on reflectance data from vitrinite has become the reference parameter for stating the thermal maturity of a rock and reflectance data from other organic macerals are converted to the vitrinite values following a linear correlation (Jacob, 1985). Furthermore, there is a correlation between vitrinite reflectance and T_{max} values that is shown graphically in Figure 4 (Teichmuller and Durand, 1983; Lafargue et al., 1998). Reflectance microscopy thermal maturity data from well file reports were converted to T_{max} values based on the relationships shown by Lafargue et al. (1998) and Teichmuller and Durand (1983).

Thermal maturity values for 88 wells were compiled using T_{max} and reflectance microscopy values (Table 1). Due to the dominance of T_{max} data, vitrinite or equivalent data were converted to T_{max} based on several correlations

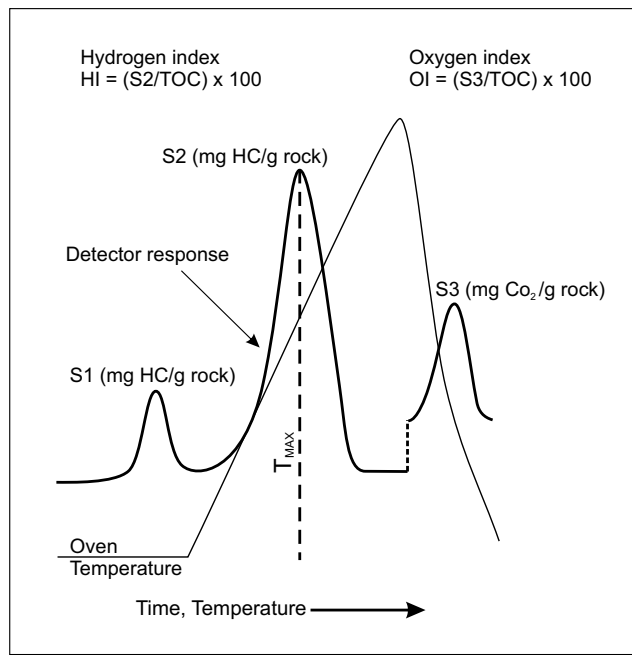


Figure 5. Schematic representation of the Rock Eval program. This instrument uses a ramped temperature pyrolysis process whereby a small amount of sample (70–100 mg) is heated in an inert atmosphere (helium or nitrogen). Any volatile hydrocarbons (i.e., those adhered to organic carbon or in pore spaces) will be released when the sample is initially heated to 300°C and the amount is referenced as the S1 peak. The sample is then heated to 600°C at 25°C/min and hydrocarbons generated during this ramped heating are produced from the cracking of kerogen in the sample. The amount of hydrocarbons produced is called S2. T_{\max} is the temperature of maximum hydrocarbon generation during this stepped heating. A separate detector registers the amount of CO and CO₂ generated, which gives the S3 value. The sample is then exposed to oxygen so that any remaining organic carbon is combusted and measured. Together with data from S1, S2 and S3, it is used to calculate the total organic carbon (TOC). A pyrogram showing the response of the detectors through time (and heating) is also produced and can provide additional information.

S1 and S2 are reported in milligrams of hydrocarbons generated from kerogen in 1 g of rock (mg HC/g rock). S3 represents milligrams of CO₂ generated from 1 g of rock. The hydrogen index (HI) is calculated from S2 and corresponds to the quantity of pyrolyzable organic matter (i.e., hydrocarbons, HC) that can be generated from 1 g of organic carbon (mg HC/g TOC). The oxygen index (OI) is calculated from S3 and represents the amount of CO₂ in 1 g of organic carbon (mg CO₂/g TOC).

and then averaged (Lafargue et al., 1998; Dewing and Sanei, 2009). Rock Eval data was first filtered using TOC and S2 cutoffs of 0.3 wt.% and 0.2 mg HC/g rock, respectively. Practice has shown that Rock Eval parameters have little significance when TOC levels are below this value and T_{\max} results are suspect when S2 is lower than 0.2 mg HC/g rock (Espitalié et al., 1985a, b, 1986; Peters, 1986).

Proper filtering of T_{\max} data is difficult in the absence of pyrograms. Some of the datasets show anomalously low

T_{\max} values (Snowdon, 2000), even within acceptable TOC and S2 parameters, suggesting either migrated oil into the sample or the use of oil-based mud additives (Peters, 1986). A systematic search of the well files to determine the mud composition during drilling of the Montney-Doig succession was not performed. In other instances, initial contour maps generated from averaged T_{\max} values produced noticeable anomalies or ‘bull’s eyes’ on the map. This led to the re-inspection of datasets and filtering based on modified criteria such as higher S2 cutoffs.

Although the Montney-Doig succession can be several hundreds of metres thick in the western part of the basin (Fig. 6), the scatter and distribution of T_{\max} values in wells with relatively complete datasets does not indicate an overall increase with depth (Fig. 7). As such, T_{\max} values for wells where data was available were averaged (88 data points, Table 1), spatially positioned and contoured (Fig. 8). Rock Eval analysis of Montney and Doig rocks indicates a predominance of type II/III kerogen (Figs. 4, 9). Unbiased contouring shows an overall maturity increase outlining the Deep Basin (as would be expected), with the peak wet gas line (T_{\max} = 460°C to 465°C; Fig. 4) trending diagonally, northwestward through the Peace River block and then northward (Fig. 8). Wells east of this line should have production that is richer in liquids and wells east of the 450°C T_{\max} value should have production dominated by oil.

LIQUIDS PRODUCTION

Although thermal maturation data can predict regions of oil, gas or wet gas potential within a formation, production records, if available in enough detail and numbers, can be spatially plotted to predict similar prospectivity. Current well counts within the Montney Formation, together with production statistics, are large enough to allow this exercise to be performed with a degree of confidence (Figs. 10–12).

Although the British Columbia Oil and Gas Commission captures the production of raw gas and some condensate at the well head, due to the centralized nature of natural gas processing, an accurate tabulation of condensate and natural gas liquids production can only be accomplished through the compilation of processing plant sales data, which are housed with the British Columbia Ministry of Finance (Fig. 13). Although condensate can be removed in the field (Fig. 13c), it is more economic to keep it in the gas stream and process it at a centralized facility. Separation of condensate in the field is dependent on the amount and composition of the condensate (e.g., amount of waxes) and distance to the nearest gas plant. When the condensate concentration exceeds approximately 50 barrels per million cubic feet of raw gas (0.28 m³/e³m³), it is necessary to separate the condensate from the raw gas stream and measure the two streams separately to accurately calculate the amount of each component before sending the combined

TABLE 1. LIST OF WELLS USED IN THE STUDY AND AVERAGE TMAX VALUES FOR ANALYZED CORE AND/OR CUTTINGS FROM THE MONTNEY AND DOIG FORMATIONS.

UWI	WA	T_{max}	n	UWI	WA	T_{max}	n
11-4-79-14W6	17427	451 ±3	5	6-10-85-25W6	5704	465 ±2	2
9-31-79-14W6	13426	451 ⁺	2	8-11-87-25W6	182	457 ±4	14
13-1-77-15W6	10621	445	1	b-4-L/93-P-7	5465	472	1
7-13-79-15W6	16639	463 ±9 ⁺	10	a-20-H/93-P-9	16615	475 ⁺	2
11-31-79-15W6	6877	462 ±4	5	d-39-F/93-P-9	10562	470 ±4 ⁺	2
1-36-79-15W6	16425	450 ±2 ⁺	4	b-32-G/93-P-9	10766	452 ±7*	15
10-22-80-15W6	7149	453 ±6*	11	b-32-G/93-P-9	13006	451 ±4	1
15-8-78-16W6	10690	452	1	a-29-H/93-P-9	10385	443 ±8	2
16-15-78-16W6	14756	438	1	a-38-H/93-P-9	16536	471 ±14 ⁺	10
8-10-79-16W6	10761	463 ±3	3	b-64-I/94-A-12	4914	447 ±1	2
11-18-79-16W6	5007	476	1	c-21-L/94-A-13	24759	464 ±15	18
12-25-79-16W6	5364	463 ±8	7	d-69-J/94-A-15	2832	447 ±3	32
11-35-79-16W6	7485	454 ±7	7	a-59-G/94-A-16	1832	442 ±2	8
1-26-86-16W6	208	441 ±3	30	c-74-I/94-B-1	24302	473 ±13*	9
13-33-78-17W6	24564	456 ±10	32	a-39-E/94-B-8	951	480 ±4	38
14-35-78-17W6	10677	447 ±16	2	c-44-L/94-B-8	25155	491 ±13	9
15-26-79-17W6	24170	461 ±5*	16	a-10-J/94-B-9	25161	483 ±20	12
14-34-79-17W6	23576	446 ±3	3	c-33-C/94-B-9	25738	453 ±12	33
8-8-80-17W6	23233	454 ±10	4	d-67-J/94-B-9	25311	490 ±10	6
11-11-80-17W6	2378	452 ±6	5	c-74-B/94-B-9	4205	449 ±8	5
4-27-88-17W6	130	453 ±3	4	d-87-I/94-B-14	554	504 ±12	15
9-33-78-18W6	24241	441 ±2*	8	a-86-C/94-B-15	827	478 ±16	7
15-34-80-18W6	24410	454 ±9	57	d-8-F/94-B-16	26622	472 ±8	9
8-10-84-18W6	6294	463	2	d-50-H/94-B-16	25568	467 ±11	21
11-28-78-19W6	25466	457 ±12	25	d-38-J/94-B-16	18509	456 ±4*	10
8-8-81-19W6	24288	451 ±6	31	b-69-A/94-B-16	253	452 ±10	30
6-17-86-19W6	1770	446 ±5	14	d-100-J/94-B-16	25392	458 ±9	4
13-21-77-20W6	24268	464	1	a-78-C/94-G-1	25788	465 ±7	16
16-29-79-20W6	25478	461 ±16	43	c-54-B/94-G-7	25640	477 ±11	22
13-11-81-20W6	24354	457 ±9	19	c-80-L/94-G-7	647	472 ±8	2
8-22-82-20W6	21910	459 ±9	11	b-10-C/94-H-1	2052	451 ±2	2
3-30-82-20W6	23346	445 ±3	5	d-13-D/94-H-1	5586	447	2
14-16-83-20W6	26789	458 ±5	14	d-25-D/94-H-1	2278	451 ±1	2
16-8-86-20W6	6124	446 ±6	7	d-81-E/94-H-1	2916	455 ±1	2
11-10-86-20W6	1190	439 ±4	34	a-78-F/94-H-1	920	443 ±4	4
8-14-86-20W6	6734	449 ±2	2	d-48-H/94-H-1	1433	436 ±4	2
7-5-87-20W6	2338	458 ±4	10	d-49-J/94-H-1	5294	434 ±2	15
4-11-81-21W6	25261	465 ±15	66	d-4-B/94-H-2	1748	451 ±2	2
3-1-83-21W6	26335	459 ±4	18	b-92-G/94-J-2	15973	464 ±9	7
11-19-83-21W6	4598	461 ±3	4	c-86-D/94-J-12	2150	455	1
10-24-86-21W6	2243	461 ±6	4	d-72-E/94-H-2	2044	444 ±3	11
13-8-82-22W6	26283	471 ±7	5	a-79-B/94-H-4	61	459 ±11	21
1-12-84-23W6	108	450 ±2	10	d-45-G/94-H-9	10189	435 ±3	4
16-17-83-25W6	25450	481 ±10	4	b-16-H/94-H-13	916	442 ±5	12

*Includes R_o values

UWI: Universal well Identifier

n: number of measurements

[†]R_o values only

WA: Well Authorization

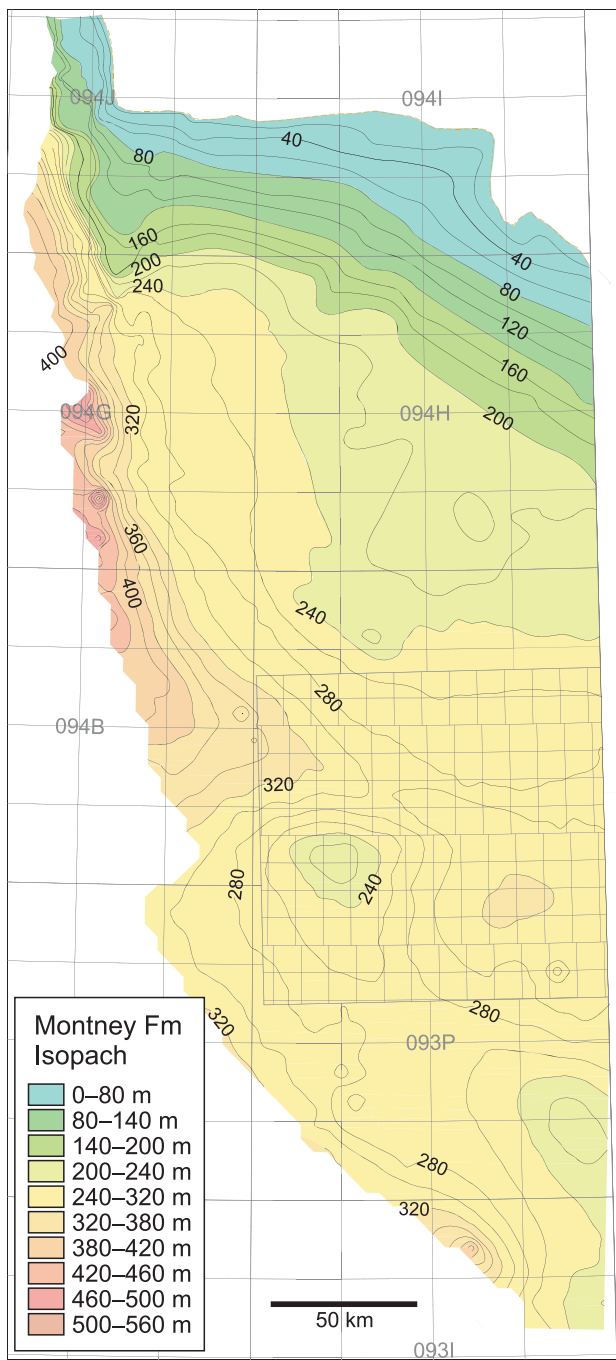


Figure 6. Isopach map of the Triassic Montney and Doig formations.

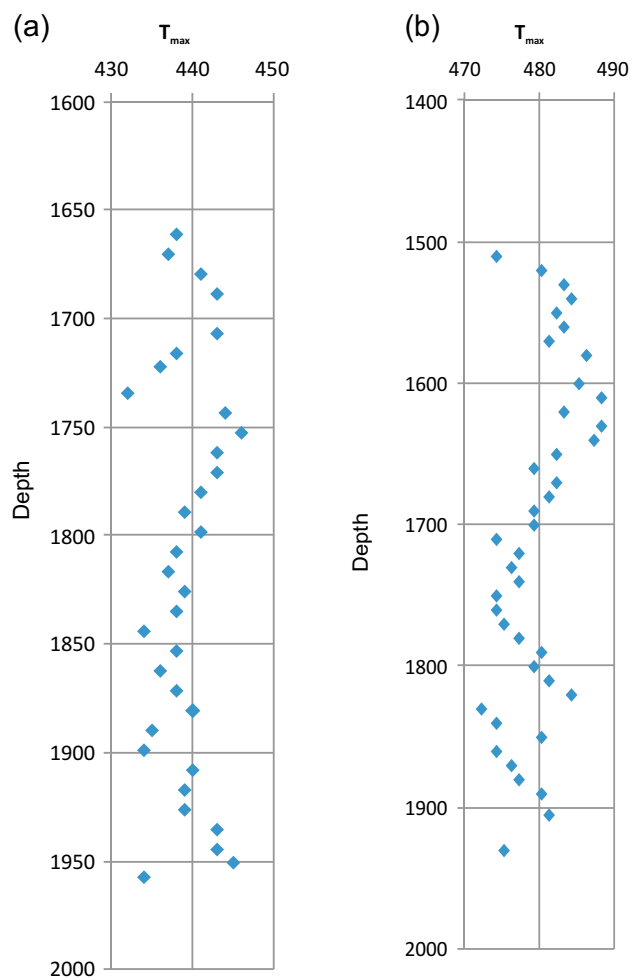


Figure 7. T_{max} versus depth for samples from the Montney and Doig formations: a) 11-10-86-20W6; b) c-029-E/94-B-08. Note that the scatter of data does not show an increase with depth.

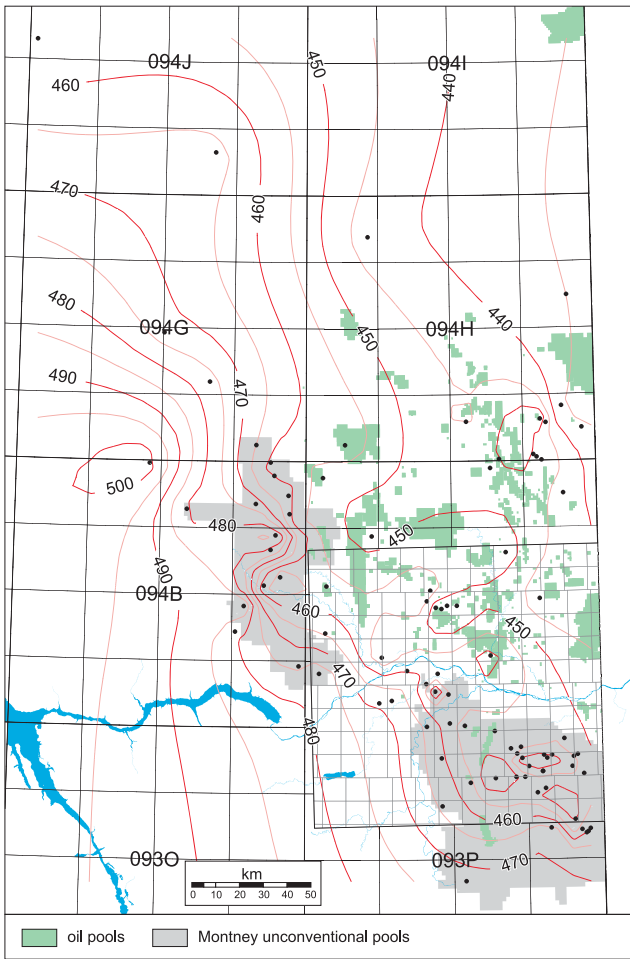
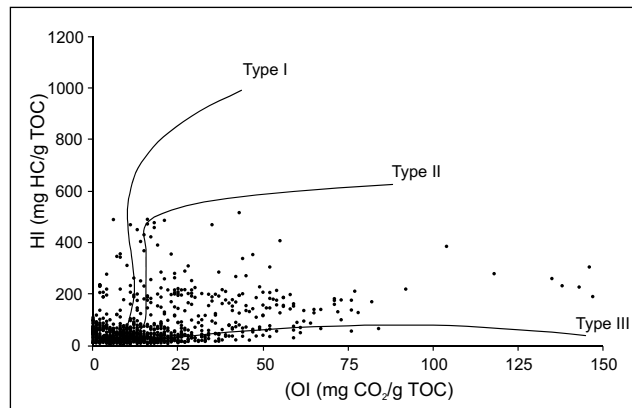


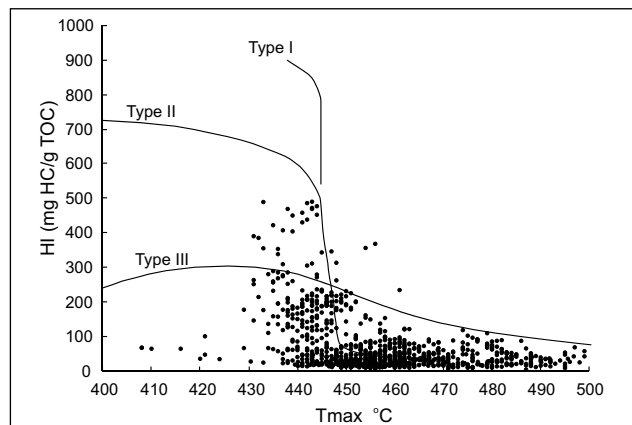
Figure 8. Contoured T_{\max} values, Montney-Doig formations. This was performed using Surfer 8™ software within GeoSCOUT™, using a kriging gridding method.

stream to the gas plant (Fig. 13b). The quantity of condensate is converted to a raw gas stream equivalent. Assigning production from a natural gas processing facility back to individual wells is calculated from a compositional analysis and flow rate of the raw gas stream.

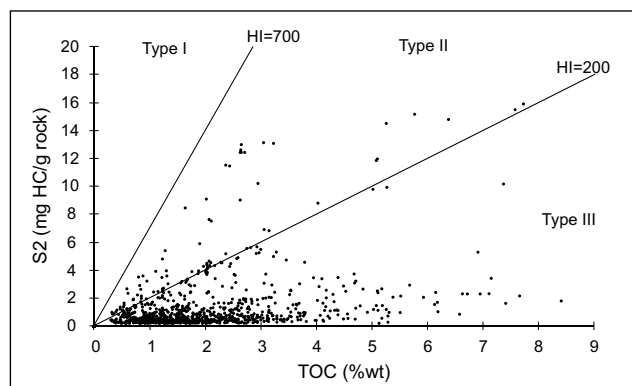
Natural gas processing plants have different capabilities and efficiencies; i.e., some only separate condensate, whereas others also have a natural gas liquids stream. Because facilities with the capacity to remove ethane (i.e., ‘deep cut’ plants) are not common, ethane-bearing gas is sold at a higher premium due to the increased calorific value. This gas can be sold directly to the end user or may be removed by more efficient gas plants in a downstream location (Fig. 13).



a)



b)



c)

Figure 9. a) Modified van Krevelen diagram (Tissot and Welde, 1984) based on filtered Rock Eval analysis of Montney and Doig samples from wells listed in Table 1; b) HI versus T_{\max} diagram based on filtered Rock Eval analysis of Montney and Doig samples from wells listed in Table 1 (modified from Bordenave, 1993); c) S2 versus total organic carbon (TOC) diagram based on filtered Rock Eval analysis of Montney and Doig samples from wells listed in Table 1 (modified from Langford and Blanc-Valleron, 1990).

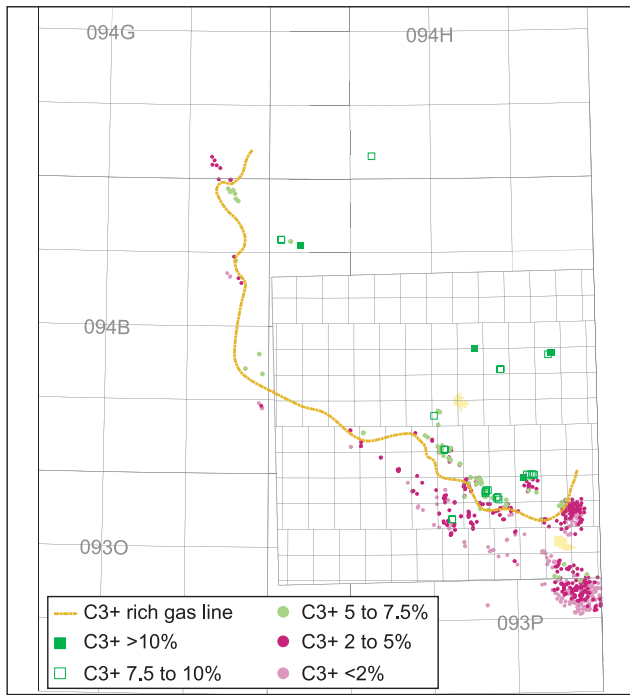


Figure 10. Gas analysis for Montney Formation production showing C3 and greater concentrations.

DISCUSSION

An attempt at outlining zones of predominantly dry gas, wet gas, wet gas to oil and oil and oil, based on mapping of T_{max} values and sales gas data is shown in Figures 14 and 15. Trends in the northern parts of both maps generally define the same zones. Although detailed sales data for the Heritage and Northern Montney fields has allowed differentiation into dry gas, wet gas and oil zones, lack of data between the two areas does not permit the same level of differentiation. It is likely that the wet gas zone and the oil zone extend to the northwest, as predicted by the thermal maturation data.

Oil to gas zones, as defined by the two methods, do not define the same trends along the southern part of the Peace River block and into the 094P map area (Figs. 14, 15). Pockets of higher liquids production are found in the dry gas zone of the southern Peace River block shown in Figure 15 (see C3 and greater gas analysis trends, C3+C4 production and pentane [C5] plus production, Figs. 10–12) and may support the lower thermal maturities defined by T_{max} values.

Gas and liquids data is very robust in the southern Peace River block, suggesting issues with the Rock Eval data. Rock Eval data cluster in this part of the study area (Figs. 8, 14, Table 1), which display a considerable range of T_{max} values (438–476°C), although the majority fall between 440–455°C. As discussed previously, suppression of T_{max} values can occur due to sample contamination from oil-based drilling fluids or from migrated oil or bitumen in

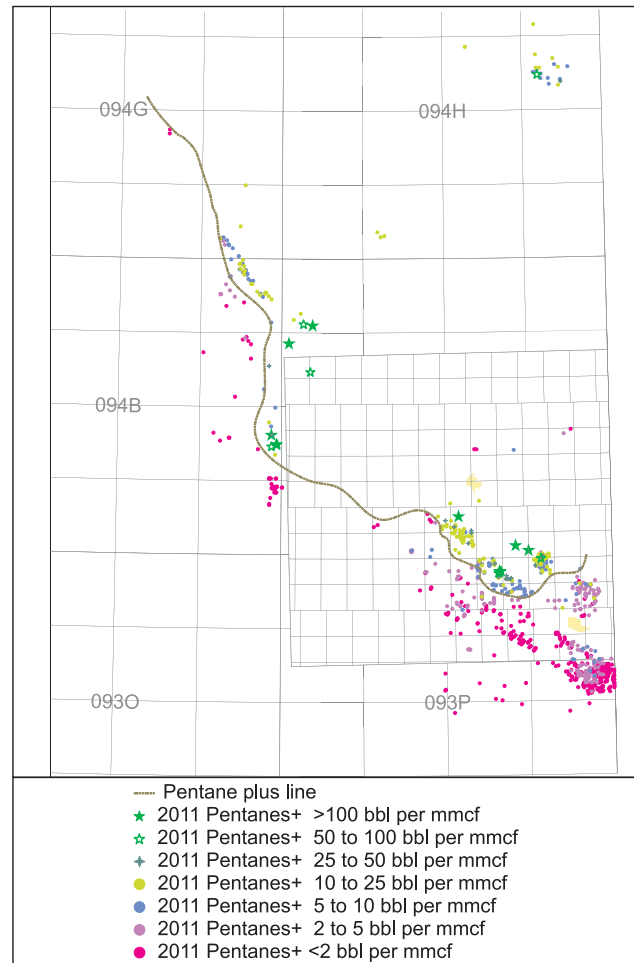


Figure 11. Liquids production map for the Montney Formation showing C5 and greater production in barrels per million cubic feet of gas.

the sample (Peters, 1986). As the original pyrograms are not available, testing either of these hypotheses would require determination of drilling fluids from drilling records and/or petrographic analysis of cuttings and core.

An alternative explanation for the lower liquids content of the wells in this area may be related to the type of kerogen present within Montney rocks. Type II/III kerogen is suggested by the Rock Eval dataset (Fig. 9) and has been described by other workers (Riediger, 1990). If kerogen in this area is closer to type III in nature, then its ability to produce liquid hydrocarbons would be considerably less than type II kerogen (Jarvie, 1991).

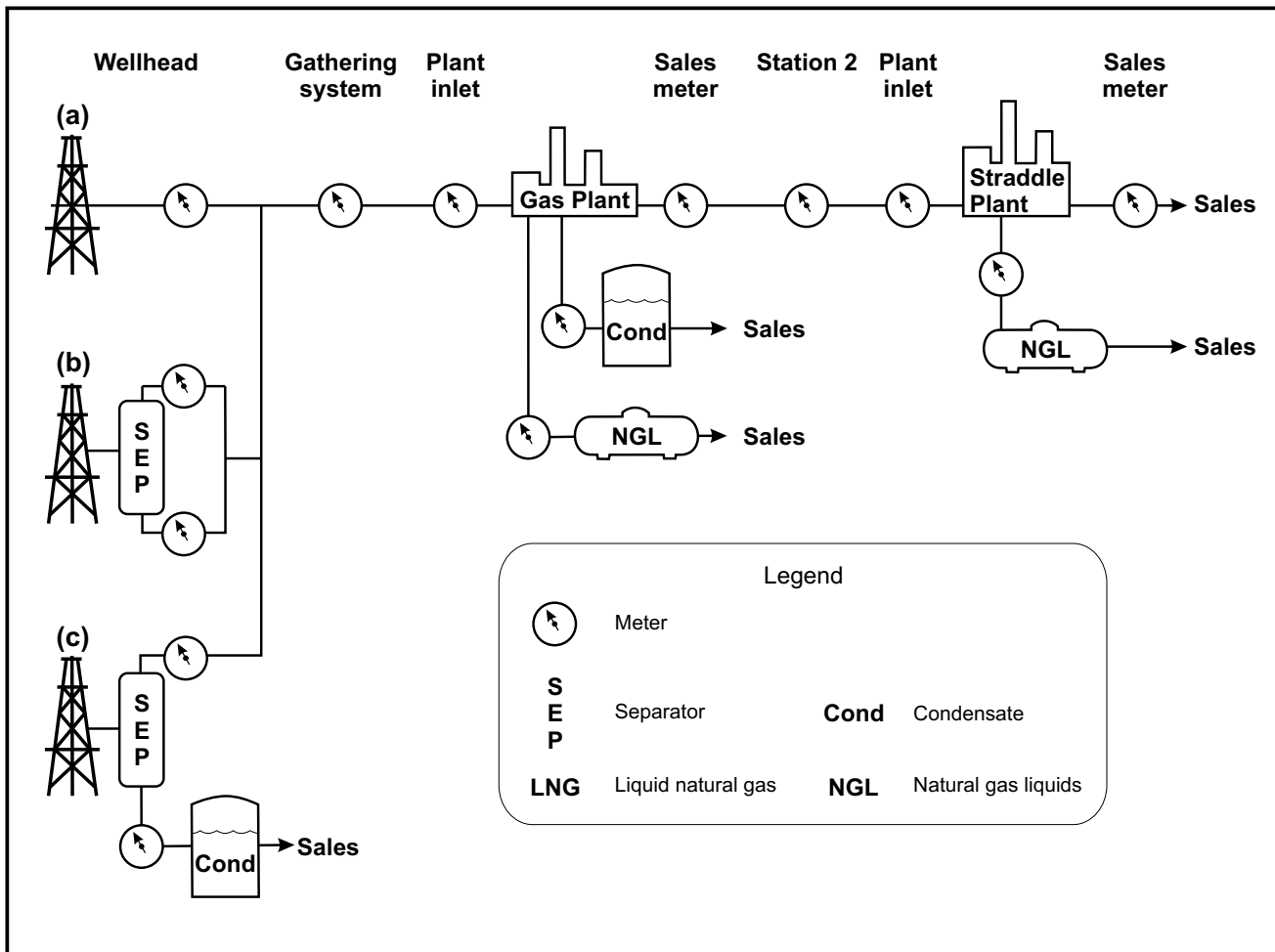


Figure 13. Three scenarios for production and processing of raw gas streams with varying proportions of condensate and natural gas liquids. In all scenarios, allocation of natural gas plant production back to the individual wells is based on both the compositional analysis and absolute flow rate of raw gas. The type of natural gas liquids produced depends on the capabilities of the gas plant; i.e., 'deep cut' plants can effectively remove ethane (C_2) from the gas stream: a) Raw gas production contains less than 50 barrels of condensate per million cubic feet of gas ($0.28 \text{ m}^3/\text{e}3\text{m}^3$) and is sent directly to the processing plant; b) Raw gas production contains greater than 50 barrels of condensate per million cubic feet of gas ($0.28 \text{ m}^3/\text{e}3\text{m}^3$). An accurate determination of raw gas production requires separation and measurement of condensate, and conversion of condensate composition to an equivalent raw gas stream flow rate; c) Condensate is removed at the well head and shipped to a sale point. Remaining liquids-rich gas is sent to the gas plant for processing.

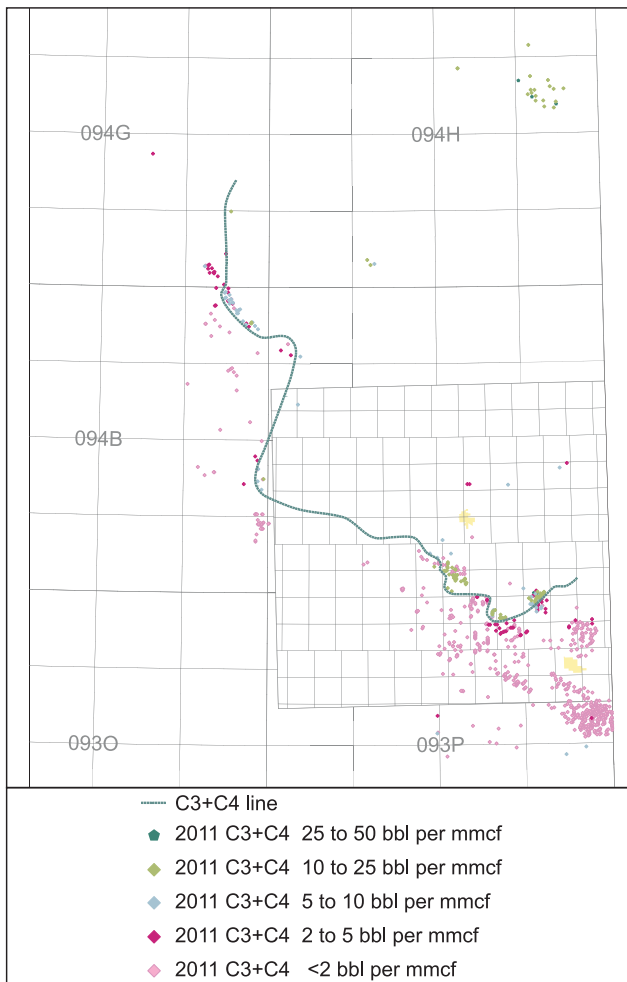


Figure 12. Liquids production for the Montney Formation showing C3+C4 production in barrels per million cubic feet of gas.

CONCLUSIONS

- Gas and liquids potential trends within the Montney Formation were determined using both T_{max} values from Rock Eval analysis of core and cuttings, and from raw gas production and gas plant sales data.
- Results from both techniques are for the most part in general agreement, but discrepancies are present in the southern part of the Montney play trend.
- These deviations may either be due to the suppression of the T_{max} value by migrated oil/bitumen or contamination by oil-based drilling fluids. Alternatively, the low production of liquids in the southern Montney trend may be due to a higher percentage of type III kerogen, which produces considerably less liquid hydrocarbons.

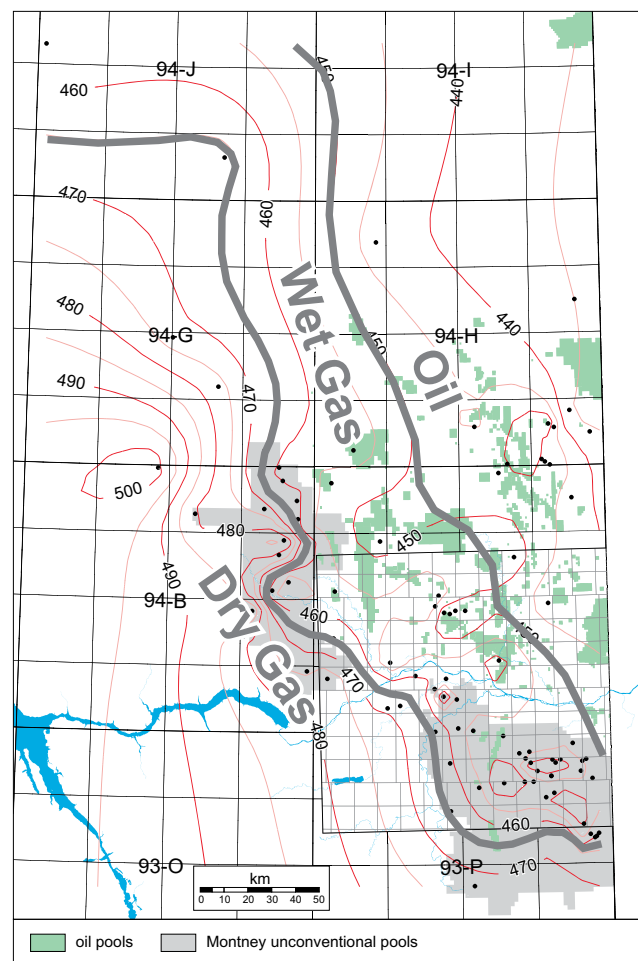


Figure 14. Zones of dry gas, wet gas and wet gas to oil within the Montney Formation derived from T_{max} data. Wet gas generation is bracketed between 450 and 465°C T_{max} values (Fig. 4), with peak wet gas generation along the 455°C line.

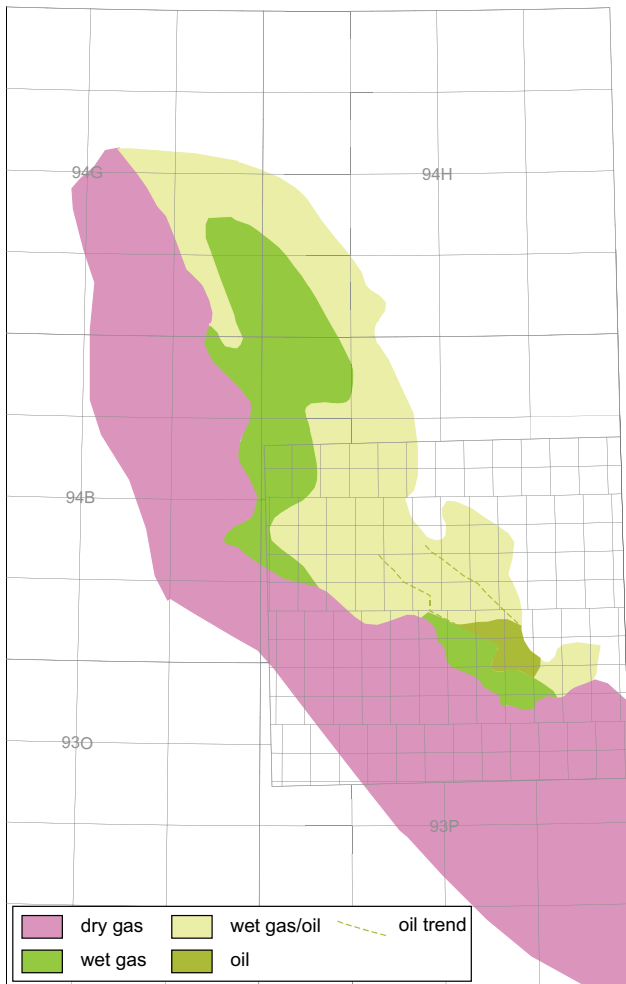


Figure 15. Zones of dry gas, wet gas, wet gas+oil and oil within the Montney Formation derived from sales gas data.

REFERENCES

- Bordenave, M.L. (1993): Applied Petroleum Geochemistry; *Tech-nip*, Paris, 531 pages.
- Dewing, K. and Sanei, H. (2009): Analysis of large thermal maturity datasets: examples from the Canadian Arctic Islands; *International Journal of Coal Geology*, Volume 77, pages 436–448.
- Espitalié, J., Deroo, G. and Marquis, F. (1985a): Rock-Eval pyrolysis and its applications (part two); *Institut Français du Pétrole, Oil & Gas Science and Technology*, Volume 40, pages 755–784.
- Espitalié, J., Deroo, G. and Marquis, F. (1985b): Rock-Eval pyrolysis and its applications (part one); *Institut Français du Pétrole, Oil & Gas Science and Technology*, Volume 40, pages 563–579.
- Espitalié, J., Deroo, G. and Marquis, F. (1986): Rock-Eval pyrolysis and its applications (part three); *Institut Français du Pétrole, Oil & Gas Science and Technology*, Volume 41, pages 73–89.
- Ferri, F., Hayes, M. and Goodman, E. (2013): Core and cuttings analysis, northeast British Columbia; *British Columbia Ministry of Natural Gas Development, Petroleum Geology Open File*, 2013-1.
- Fowler, M.G., Obermajer, M. and Snowdon, L.R. (2007a): Rock-Eval/TOC data for eleven NE British Columbia boreholes (map areas 94-I to 94-P); *Geological Survey of Canada, Open File* 5672.
- Fowler, M.G., Obermajer, M. and Snowdon, L.R. (2007b): Rock-Eval/TOC data for eight NE British Columbia boreholes (map areas 93-O to 94-H); *Geological Survey of Canada, Open File* 5673.
- Fowler, M.G. and Snowdon, L.R. (2001): Rock-Eval/TOC data for ten northern Alberta and British Columbia wells; *Geological Survey of Canada, Open File* 4124.
- Ibrahimbas, A. and Riediger, C.L. (2004): Hydrocarbon source rock potential as determined by Rock-Eval 6/TOC pyrolysis, northeast British Columbia and Northwest Alberta; in Summary of Activities 2004, *British Columbia Ministry of Energy, Mines and Natural Gas*, pages 8–18.
- Jacob, H. (1985): Disperse solid bitumen as an indicator for migration and maturity in prospecting for oil and gas; *Erdöl Kohle*, Volume 38, pages 365–374.
- Jarvie, D.M. (1991): Total organic carbon (TOC) analysis; in Source migration processes and evaluation techniques; Merrill, R.K., Editor, *American Association of Petroleum Geologists, Treatise of Petroleum Geology*, pages 113–118.
- Langford, F.F. and Blanc-Valleron, M.-M. (1990): Interpreting Rock-Eval pyrolysis data using graphs of pyrolyzable hydrocarbons vs. total organic carbon; *American Association of Petroleum Geologists Bulletin*, Volume 74, pages 799–804.
- Lafargue, E., Marquis, F. and Pillot, D. (1998): Rock-Eval 6 applications in hydrocarbon exploration, production, and soil contamination studies; *Revue de L'institut Français du Pétrole*, Volume 53, pages 421–437.
- Peters, K.E. (1986): Guidelines for evaluating petroleum source rock using programmed pyrolysis; *American Association of Petroleum Geologists Bulletin*, Volume 70, pages 318–329.

- Riediger, C.L. (1990): Rock-Eval/TOC data from the Lower Jurassic “Nordegg Member”, and the Lower and Middle Triassic Doig and Montney formations, Western Canada Sedimentary Basin, Alberta and British Columbia; *Geological Survey of Canada*, Open File 2308.
- Snowdon, L.R. (2000): Rock-Eval/TOC data for three British Columbia wells; *Geological Survey of Canada*, Open File 3910.
- Teichmuller, M. and Durand, B. (1983): Fluorescence microscopical rank studies on liptinites and vitrinites in peat and coals, and comparison with results of the rock-eval pyrolysis; *International Journal of Coal Geology*, Volume 2, Issue 3, pages 197–230.
- Tissot, B. and Welte, D.N. (1984): Petroleum Formation and Occurrence, 2nd edition; *Springer Verlag*, Heidelberg, 699 pages.
- Walsh, W. and McPhail, S. (2007): Shale gas potential: core and cuttings analysis, northeast British Columbia; *British Columbia Ministry of Energy, Mines and Natural Gas*, Petroleum Geology Open File 2007-1.

SUMMARY OF FIELD ACTIVITIES IN THE WESTERN LIARD BASIN, BRITISH COLUMBIA

*Filippo Ferri¹, Margot McMechan², Tiffani Fraser³, Kathryn Fiess⁴,
Leanne Pyle⁵ and Fabrice Cordey⁶*

ABSTRACT

The second and final year of a regional bedrock mapping program within the Toad River map area (NTS 094N) was completed in 2012. The program will result in three– 100 000 scale maps of the northwest, northeast and southeast quadrants of 094N and with four 1:50 000 scale maps covering the southwest quadrant. Surface samples were also collected for Rock Eval™, reflective light thermal maturity and apatite fission-track analysis. Cuttings from several petroleum wells in the map area were also sampled for Rock Eval analysis and vitrinite reflectance.

Composite sections of the Besa River Formation were measured in the southern Caribou Range and along the Alaska Highway, south of Stone Mountain. Approximately 170 m of the Besa River Formation were measured in three separate sections in the southern Caribou Range. Lithological, gamma-ray spectrometry and lithogeochemical data are similar to those observed in other sections of the formation, suggesting similar depositional conditions within the western Liard Basin. Changes in abundances of several trace elements, particularly, V, Mo, Ba and P, suggest variations in redox conditions during the deposition of the formation. Radiolarian and conodont fragments from the upper part of the section in the Caribou Range indicate a mid-Tournaisean age. Characteristics of the lower Besa River Formation observed along the Alaska Highway south of Stone Mountain are similar to the Evie member of the Horn River Formation.

Ferri, F., McMechan, M., Fraser, T., Fiess, K., Pyle, L. and Cordey, F. (2013): Summary of field activities in the western Liard Basin, British Columbia; in Geoscience Reports 2013, British Columbia Ministry of Natural Gas Development, pages 13–31.

¹Geoscience and Strategic Initiatives Branch, Oil and Gas Division, British Columbia Ministry of Natural Gas Development, Victoria, BC, Fil.Ferri@gov.bc.ca

²Geological Survey of Canada, Calgary, AB

³Yukon Geological Survey, Whitehorse, YT

⁴Northwest Territories Geoscience Office, Yellowknife, NWT

⁵VI Geosciences Services Ltd., Victoria, BC

⁶Université Claude Bernard Lyon 1, Lyon, France

Key Words: Besa River Formation, Liard Basin, Horn River Basin, Toad River, regional mapping, shale gas, lithogeochemistry, gamma ray spectrometry, measured section, radiolarians, Caribou Range, British Columbia, Yukon, Northwest Territories.

INTRODUCTION

The British Columbia Geoscience and Strategic Initiatives Branch participated in two co-operative geosciences programs in the western Liard Basin during the summer of 2012 (Fig. 1): 1) regional mapping within the Toad River map area (NTS 094N) and 2) examination of the Besa River Formation in the western and northern Liard Basin. The regional mapping program is in its second year (McMechan et al., 2012) and is part of the Geological Survey of Canada's (GSC) ongoing Geomapping for Energy and Minerals

(GEM) Yukon Sedimentary Basins project. Examination of the Besa River Formation is in its third year and in 2012 was conducted as part of a multijurisdictional project between the governments of Yukon, Northwest Territories and British Columbia. This work was also supported by the GEM program through use of analytical laboratories at the Geological Survey of Canada (GSC).

Besa River stratigraphy exposed along the western margins of the Liard Basin contains equivalents to the Horn River Formation, currently being developed for its shale gas potential in the eastern Horn River Basin (Fig. 2; Ferri

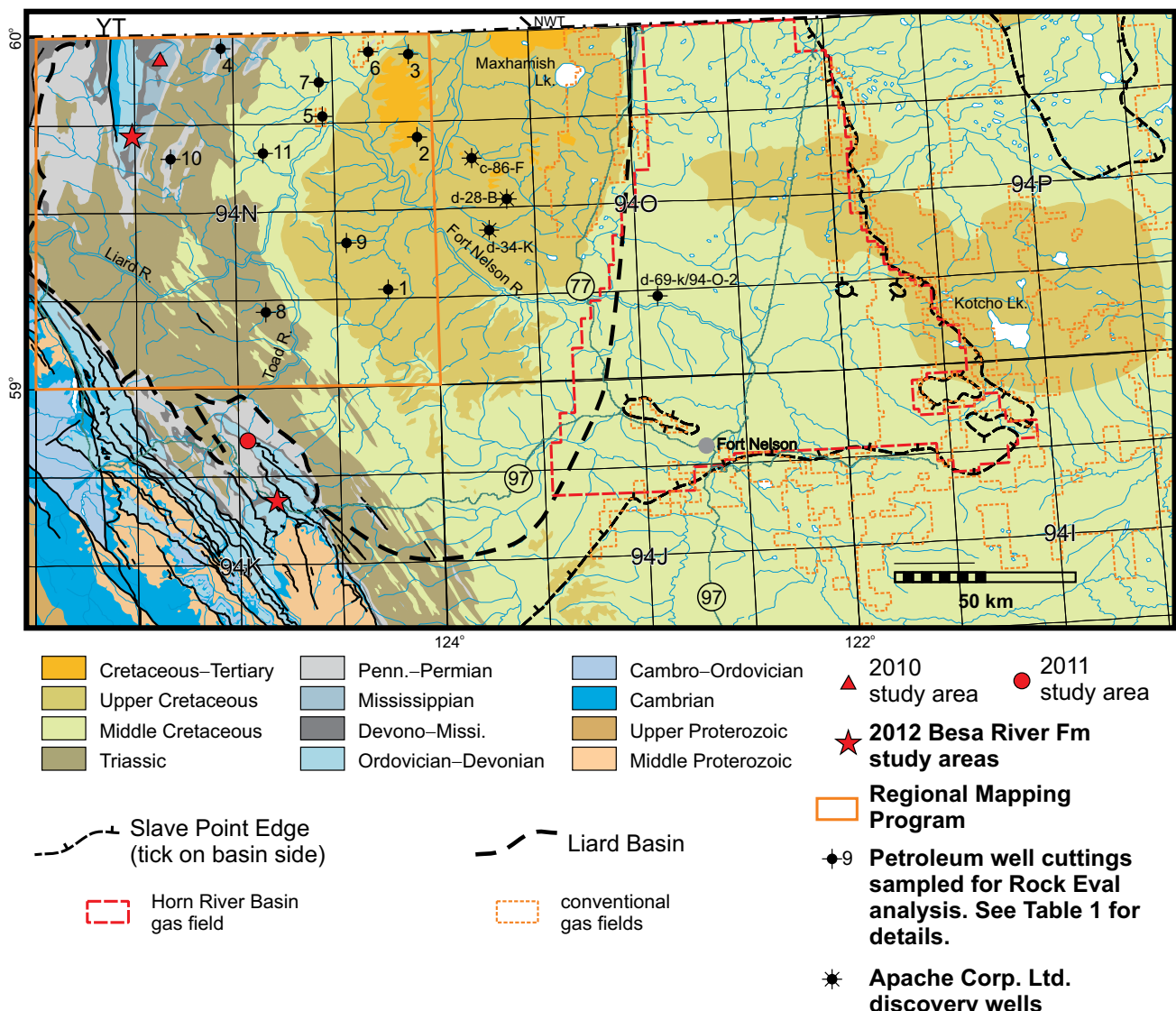


Figure 1. Regional geological map of northern British Columbia showing the location of the regional mapping project in the Toad River map area (094N) and stratigraphic sections of the Besa River Formation measured in the southern Caribou Range and along the Alaska Highway, southeast of Toad River. Geological database from Massey et al. (2005). The edge of Horn River Basin follows the Slave Point edge as defined by Petrel Robertson Consulting Ltd. (2003). Well locations refer to data in Table 1.

et al., 2011, 2012). The recent announcement by Apache Canada Ltd. of initial, average one-month production of 21.3 million cubic feet (mmcf; $6.03 \times 10^5 \text{ m}^3$) per day from a well within the central Liard Basin (d-34-K; Figure 1) underscores the potential for shale sequences in this area to hold significant potential. This well was drilled to a depth of 3800 m and laterally almost 900 m into the upper Besa River Formation. Apache Canada Ltd. estimates ultimate production of 17.9 billion cubic feet ($5.06 \times 10^8 \text{ m}^3$) from this well and suggests a net resource of 48 trillion cubic feet ($1.36 \times 10^{12} \text{ m}^3$) on its 430 000 acre (174 021 Ha) land holdings (Apache Corporation Ltd., 2012; Macedo, 2012).

Rocks of the Besa River Formation represent western shale equivalents of Middle Devonian to Early Mississippian

carbonate and shale sequences of the Western Canada Sedimentary Basin (Fig. 2). Ferri et al. (2011, 2012) summarize the regional geological setting and stratigraphic framework of these rocks.

TOAD RIVER MAPPING PROJECT (094N)

This is the second year of a regional mapping program within the Toad River map area, spearheaded by the GSC. A summary of the geological setting, and stratigraphic and structural framework, together with initial interpretations, can be found in McMechan et al. (2012).

Two weeks were spent collecting field data within the Toad River map area (094N) from base localities in Fort

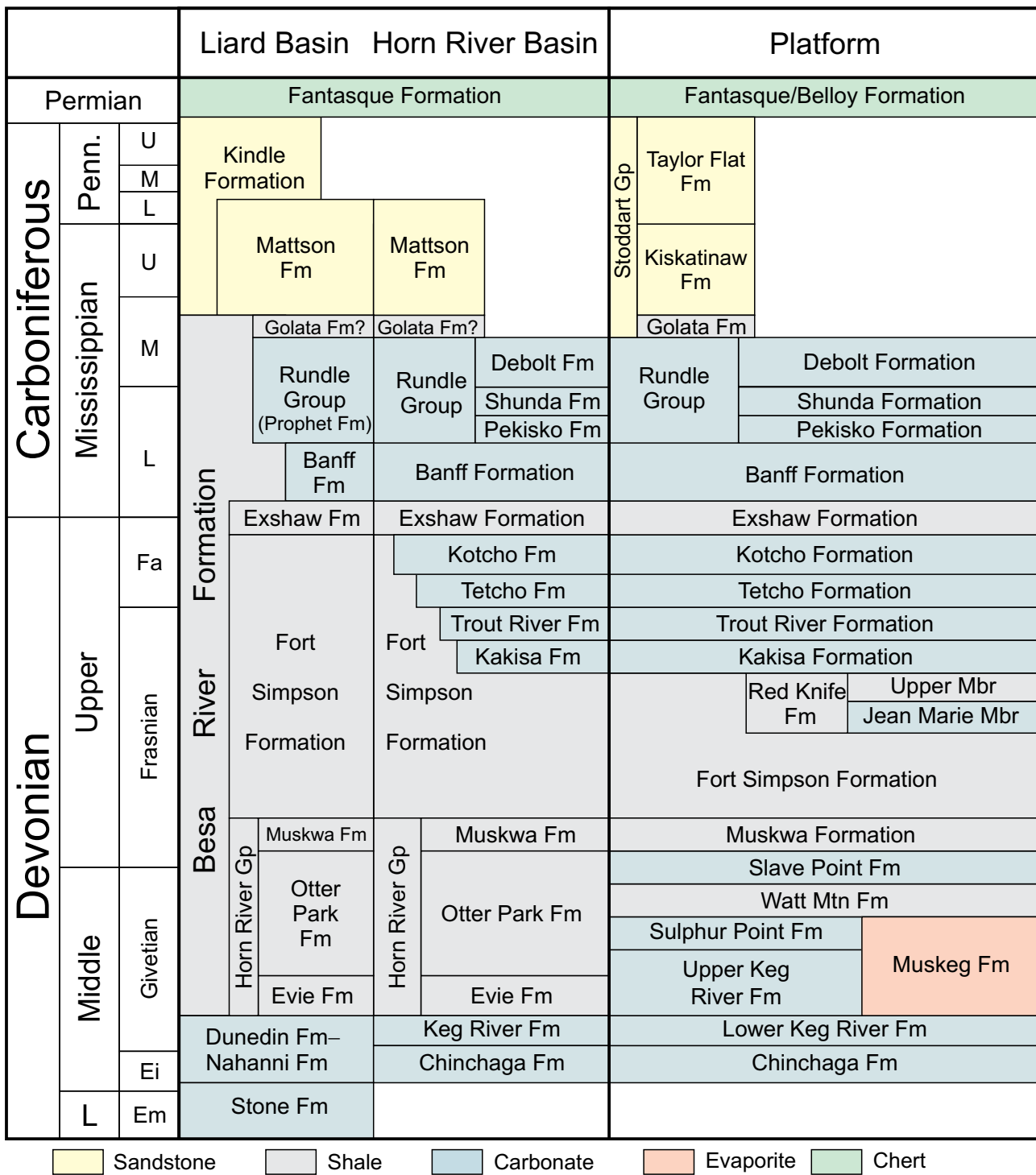


Figure 2. Stratigraphic chart showing the relationship of the Besa River Formation to other shale units and carbonates within the Western Canada Sedimentary Basin.

Nelson and at the small community of Liard River. A total of 260 field stations were added during the 2012 field season, resulting in a total of nearly 1200 localities (Fig. 3). This includes BC Hydro coverage from the early 1980s along the Liard River corridor and published and unpublished GSC data from the 1940s and late 1990s. In addition,

approximately 75 samples were collected for fossil identification (unit age determination), thermal maturation via reflective light microscopy, Rock Eval analysis and apatite fission track analysis for low-temperature thermal modelling (i.e., burial and uplift history; Fig 3b).

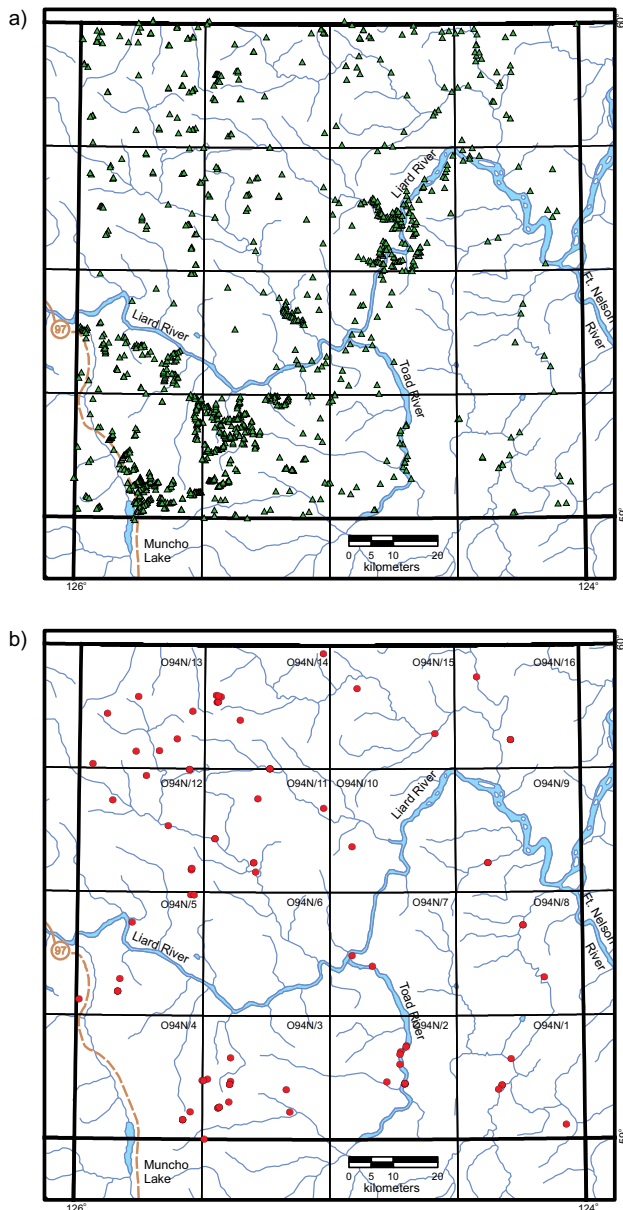


Figure 3. a) Station locations and b) 2012 sample locations of the regional mapping program in the Toad River map area.

Cuttings from the Garbutt, Toad-Grayling and Besa River shale successions in 11 oil and gas wells were also sampled for Rock Eval analysis and vitrinite reflectance (Table 1). Results of this sampling and analyses will be released in a future publication.

The primary goal of this project is to update the surface geological database through the production of three 1:100 000 scale maps of the northeast, southeast and northwest quadrants and four 1:50 000 scale maps of the southwest quadrant of the 094N map area. This data will also be available online in GIS format.

BESA RIVER FORMATION

This is the third year of a detailed stratigraphic and lithogeochemical examination of the Besa River Formation within the western Liard Basin (Ferri et al., 2011, 2012). In 2012, this project was carried out as part of a cooperative undertaking between the British Columbia Geoscience and Strategic Initiatives Branch, the Yukon Geological Survey and the Northwest Territories Geoscience Office. Because Besa River rock types occur in all three jurisdictions, an approach using data from throughout this area would not only present a more complete picture of this emerging shale gas succession, it would also highlight the economic potential within all three regions.

During the 2012 field season, all three organizations combined efforts and measured sections of the Besa River Formation, or its equivalent, in each jurisdiction (Fig. 4). This report will summarize initial results from 2012 investigations within British Columbia and include a summary of lithogeochemical data from 2011 sampling of the Besa River Formation in the Stone Mountain area, just east of Toad River (Ferri et al., 2012; Fig. 1). The reader is referred to Fraser et al. (2013) and Fiess et al. (2013) for a summary of 2012 activities within the Yukon and Northwest Territories, respectively. In addition, this report summarizes data collected along a section of the lowermost Besa River Formation that was measured by the senior author along the Alaska Highway, south of the section described by Ferri et al. (2012) and east of Toad River (Fig. 1).

Much of the analytical work in this investigation (Rock Eval, X-ray diffraction and thermal maturation through reflective light microscopy) and some field assistance (gamma-ray spectrometer) was supported through the GSC's GEM program, specifically the Yukon Sedimentary Basins project. The following is the procedure for data collection and analysis of samples that was carried out during the 2010 and 2011 field seasons, specifically

- detailed measurement and description of the section,
- acquisition of gamma ray spectrometer data (total counts; U, Th and K concentrations) on a 1 m spacing and
- representative chip samples of the section collected on a 2 m spacing that were crushed, split and analyzed for Rock Eval and lithogeochemistry (inductively coupled plasma–emission spectrometry [ICP-ES] and inductively coupled plasma–mass spectrometry [ICP-MS]).

A smaller representative subset of samples will be analyzed for semi-quantitative mineral composition through X-ray diffraction and a level of thermal maturity by reflective light microscopy.

TABLE 1. WELL CUTTINGS SAMPLED FOR ROCK EVAL ANALYSIS.

Well Name	Location	Location Figure 1	Unit Sampled—Cutting Intervals (original units)		
			Garbutt Fm.	Toad—Grayling Fms	Besa River Fm
Suncor et al Dunedin	a-039-B 094-N-08	1	1700–1760 m		
Suncor Westar La Jolie	b-037-I 094-N-09	2	1885–2005 m	2020–2055 m	
Talisman Beaver	b-037-I 094-N-16	3	1395–1690 m	2010–2385 m	
TPOC Clark Beavercrow	b-067-I 094-N-14	4			1020–4270 ft
Devon NEC Crow	c-016-A 094-N-15	5	700–780 m	1290–1490 m	2515–3640 m
Pan Am Beaver	c-045-K 094-N-16	6		1110–1830 ft	9520–11870 ft
Amoco Chevron Crow	d-036-H 094-N-15	7	1000–1500 ft	2850–3750 ft	7480–11980 ft
KMCL Shell Toad	d-057-K 094-N-02	8			7430–10016 ft
IOE Dunedin	d-075-E 094-N-08	9	5930–7260 ft	8800–10380 ft	11130–12050 ft
Shell E Grayling	d-095-F 094-N-11	10			1330–4010 ft
Oakwood IOE et al. Scatter	d-098-F 094-N-10	11	420–1700 ft	3850–4830 ft	7650–11 880 ft

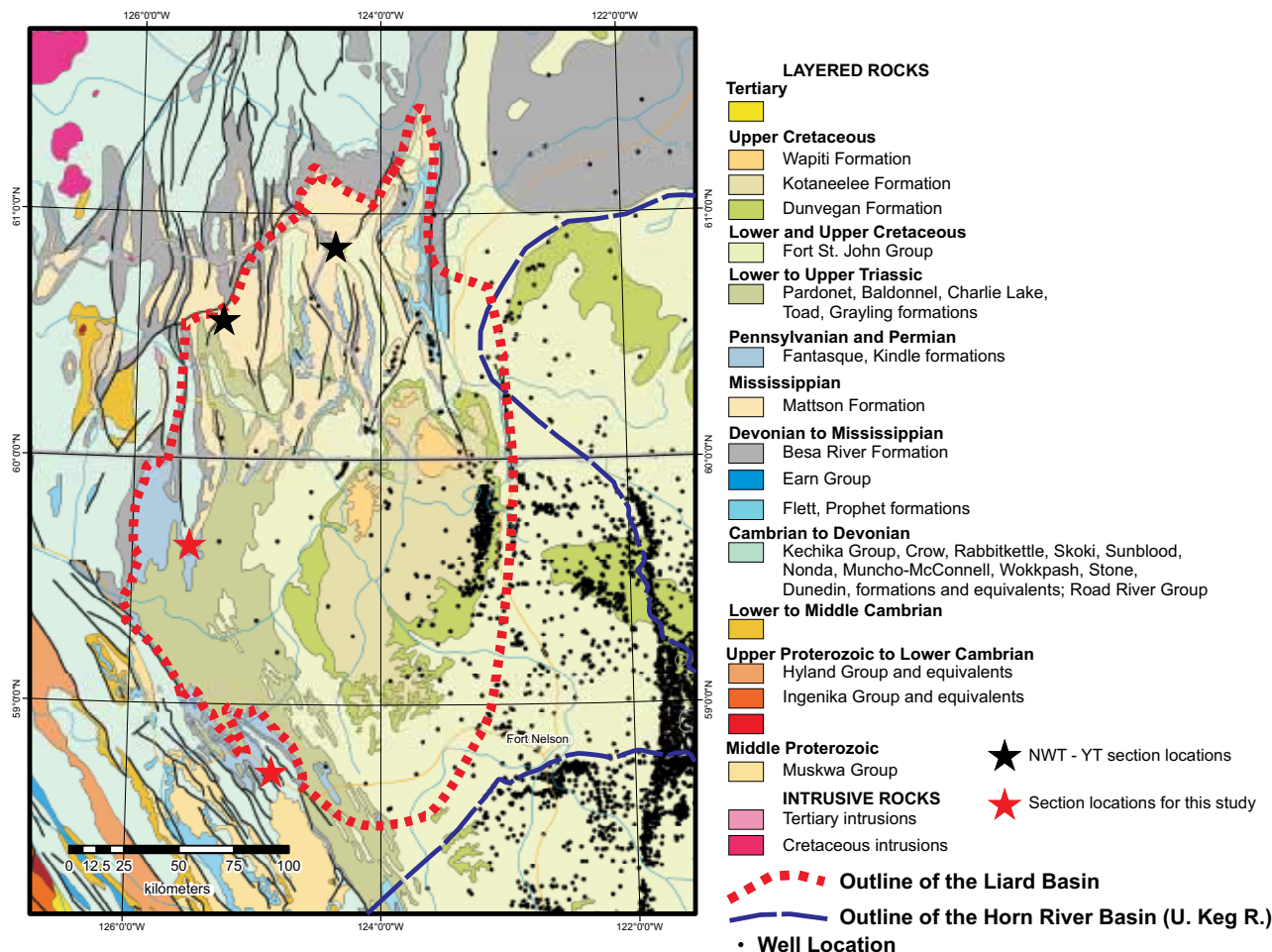


Figure 4. Regional geological map of northern British Columbia, southeastern Yukon and southwestern Northwest Territories with locations of Besa River Formation sections measured in each jurisdiction. Also shown are the outline of the Liard Basin and the eastern margin of the Horn River Basin as defined by the Upper Keg River Formation. Geological database from Wheeler and McFeely (1991).

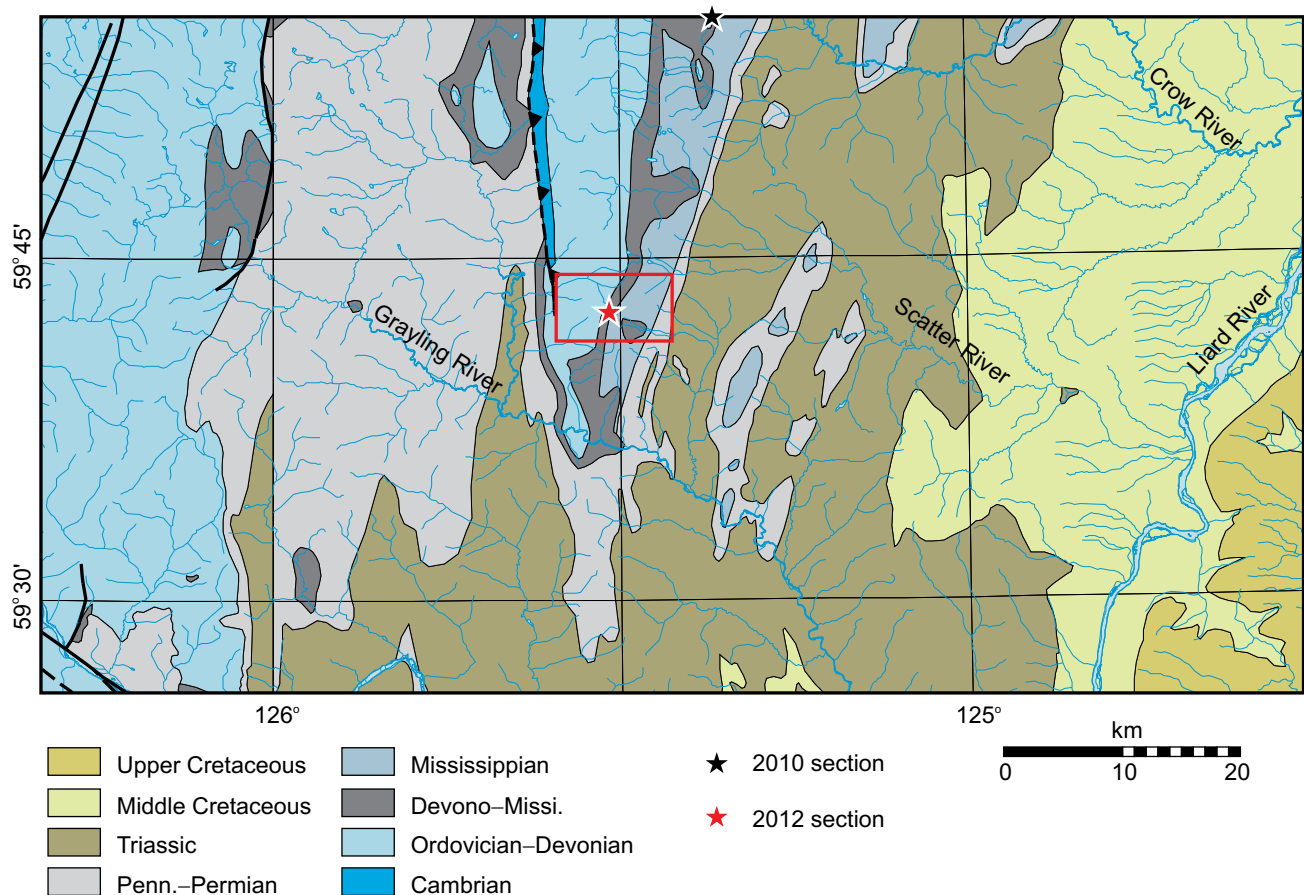


Figure 5. Geology of the southern Caribou Range showing locations of the sections measured in 2010 and 2012. Red rectangle shows the location of Figure 6. Geological database from Massey et al. (2005).

Location

Two composite sections of the Besa River Formation were measured in the western Liard Basin during the 2012 field season: 1) approximately 190 m of semicontinuous exposure within the southern Caribou Range, approximately 45 km south of the section measured in 2010 (Figs. 5, 6; Table 2) and 2) approximately 25 m of the lowermost Besa River Formation located along the north side of a creek, approximately 100 m east of the Alaska Highway, approximately 50 km south-southeast of the 2011 section (Figs. 1, 7; Table 2).

CARIBOU RANGE

Lithology

In the Caribou Range, nearly 190 m of lower and middle Besa River stratigraphy was measured in three separate sections (Figs. 8–10). Although correlations based on lithology, lithogeochemistry and gamma-ray scintillometer profiles suggest that there is approximately 60 m of unexposed stratigraphy between the three measured sequences, it is

TABLE 2. SECTION COORDINATES

Section	Level above base	Easting	Northing
CR - Section 1	0 m	358534	6622051
CR - Section 1	10 m	358560	6622048
CR - Section 2	0 m	358622	6622055
CR - Section 2	3 m	358630	6622051
CR - Section 3	0 m	358662	6621990
CR - Section 3	170 m	358961	6621893
AH	0 m	395145	6505895
AH	27 m	395099	6505887

NAD 83, Zone 10

CR - Caribou Range; AH - Alaska Highway

difficult to precisely position the middle section (section 2) within Besa River stratigraphy. The barite nodules found at the 115 m level of the upper section are likely equivalent to the barite nodules observed in the upper parts of the sections measured in 2010 and 2011 (Ferri et al., 2011, 2012). This is further corroborated by the up-section increase in barium levels beginning at this horizon (observed in all three sections) and the location of these nodules stratigraphically above vanadium anomalies (also seen in all three measured

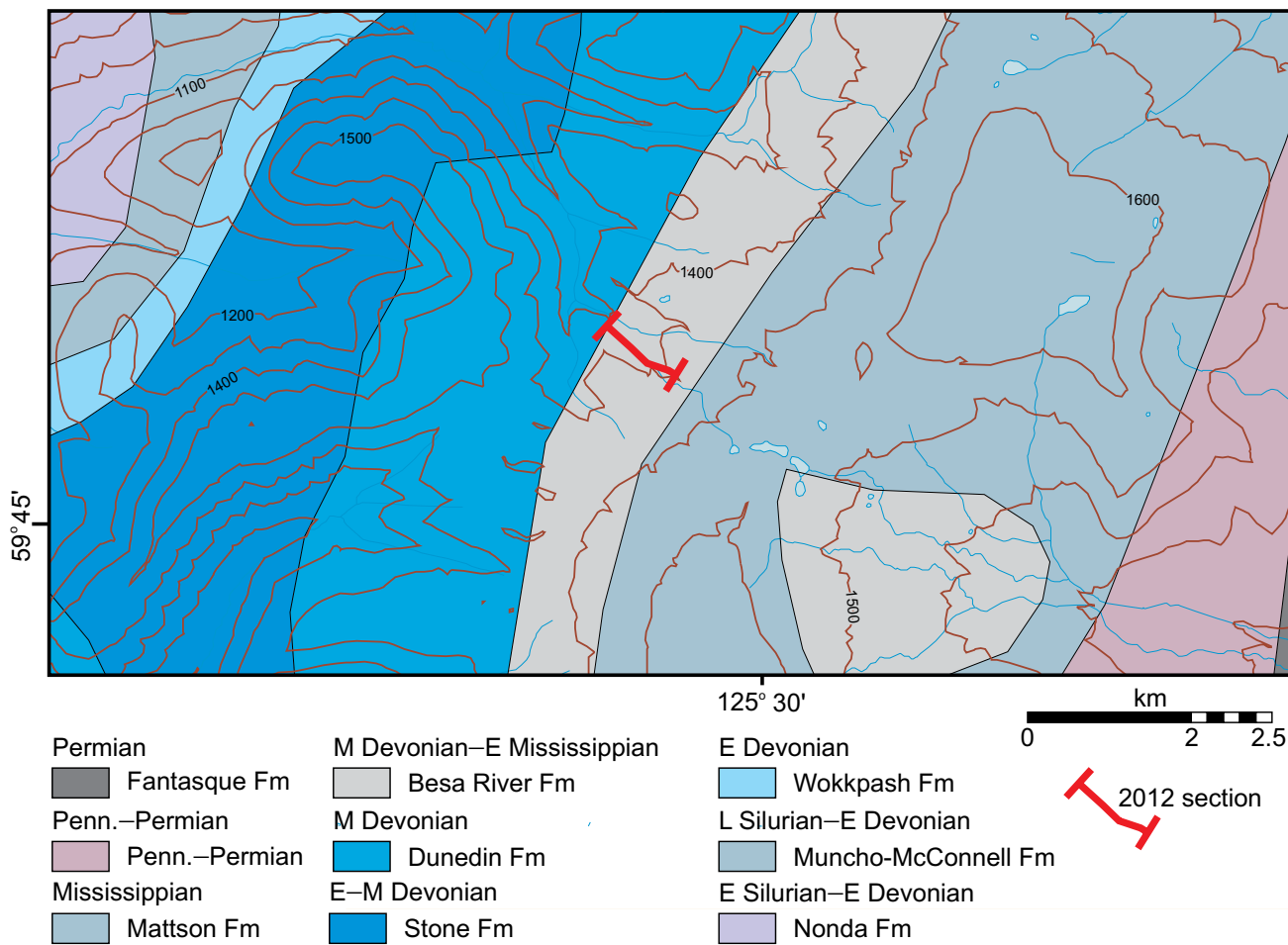


Figure 6. Location of the 2012 Besa River Formation section measured in the southern Caribou Range with respect to the local geology.

successions). In the northern Caribou Range and Stone Mountain, these nodules occur above a resistive section of silty mudstone to mudstone that has higher silica contents, a feature also observed in the 2012 section.

Resistive, black silty mudstone dominates the lower two sections of the Besa River Formation in the southern Caribou Range (Figs. 11, 12). The more recessive, tentaculitid-bearing carbonaceous shales sitting on the Dunedin Formation at the Alaska Highway section (see below) were not exposed. The lower 30 m of the upper section contains more recessive silty mudstone with a large portion of the section consisting of papery shale to platy siltstone (Figs. 11, 12). Above this is nearly 70 m of more resistive, blocky mudstone up to 15 cm thick, separated by thinner, shalier horizons up to several centimetres in thickness (Fig. 12). Barite nodules up to 20 cm in diameter, which are fetid when broken and display hollow cores with prismatic crystals, were found at the top of this mudstone section (115 m level, upper section; Fig. 12). These are very similar in morphology to those seen in the 2010 section in the northern part of the Caribou Range and to barite nodules in the Stone Mountain section measured in 2011. The succeeding 45 m of the section is dominated by more recessive crumbly

to fissile shaly sequences punctuated by several horizons of silty mudstone in the upper part.

The character of the succession above the barite nodules in section 3 of the southern Caribou Range is very similar to unit 6 of Ferri et al. (2010) from the northern Caribou Range. The underlying resistive and siliceous section (see Fig. 8) below these nodules has overall similarities with units 4 and 5 of the northern Caribou Range (Ferri et al., 2010), although the light grey weathering rocks of unit 4 are not observed in the south. Blocky to platy, silty mudstone and shale in the lowermost part of section 3 has similarities to unit 3 of the northern Caribou Range (Ferri et al., 2010).

Gamma ray spectrometry

Gamma ray spectrometer data of total counts and uranium, thorium and potassium concentrations across the three sections in the southern Caribou Range, are shown in Figure 13. The trace of total counts (or dose) mimics that for uranium, similar to observations in the other sections of the Besa River Formation (Fig. 13; Ferri et al., 2011, 2012). Uranium levels decrease upsection and are less than or

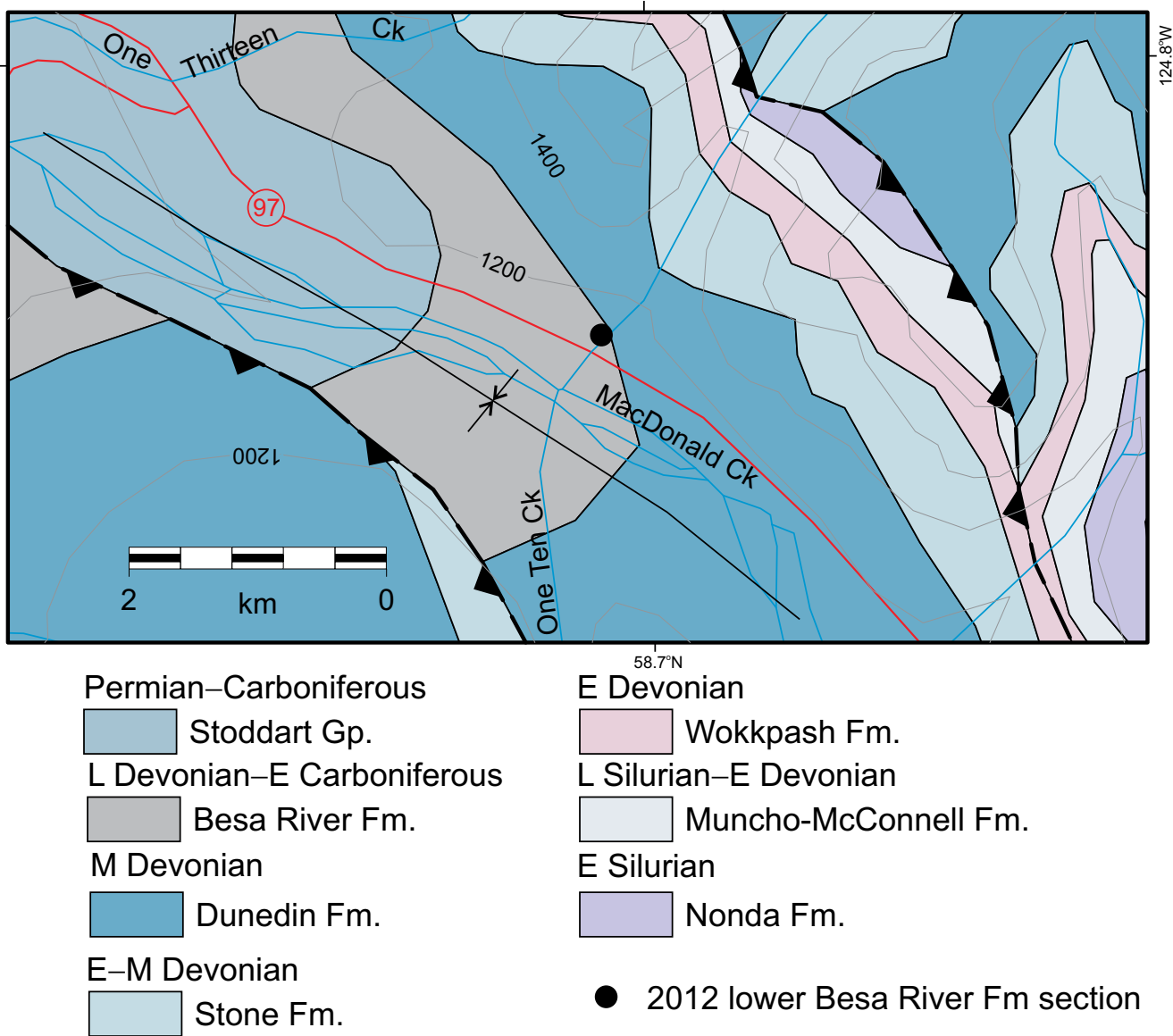


Figure 7. Local geology in the vicinity of the Besa River Formation section measured along the Alaska Highway, southeast of Toad River. Geological database from Massey et al. (2005).

equal to thorium values at the top of the upper section. Uranium concentrations appear to be highest in the lowest parts of the Besa River Formation and within the middle part of the upper section (60–110 m level). Although no Rock Eval data was available prior to publication, based on experience with the Besa River Formation and other shale sequences, the trace of organic carbon levels will likely mimic the trace of uranium concentrations and will be highest where uranium levels are at maximum levels. Potassium concentrations increase upsection, which is likely an indication of higher clay content.

Lithogeochemistry

Preliminary results of 2012 lithogeochemistry are presented in a format similar to that used in Ferri et al. (2011) in order to compare the two datasets (Figs. 14, 15). In addition, lithogeochemistry results from 2011 sampling, which were not available prior to publication of Geoscience Reports 2012, are also shown in Figure 16.

In the southern Caribou Range, the SiO_2 content averages 78 wt.% and is greater than 68 wt.%. There are peak values more than 87 wt.% in the lower and upper part of the upper section (Fig. 14). The concentration of Al_2O_3 mirrors that of SiO_2 and becomes highest in the upper part of the section. The concentration of Ca and Na is generally very low (<1 wt.%), although there are anomalous values above 2 wt.%, likely related to thin carbonate beds. This

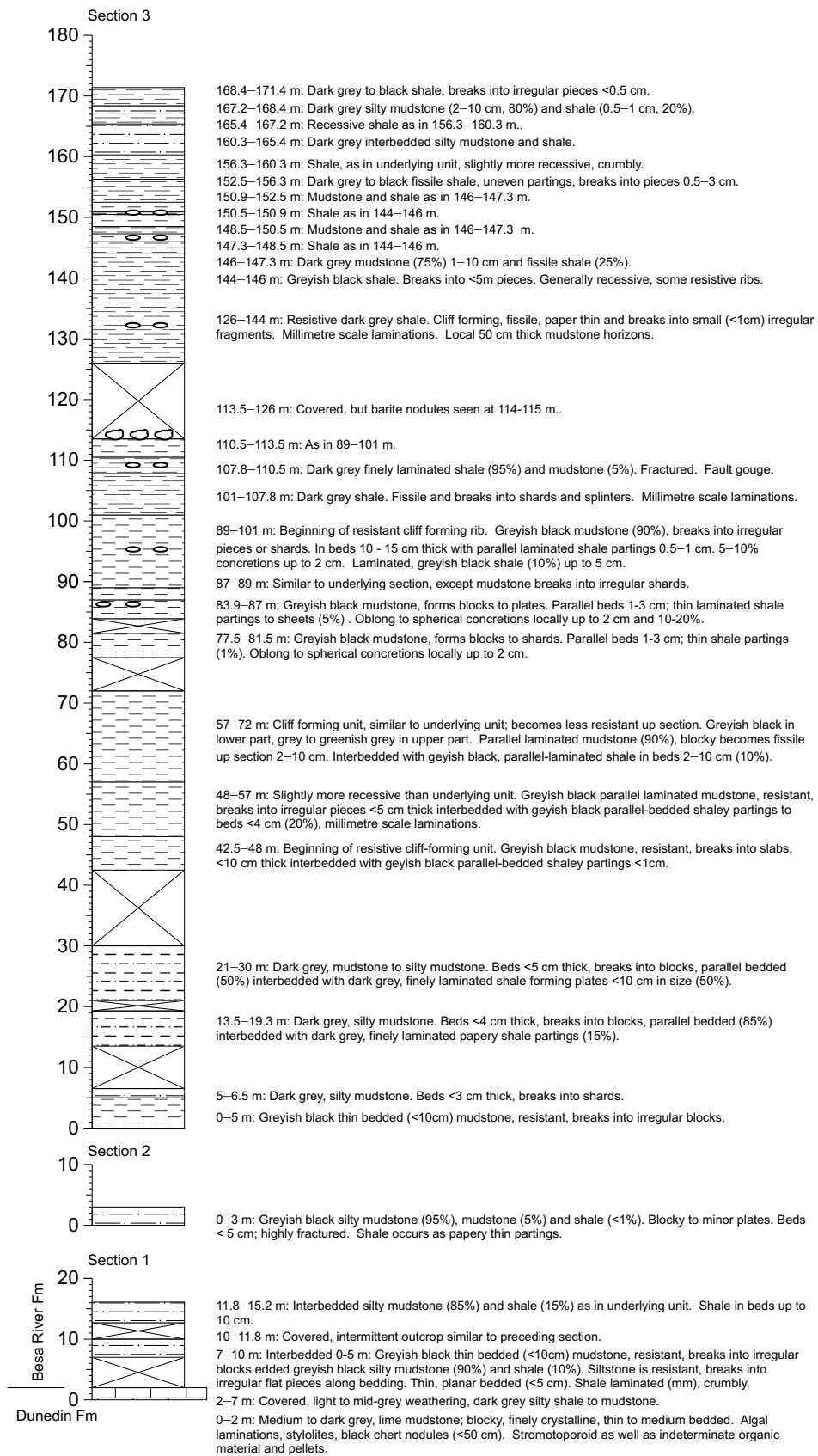


Figure 8. Lithological description of three separate sections of Besa River Formation measured in the southern Caribou Range. Although the three sections are in relative stratigraphic order, the exact distance between each is not known. The legend is the same as Figure 17.



Figure 9. Areal view of the three sections of the Besa River Formation measured in the southern Caribou Range. Arrows indicate viewing direction of photographs for sections 1 and 3 shown in Figures 10a and b.

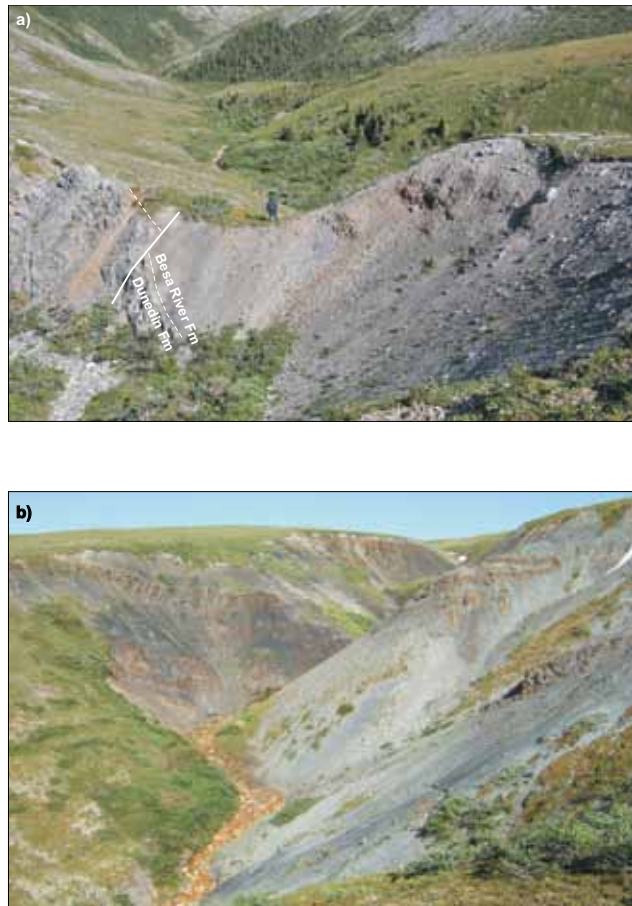


Figure 10. a) Looking south at section 1 of the Besa River Formation showing the lowermost 15 m of this formation sitting on top of Dunedin Formation carbonate rocks; b) Looking northwest at the upper section 3 of the Besa River Formation.

is also displayed in data from the 2011 section near Stone Mountain, where Ca and Na concentrations are greater than 10 wt.%. Thicker, cleaner carbonate horizons in the Stone Mountain area may be a reflection of closer proximity to the carbonate bank edge (Figs. 1, 16). The Mn and Fe levels are low, <0.01 wt.% and 5 wt.%, respectively, indicative of the reducing environment during deposition of the shales (Ferri et al., 2011). The Fe levels increase in the upper part of the section, suggesting a less reducing water column.

Redox-sensitive elements, such as Mo, V, Ba and P, show varying concentrations within the section. The Mo and V concentrations display elevated values below the 120 m level of the upper section, suggesting highly reducing conditions. The V concentrations are greater than or near 1000 ppm between 70 and 110 m level of the upper section, suggesting euxinic conditions (Quinby-Hunt and Wilde, 1994). These drop to well below 500 ppm above this horizon. There are elevated values of Mo below the 110 m level of the upper section, but as with V, concentrations drop considerably above this horizon, to less than 5 ppm. Phosphorous concentrations are also highest across this horizon (i.e., 70 to 110 m level, upper section; Fig. 15).



Figure 11. a) Lowermost few metres of section 1 in the southern Caribou Range, showing fault-offset contact between carbonate rocks of the Dunedin Formation and light grey weathering shale of the lower Besa River Formation; b) Interbedded rusty weathering, dark grey mudstone and shale of the Besa River Formation in the upper part of section 1; c) Rusty weathering, grey-black silty mudstone and thin shale partings in the Besa River Formation of section 2; d) Greyish black, thin bedded mudstone in the lower 5 m of Besa River Formation, section 3; e) Rusty to tan weathering, dark grey, thin bedded silty mudstone of the Besa River Formation at the 25 m level of section 3; f) Tan to rusty weathering, greyish black mudstone of the Besa River Formation at the 44 m level of section 3. This rock type is resistant because of its higher silica content.

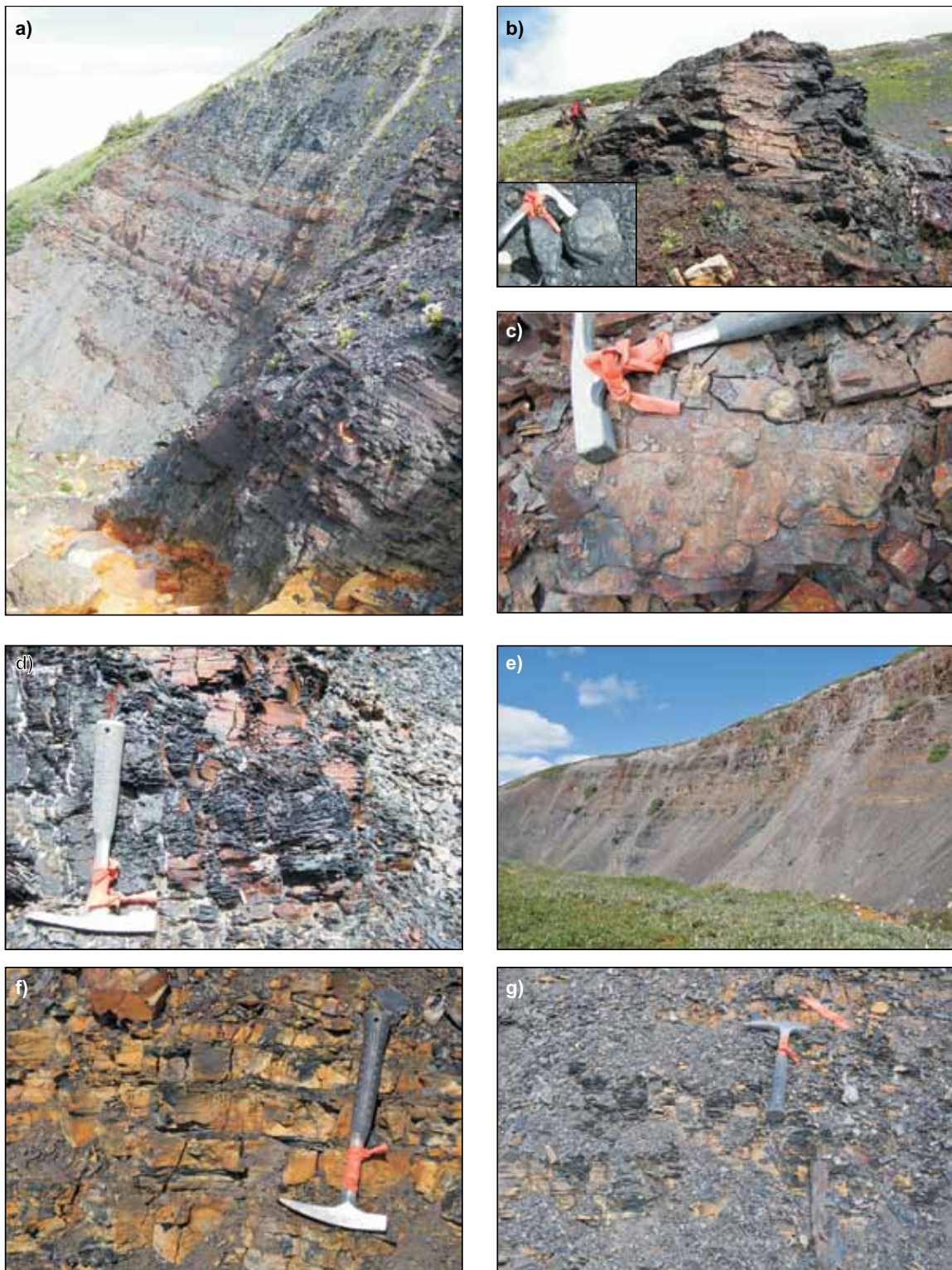


Figure 12. a) Looking southwest at blocky, greyish black parallel laminated resistive mudstone of the Besa River Formation between the 57–72 m level of section 3. These rocks become less resistive upsection; b) Blocky, resistive, greyish black mudstone between 110–113 m of section 3. Barite nodules are found weathering out of the covered section just above this (inset); c) Nodules within greyish black mudstone of the Besa River Formation at the 88 m level of section 3; d) Dark grey, fissile shale of the Besa River Formation at the 105 m level of section 3; e) Looking southwest at Besa River Formation rocks between the 120–170 m level of section 3; f) Rusty weathering, dark grey to black, silty mudstone and thinly interlayered shale of the Besa River Formation at the 150 m level of section 3; g) Dark grey to black shale of the Besa River Formation at the 154 m level of section 3. Rocks shown in f) and g) are dominant in the upper 40 m of section 3.

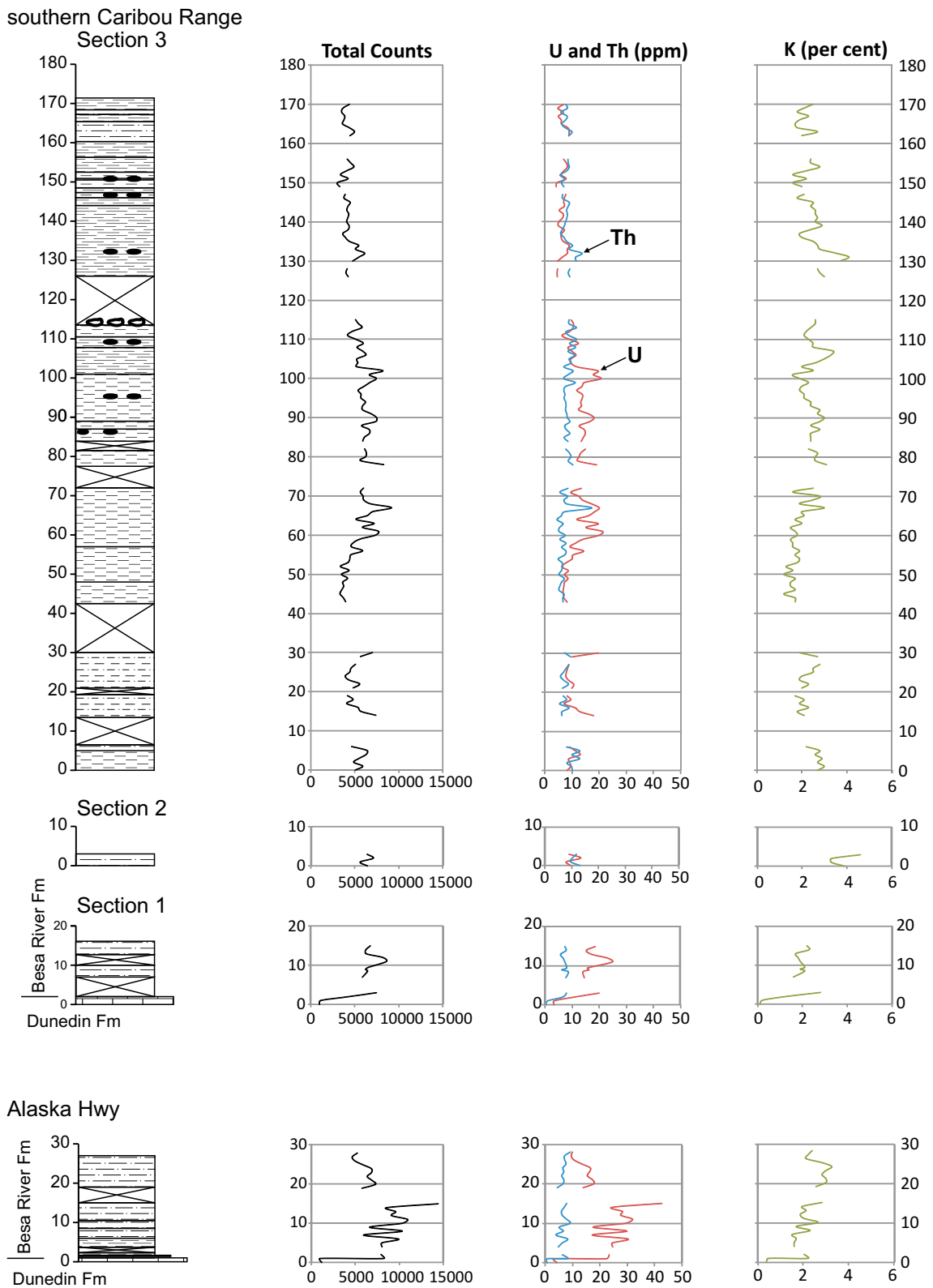


Figure 13. Gamma ray spectrometer data showing trace of total counts, uranium, thorium and potassium concentrations across the sections of the Besa River Formation measured in the southern Caribou Range and along the Alaska Highway.

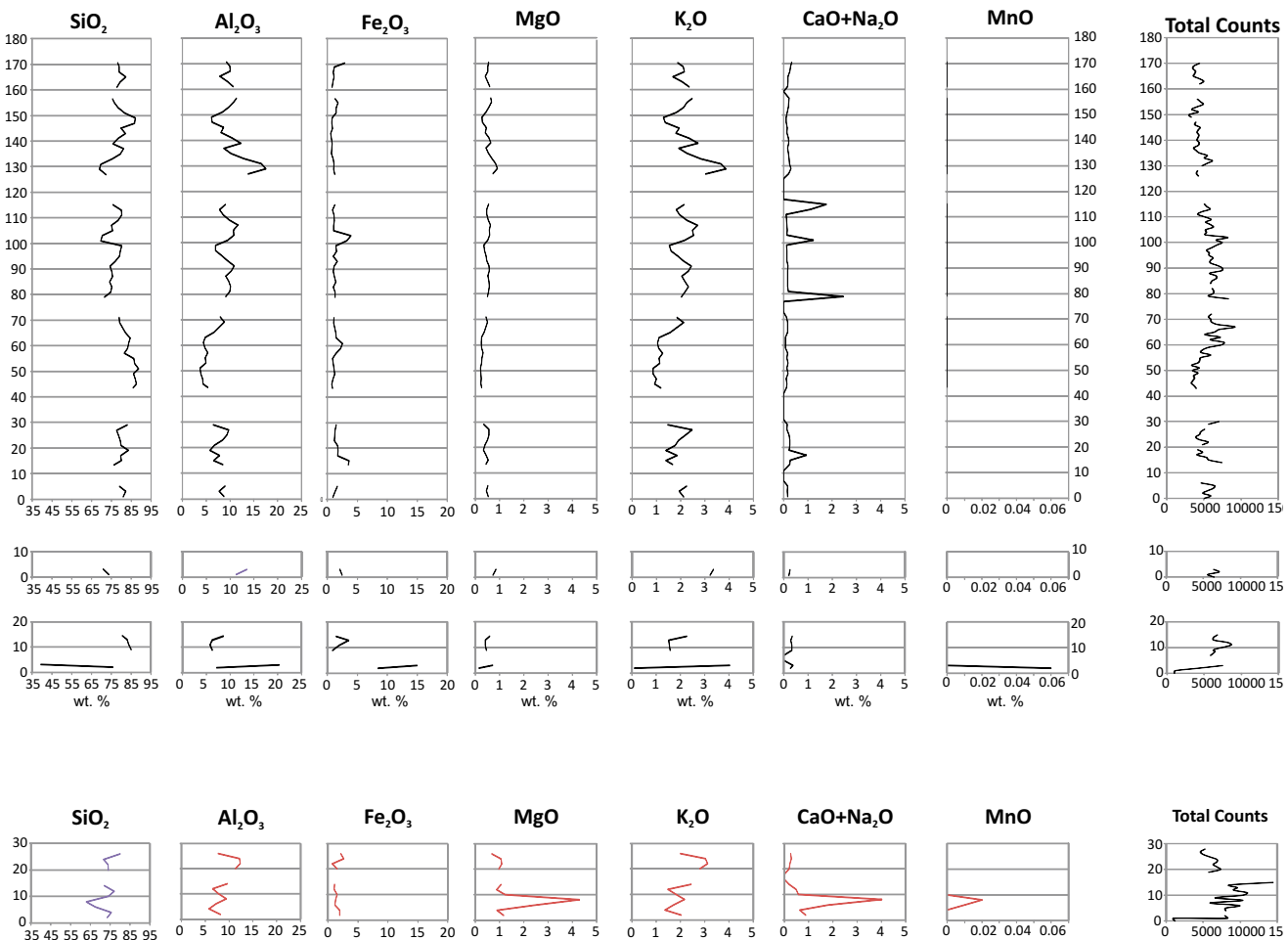


Figure 14. Major elemental abundances across the sections of the Besa River Formation measured in the southern Caribou Range and southwest of Toad River.

Barium is generally less than 2000 ppm below the 110 m level of the upper section but then increases to values in excess of 3000 ppm above this stratigraphic horizon. This increase in Ba within the sediments roughly corresponds to the occurrence of barite nodules at the 115 m level of the upper section. Barite nodules suggest that Ba may be precipitating from the water column due to a greater availability of sulphate. Below this stratigraphic level, conditions were likely more reducing, leading to the conversion of sulphate to sulphide. The Ba found in this environment would have accumulated in the water column, but would have started to precipitate out when sulphate became more abundant due to less reducing conditions. In this model, Ba levels in the water column would have been highest just before redox conditions changed, thus leading to an initial spike of barite precipitation represented by the barite nodules (Jewell, 2000; Huston and Logan, 2004; Griffith and Paytan, 2012).

Micropaleontology

Two samples of Besa River rocks (from the 43.5 m level and 151 m level of the upper section) were taken for processing and extraction of radiolarians for age determination. Although radiolarians were recovered from the 43.5 m level, these were flattened parallel to bedding and unidentifiable. Well-preserved radiolarians and a conodont ramiform element were recovered from the 151 m sample, which suggests a Frasnian to Tournaisian age, with the conodont fragment possibly of late Tournaisian age (Cordey, 2013; M. Orchard, pers comm, 2013).

ALASKA HIGHWAY SECTION

Lithology

Approximately 26 m of the lowermost Besa River Formation were measured immediately south of Stone Mountain, approximately 100 m north of the Alaska Highway and on the north side of a creek flowing into MacDonald Creek (Figs. 7, 17 and 18). Besa River shales sit sharply

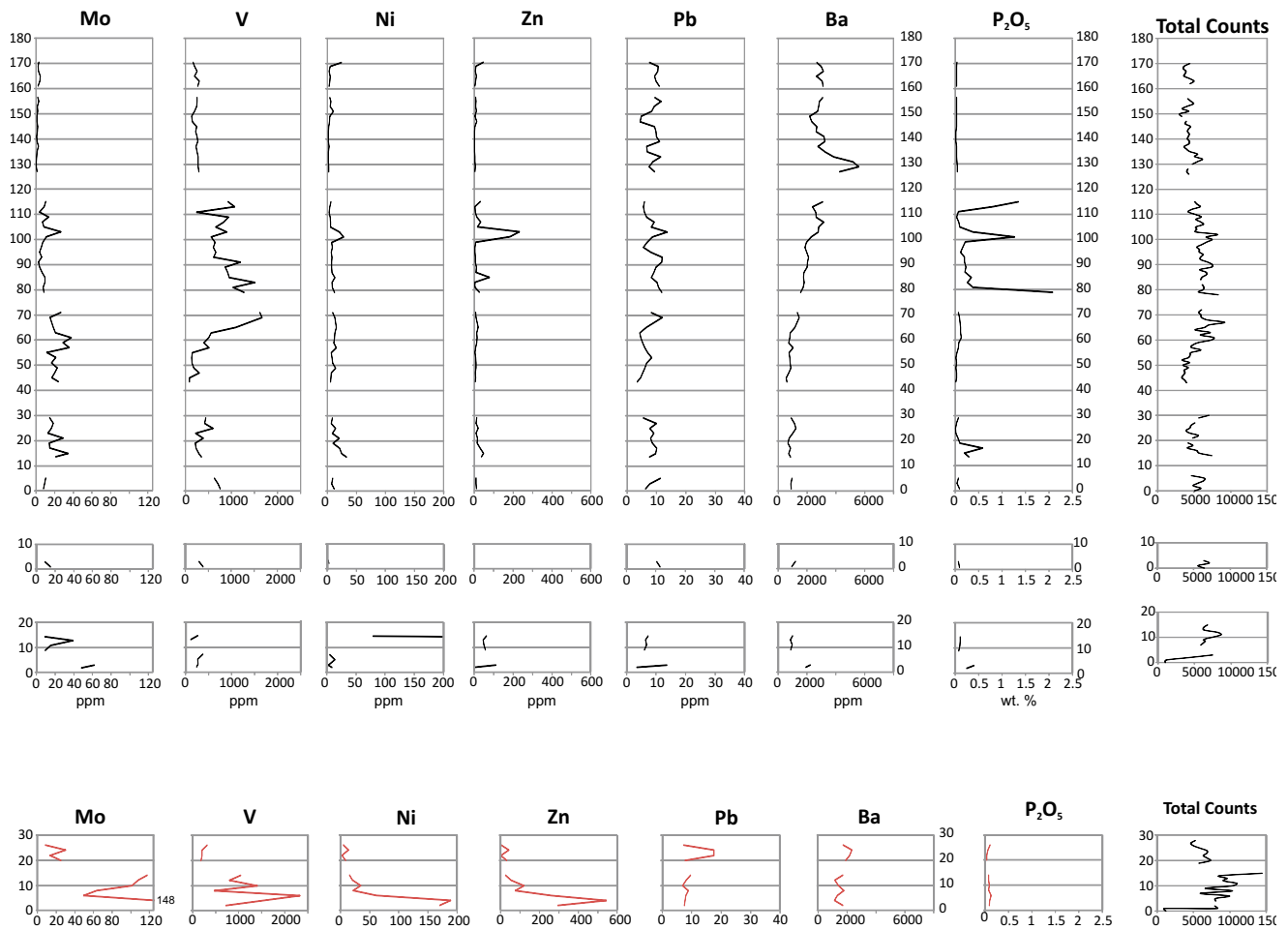


Figure 15. Minor and trace elemental abundances across sections of the Besa River Formation measured in the southern Caribou Range and southeast of Toad River.

above fossiliferous (coral, crinoids and shell fragments) limestone of the Dunedin Formation (Fig. 18a). The basal 6 m of the Besa River Formation consists of dark grey to black, tentaculitid-bearing (less than 5 mm long), soft, friable, carbonaceous shale (Fig. 18b). A thin, dark grey to black, carbonaceous limestone bed is found 1 m above the Dunedin Formation contact. These soft shales grade upward into 5–20 cm thick, carbonaceous mudstone to silty mudstone beds separated by thin shale horizons (Fig. 18c). The uppermost part of this section is massive (i.e., no bedding planes observed) and breaks into uneven, shard-like pieces (Fig. 18d).

Gamma ray spectrometry

The trace of total counts per second across the section has similarities to the lower part of the 2012 section investigated in the southern Caribou Range (Fig. 13). Uranium concentrations are higher than thorium and the profile of this concentration across the section mimics the total counts.

Lithogeochemistry

Major element abundances within the Alaska Highway section of the Besa River Formation are similar to those seen in the Caribou Range and within the 2011 section (Figs. 14, 15). Trace elements, including Mo, V, Ni and Zn, show elevated concentrations within the lower radioactive zone (2–15 m). These abundances are similar to those seen within the upper part of the succession in the southern Caribou Range (70–110 m level of section 3) and are at similar concentrations to those in Besa River sections sampled in 2010 and 2011. These abundances suggest very reducing (euxinic) conditions and likely will be accompanied by high organic carbon contents.

DISCUSSION

Lithological and geochemical characteristics of the Besa River Formation within the southern Caribou Range have overall similarities with sections measured in the northern Caribou Range and within the Stone Mountain area, suggesting uniform depositional conditions over a

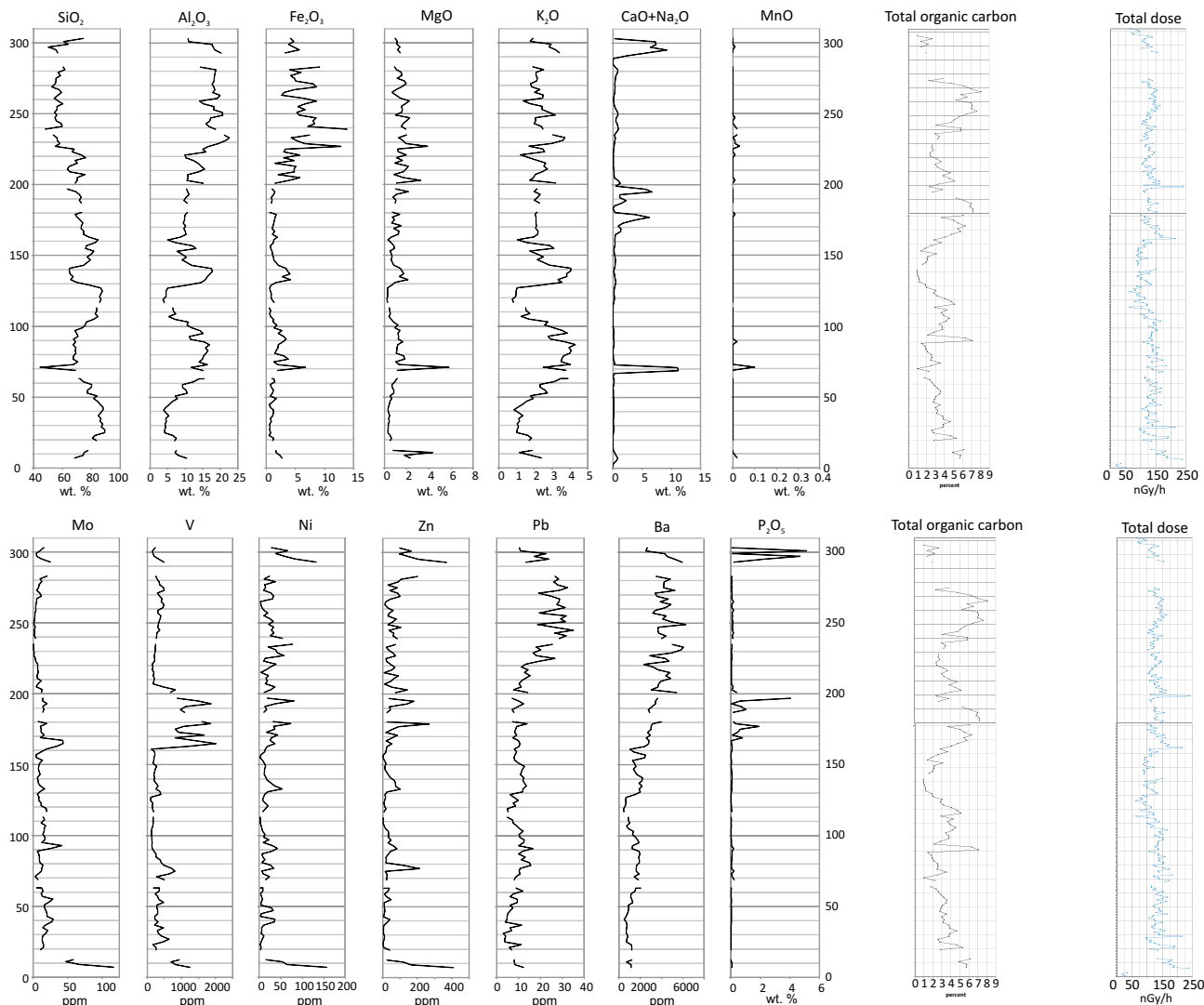


Figure 16. Major, minor and trace element abundances across the section of Besa River Formation measured in the Stone Mountain area by Ferri et al. (2012).

widespread area. Tentative correlation of the section in the southern Caribou Range with other sections is shown in Figure 19. Note that the 70–110 m portion of the upper section is tentatively correlated with rocks that are believed to be equivalents to the Exshaw Formation in the subsurface (Ferri et al., 2011, 2012). The postulated late Tournaisian age for radiolarian and conodont taxa from the 151 m level of the section would corroborate this because the Exshaw Formation has been shown to be late Famennian to middle Tournaisian in age (Richards et al., 2002).

The radioactive, tentaculitid-bearing shale section seen along the Alaska Highway is similar to Evie rocks observed by the senior author within the Imperial Komie, d-69-K/94-O-2 well of the Horn River Basin (Figs. 1, 18). This further supports the correlation of Horn River Basin rocks westward into the lower parts of the Besa River Formation (Ferri et al., 2011, 2012).

Rocks of the Besa River Formation in the Yukon have overall similarities to those of the Caribou Range and Stone Mountain area (Fraser et al., 2013). Although scintillometer and lithogeochemical data may assist with correlation of the sections, the Besa River Formation in the Yukon is much thicker, suggesting either (or a combination of) shale-out of underlying Dunedin Formation limestone, localized depositional thickening or structural complications.

The Golata Formation in the Northwest Territories (Fiess et al., 2013) contains rocks similar to those observed in the upper Besa River Formation within British Columbia (Ferri et al., 2011, 2012). Golata Formation rocks in the Northwest Territories are located immediately southeast of the Prophet Formation shale-out into rocks of the Besa River Formation.

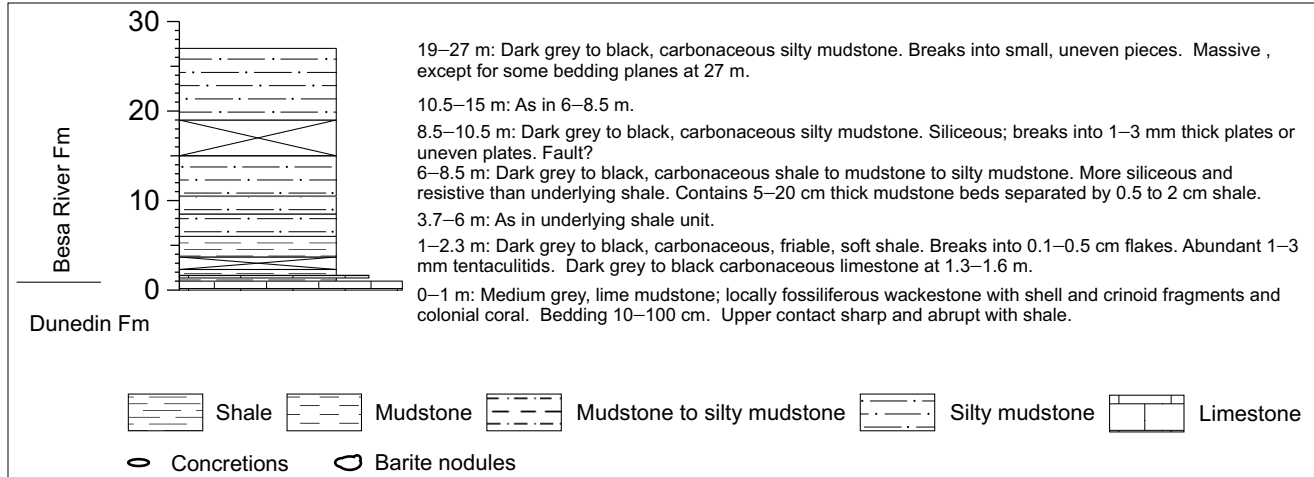


Figure 17. Lithological description of the Besa River Formation measured along the Alaska Highway, southeast of Toad River.

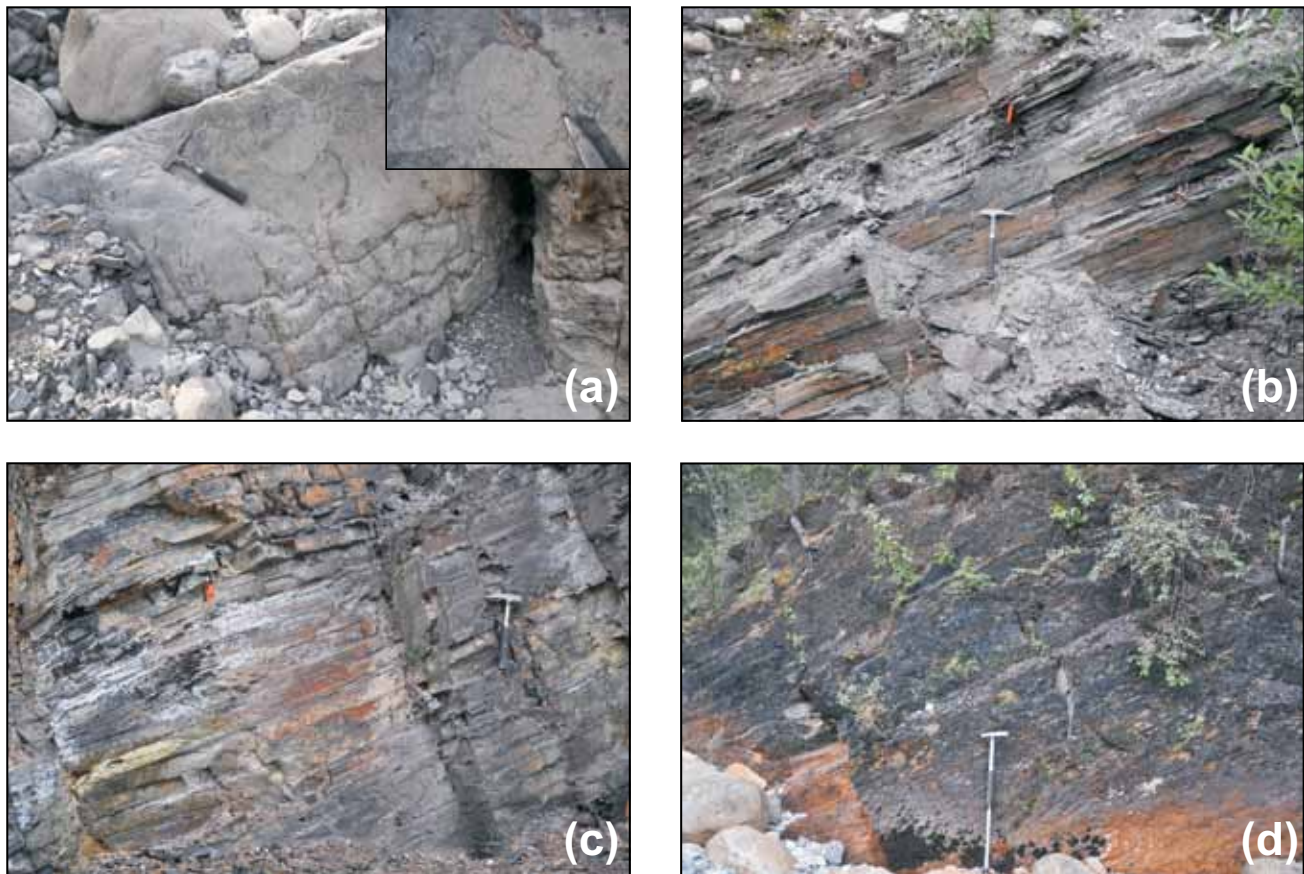


Figure 18. a) Upper two metres of fossiliferous limestone belonging to the Dunedin Formation within the section measured along the Alaska Highway, southeast of Toad River. Inset shows coral on the bedding surface immediately below the contact with the Besa River Formation; b) Lower several metres of tentaculitid-bearing soft shales of the Besa River Formation along the Alaska Highway section; c) More resistive, blocky shales to siltstone with fissile partings across the 11–13 m part of the Besa River section measured just north of the Alaska Highway; d) Splintery shale to siltstone in the upper part of the Besa River section just north of the Alaska Highway.

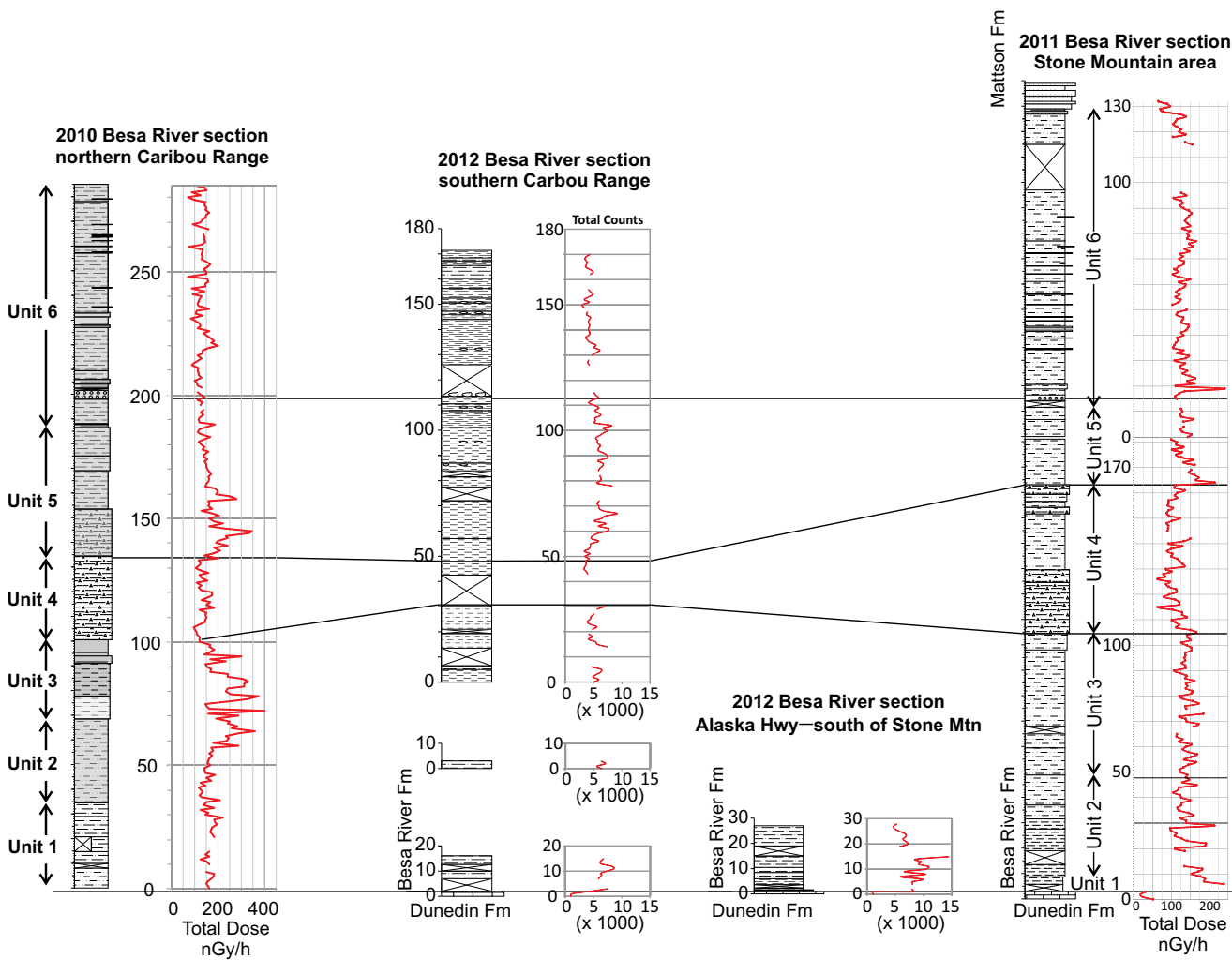


Figure 19. Correlation of Besa River Formation sections measured in this study with Besa River Formation sections measured in the northern Caribou Range and the Stone Mountain area by Ferri et al. (2011) and Ferri et al. (2012), respectively.

SUMMARY

- Regional mapping was concluded in the Toad River map area (NTS 094N) and will lead to the production of 1:100 000 scale maps of the northeast, southeast and northwest quadrants and 1:50 000 scale maps of 094N/3, 4, 5 and 6. This is a co-operative program with the GSC.
- Several composite sections of the Besa River Formation were measured in the southern Caribou Range and along the Alaska Highway, south of Stone Mountain. Data collection follows the methods used by Ferri et al. (2011, 2012). This was part of a larger project looking at sections of the Besa River Formation in the Yukon and its equivalents in the Northwest Territories (Fiess et al., 2013; Fraser et al., 2013).
- Overall lithological, gamma-ray spectrometry and lithogeochemical data across the Besa River Formation in the southern Caribou Range are similar

to those observed in the northern Caribou Range and the Stone Mountain area, suggesting similar depositional conditions over a wide area.

- Lithogeochemistry indicates changes in redox conditions during deposition of the Besa River Formation.
- Radiolarian and conodont fossils collected from the top of the section indicate a late Tournaisian age.
- Characteristics of the lower Besa River Formation observed along the Alaska Highway south of Stone Mountain are similar to the Evie member of the Horn River Formation.

ACKNOWLEDGMENTS

The authors thank Trevor Wilson of Bailey Helicopters for excellent service during regional mapping in Toad River map area. We would also thank Benedikt Segura of Great Slave Helicopters, not only for his excellent piloting skills, but also for willingness to help in collecting data at the outcrop. The efforts of Lindsay Kung and Arend Stamhuis in the field are greatly appreciated.

REFERENCES

- Apache Corporation Ltd. (2012): Liard discovery truly a world-class play; *Explore Newsletter*, Apache Corporation Ltd., URL <http://www.apachecorp.com/News/Articles/View_Article.aspx?Article.ItemID=2877> [November 2012].
- Cordey, F. (2013): Microfossil report, Besa River Formation, Caribou Range, northeastern *British Columbia*; *British Columbia Ministry of Natural Gas Development*, Oil and Gas Maps and Miscellaneous 2013-1, 4 pages.
- Ferri, F., Hickin, A. and Reyes, J. (2012): Horn River Basin-equivalent strata in Besa River Formation shale, northeastern British Columbia; in *Geoscience Reports 2012*, *British Columbia Ministry of Energy, Mines and Natural Gas*, pages 1–15.
- Ferri, F., Hickin, A.S. and Huntley, D.H. (2011): Besa River Formation, western Liard Basin, British Columbia (NTS 094N): geochemistry and regional correlations; in *Geoscience Reports 2011*, *British Columbia Ministry of Energy, Mines and Natural Gas*, pages 1–18.
- Fiess, K., Ferri, F., Pyle, L., Fraser, T. and Rocheleau, J. (2013): Liard Basin Hydrocarbon Project: shale gas potential of Devonian-Carboniferous strata in the Northwest Territories, Yukon and northeastern British Columbia; *Geoconvention 2013*, program with abstracts, Canadian Society of Petroleum Geologists, in press.
- Fraser, T., Ferri, F., Fiess, K. and Pyle, L. (2013): Besa River Formation in Liard basin, southeast Yukon: report on 2012 reconnaissance fieldwork; in Yukon Exploration and Geology 2012, MacFarlane, K.E. and Nordling, M.G., Editors, *Yukon Geological Survey*, pages 37–46.
- Griffith, E.M. and Paytan, A. (2012): Barite in the ocean—occurrence, geochemistry and palaeocenographic applications; *Sedimentology*, Volume 59, pages 1817–1835.
- Huston, D.L. and Logan, G.A. (2004): Barite, BIF's and bugs: evidence for the evolution of the Earth's early hydrosphere; *Earth and Planetary Science Letters*, Volume 220, pages 41–55.
- Jewell, P.W. (2000): Bedded barite in the geologic record; in *Marine authigenesis: from global to microbial*, Glenn, C.R., Lucas, J. and Prevot, L., Editors, *Society for Sedimentary Geology*, Special Publication 66, pages 147–161.
- Macedo, R. (2012): Apache validates new shale play in B.C.'s Liard Basin; *Daily Oil Bulletin*, June 14, 2012.
- Massey, N.W.D., MacIntyre, D.G., Desjardins, P.J. and Cooney, R.T. (2005): Digital geology map of British Columbia: whole province; *British Columbia Ministry of Energy, Mines and Natural Gas*, GeoFile 2005-1, scale 1:1 000 000.
- McMechan, M., Ferri, F. and MacDonald, L. (2012): Geology of the Toad River area (NTS 094N), northeast British Columbia; in *Geoscience Reports 2012*, *British Columbia Ministry of Energy, Mines and Natural Gas*, pages 17–39.
- Petrel Robertson Consulting Ltd. (2003): Exploration assessment of deep Devonian gas plays, northeastern British Columbia; *British Columbia Ministry of Energy, Mines and Natural Gas*, Petroleum Geology Open File 2003-4.
- Quinby-Hunt, M.S. and Wilde, P. (1994): Thermodynamic zonation in the black shale facies based on iron-manganese-vanadium content; *Chemical Geology*, Volume 113, pages 297–317.
- Richards, B.C., Ross, G.M. and Utting, J. (2002): U Pb geochronology, lithostratigraphy and biostratigraphy of tuff in the upper Famennian to Tournaisian Exshaw Formation: evidence for a mid-Paleozoic magmatic arc on the northwestern margin of North America; in Carboniferous and Permian of the world, Hills, L.V., Henderson, C.M. and Bamber, E.W., Editors, *Canadian Society of Petroleum Geologists*, Memoir 19, pages 158–207.
- Wheeler, J.O. and McFeely, P. (1991): Tectonic assemblage map of the Canadian Cordillera and adjacent parts of the United States of America; *Geological Survey of Canada*, Map 1712A.

CHARACTERIZING POROSITY IN THE HORN RIVER SHALE, NORTHEASTERN BRITISH COLUMBIA

Nicholas B. Harris¹ and Tian Dong¹

ABSTRACT

Models for controls on porosity and permeability are critical to building robust reservoir models. Relationships between porosity, pore size, total organic carbon and mineralogy can help to identify sites of porosity and possible mechanisms for porosity development. The authors analyze porosity, organic carbon and mineral abundance data from two Horn River shale cores, taken from well files at the British Columbia Ministry of Energy, Mines and Natural Gas, quantitative assessment of pore sizes determined from scanning electron microscope (SEM) images and nitrogen adsorption-desorption and high-pressure mercury injection capillary pressure (MICP) experiments at the University of Alberta.

Porosity is moderately strongly correlated with total organic carbon content in samples from the Evie and Otter Park members of the Horn River Formation, suggesting that porosity dominantly occurs in organic matter, possibly as a function of kerogen cracking, and that porosity can be predicted from models of organic carbon distribution. Data from the Muskwa Formation shows no clear relationship between porosity and organic carbon or any one mineral, indicating a more complicated distribution of porosity.

Estimates of pore size depend on the analytical technique applied. SEM images show pores in the size range of 20 nm to more than 1000 nm; however, MICP data and nitrogen adsorption-desorption experiments indicate that the preponderance of pores are in the size range of 2–10 nm. This demonstrates that most pores are smaller than the resolution of most SEM imaging systems, which accounts for the systematic underestimation of total porosity in SEM images.

Harris, N.B. and Dong, T. (2013): Characterizing porosity in the Horn River shale, northeastern British Columbia; in Geoscience Reports 2013, *British Columbia Ministry of Natural Gas Development*, pages 33–40.

¹Department of Earth and Atmospheric Sciences, University of Alberta, Edmonton, Alberta; nharris@ualberta.ca Ferri, F., Hickin,

Key Words: Horn River Basin, Horn River Formation, Muskwa Formation, Shale, Porosity, Permeability, Pore size, Mineralogy

INTRODUCTION

The size, distribution and interconnectivity of pores in any reservoir are key to understanding permeability, which in turn substantially dictates flow rates in wells. In most sandstone reservoirs, pores typically occupy the intergranular volume, with a smaller porosity fraction in the interior of grains resulting from dissolution. Pore throats decrease in size and specific surface area increases as grain size decreases, giving rise to the familiar relationship between porosity, permeability and grain size described by the Kozeny-Carman equation (Dvorkin, 2009). In carbonate reservoirs, porosity is commonly the product of recrystallization and dissolution of primary components, but still largely depends on particle size (Lucia, 1995).

The characterization of porosity in shale reservoirs is considerably more challenging than in sandstone or carbonate reservoirs. Complexities arise simply because the pores are so small. Multiple lines of evidence, including mercury injection capillary pressure (MICP) data, adsorption-desorption experiments and high-resolution scanning

electron microscope (SEM) analysis, suggest that much of the porosity occurs in pores with diameters of a few nanometres, smaller than can be observed through any optical methods. Pore sizes are smaller than particles in polishing compounds historically used to prepare rock samples; it is now thought that observations of porosity in conventionally polished samples are largely of artifacts induced by the polishing. In a benchmark paper on the Barnett Shale, Loucks et al. (2009) described the application of a wholly different polishing technique taken from the electronics industry, ion milling, to shale samples. Application of this technique, combined with SEM imaging, revealed pore networks not previously imagined. That approach has now expanded to a number of other formations.

A set of key papers now describe basic properties of porosity in shale reservoirs. Pores are most commonly in the range of one to a few hundreds of nanometres (Loucks et al., 2009). Much of the porosity occurs in organic matter, although pores in some formations are also observed between clay particles, in pyrite framboids and in voids

in microfossils (Slatt and O'Brien, 2011; Chalmers et al., 2012; Curtis et al., 2012). Researchers have suggested that porosity in organic matter forms as a consequence of thermal maturation, hydrocarbon generation and expulsion (Bernard et al., 2012), although a recent study of the Kimmeridge Clay Formation (Fishman et al., 2012) suggests that interpretation may not apply to all organic-rich shales.

Shale permeability is not simply a function of the volume and size of pores; it also depends on the degree to which pores are interconnected. Establishing the three-dimensional pore networks of shales presents even more challenges. The size distribution of pore throats can be characterized through high-pressure MICP, but such measurements do not identify the location of pores. Sequential ion milling combined with SEM imaging avenues has produced more detailed information. This involves the erosion of successive thin sheets of material from a cube of shale, imaging the surface between each excavation. Images of pores and minerals are stacked and integrated, creating a three-dimensional volume.

Such studies have contributed greatly to the authors' understanding of porosity and permeability in shale reservoirs; however, shale formations have great stratigraphic variability in terms of organic carbon content, mineralogy and trace-metal composition, and rock mechanical properties. It is likely that shale formations also vary stratigraphically in porosity and permeability, but such variation has not been rigorously demonstrated.

In this paper, the authors present initial results from a multidisciplinary study of the Horn River Formation in northeastern British Columbia now underway at the University of Alberta. The Horn River shale is a successful shale gas play with documented producible reserves in excess of 100 trillion cubic feet (TCF; $2.8 \times 10^{12} \text{ m}^3$) of gas (Reynolds and Munn, 2010). Operating companies in the play have acquired a large number of cores, many of which now have released datasets. This research applies sedimentology, stratigraphy, geochemistry and petrophysics to develop an integrated model for controls on reservoir quality. This paper summarizes porosity relationships in two Horn River wells, the Nexen Komie D-94-A/94-O-8 and the EOG Maxhamish D-012-L/094-O-15. First, the authors investigate data relating total porosity to gas-filled porosity, total porosity to total organic carbon (TOC) content, and the possible function of mineralogy. Second, porosity in samples is characterized, involving measurements of total porosity and pore dimensions measured by MICP, adsorption-desorption experiments and SEM image analysis on ion-milled samples. The latter work is described in more detail in Dong and Harris (in press).

GEOLOGICAL BACKGROUND

The Horn River Basin in northeastern British Columbia represents a prominent deepwater embayment on the west-facing margin of North America in the Middle and Late Devonian (Fig. 1). The basin was flanked by carbonate platforms of the Hay River bank to the northeast, east and south, and by the Bovie fault to the west, on which there is substantial down-to-the-west displacement (Ross and Bustin, 2008; Ferri et al., 2011).

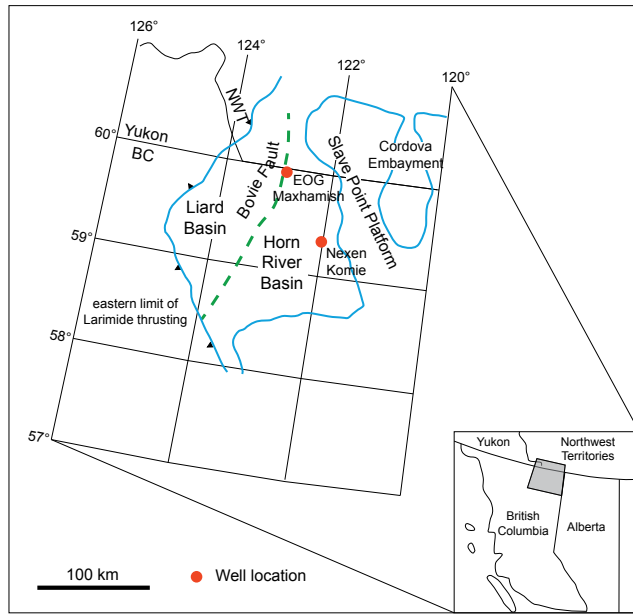


Figure 1. Map of the Horn River Basin, showing the location of wells described in this report (from Dong and Harris, in press; modified after Ross and Bustin, 2008).

Devonian shale stratigraphy in the Horn River Basin consists of the Givetian to lowermost Frasnian (Middle to the base of the Upper Devonian) Evie and Otter Park members of the Horn River Formation (Fig. 2), overlain by the lower Frasnian Muskwa Formation and the Frasnian to Famennian Fort Simpson Formation and Red Knife–Kakisa formations (McPhail et al., 2008; Ferri et al., 2011). This entire sequence rests on Lower Keg River carbonate rocks. Potma et al. (2012) interpret the entire package—from Lower Keg River to Red Knife–Kakisa—to represent two second-order sea level cycles with maximum flooding surfaces in the Evie member and Muskwa Formation.

Of this sequence, the Evie, Otter Park and Muskwa are known to be organic rich; McPhail et al. (2008) report total organic carbon (TOC) contents of 0.3–9.57% in the Evie, 1.6–7.97% in the Otter Park and 0.15–4.99% in the Muskwa. Thermal maturities are considered to be high, between 2.2 and 2.8% Ro according to Reynolds et al. (2010). TOC contents in the overlying Fort Simpson are much lower, averaging 0.25% in data published by Ross and Bustin (2008).

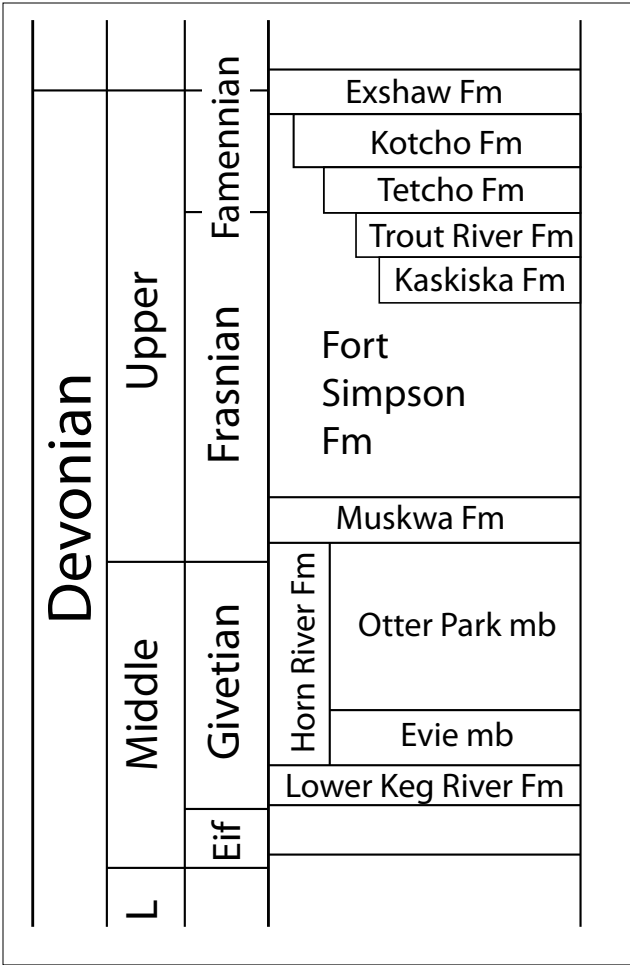


Figure 2. Middle and Upper Devonian stratigraphy of the Horn River Basin (modified after McPhail et al. 2008 and Ferri et al., 2011).

DATA AND SAMPLES

Samples and data from two wells are analyzed: the Nexen Komie D-94-A/94-O-8 well is located near the margin of the eastern Horn River Basin and the EOG Maxhamish D-012-L/094-O-15 is located in the northern part of the basin, somewhat farther from the carbonate platform edge. Porosity and data are taken from files at the British Columbia Ministry of Energy, Mines and Natural Gas. Analysis of the Maxhamish core was carried out by TerraTek and analysis of the Komie core was carried out by CBM Solutions. Work at the University of Alberta included quantitative analysis of SEM images using Image-Pro Plus software to outline and measure all the individual pores and fractures in the area of interest, nitrogen adsorption-desorption experiments (also called BET analysis) on an Autosorb-1 instrument produced by Quantachrome and high-pressure MICP measurements using an Autopore IV 9500 by Micromeritics Instrument Corp., using a maximum pressure of 413.3 MPa (59 944 psi). Additional details on image analysis and the adsorption-desorption experiments are found in Dong and Harris (in press).

RESULTS

Shale composition

The Horn River shales show a range of compositions in the Maxhamish and Komie wells. The major mineral components are quartz, clay and carbonate, with subsidiary pyrite and feldspar. When plotted on a ternary diagram representing quartz, total carbonate and total clay (Fig. 3), compositions in most samples are dominated by quartz with subsidiary clay. Evie samples and a small fraction of the Otter Park samples contain significant carbonate. Muskwa samples generally contain very little carbonate. The range of Muskwa compositions in the Maxhamish and Komie wells are very similar.

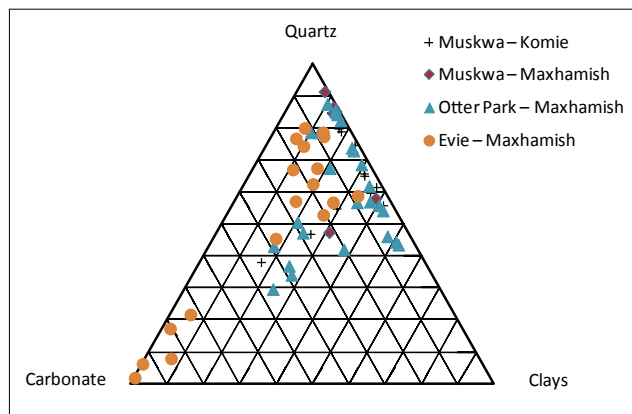


Figure 3. Composition of Horn River shale units in the EOG Maxhamish and Nexen Komie wells, based on data from well files; see text for details.

Organic carbon content

The Muskwa, Otter Park and Evie all contain elevated organic carbon content, summarized in Table 1. Data obtained by TerraTek from the Maxhamish well indicate that the Muskwa is somewhat enriched relative to the other two units, with an average of 4.8% TOC compared to a 3.3% average TOC in the Otter Park and a 3.8% average TOC in the Evie.

The average TOC content of the Muskwa Formation is significantly lower in the Komie well than in the Maxhamish well. The reason for this is not clear. TOC content was obtained through a combustion technique for the Komie well (Leco or equivalent). Well files do not indicate the method used by TerraTek for the Maxhamish core. Different methods (for example, TOC from Leco versus TOC from Rock Eval) yield somewhat different results; nonetheless, these data represent an almost 100% difference, probably more than can be accounted for by a difference in analytical method.

TABLE 1. SUMMARY OF TOTAL ORGANIC CARBON CONTENT (TOC) IN THE MAXHAMISH AND KOMIE WELLS.

	Muskwa–Maxhamish	Muskwa–Komie	Otter Park–Maxhamish	Evie–Maxhamish
Average TOC	4.80%	2.50%	3.30%	3.80%
Maximum TOC	6.40%	3.60%	7.00%	6.50%
Minimum TOC	3.66%	1.40%	1.16%	0.38%

Porosity

ASSOCIATIONS WITH MINERALS AND ORGANIC CARBON

Porosity data measured by TerraTek from the Muskwa, Otter Park and Evie in the Maxhamish well show similar ranges, each unit averaging between 5.1% and 5.6% porosity (Fig. 4). The range of porosities is somewhat smaller for the Muskwa dataset than for the Otter Park and Evie, but few Muskwa samples were analyzed, which may account for the difference in the range of values. Porosities measured in the Komie well by CBM Solutions are considerably higher; they report an average total porosity of 10.9% in 14 Muskwa samples (range from 6.7 to 14.4%). The range of values reported for effective porosities by CBM Solutions (total porosity \times (1-Sw)) is in fact similar to the total porosity reported by TerraTek for the same formation.

The underlying reason for the difference between the two datasets in measured porosity is not immediately apparent. It is generally recognized that different labs produce measurements for important reservoir properties such as porosity and permeability, and the two datasets may simply reflect that. Alternatively, real differences in porosity between the two wells are perhaps due to differences in rock compositions.

Possible controls on porosity can be assessed by comparing porosity to compositional parameters. Porosity has been associated in particular with organic matter in other shale formations, for example, the Barnett Shale (Loucks et al., 2009); if porosity is present in organic matter and results from the cracking of kerogen to hydrocarbons, then a correlation might exist between porosity and TOC content. In the Maxhamish dataset, relatively strong associations exist between TOC and porosity for the Evie and Otter Park members (Fig. 4; correlation coefficients of +0.61 and +0.71, respectively). No such relationship exists between TOC and porosity for the Muskwa Formation (correlation of -0.33).

If, on the other hand, porosity is largely associated with specific minerals such as clays or pyrite, this could be recognized through high positive correlation coefficients between porosity and these minerals. No such correlations exist between porosity and any reasonable mineral phase in the Maxhamish dataset for any stratigraphic unit, although it is appropriate to note the difficulty of obtaining accurate

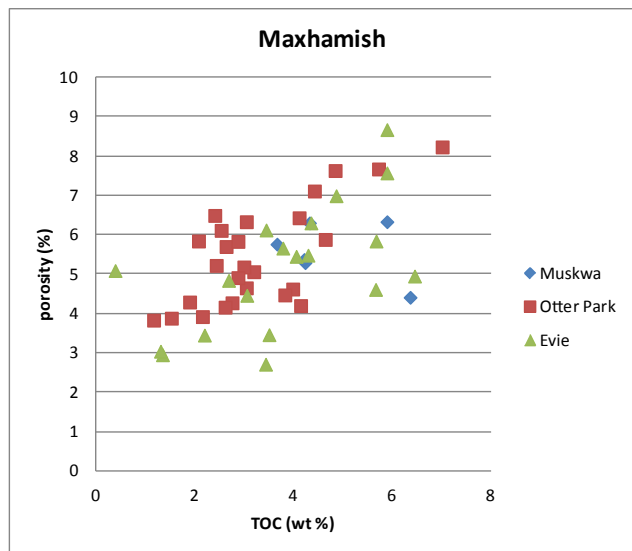


Figure 4. Total porosity versus total organic carbon (TOC) in samples from the EOG Maxhamish well, based on data from well files.

quantitative mineralogical compositions from X-ray diffraction analysis.

Based on these relationships in the Maxhamish data, it can be concluded that porosity is primarily associated with organic matter in the Evie and Otter Park members. The mode of porosity development in the Muskwa is apparently very different than in the deeper shale reservoir units. The lack of any strong associations in this unit suggests that porosity is dispersed among a number of hosts.

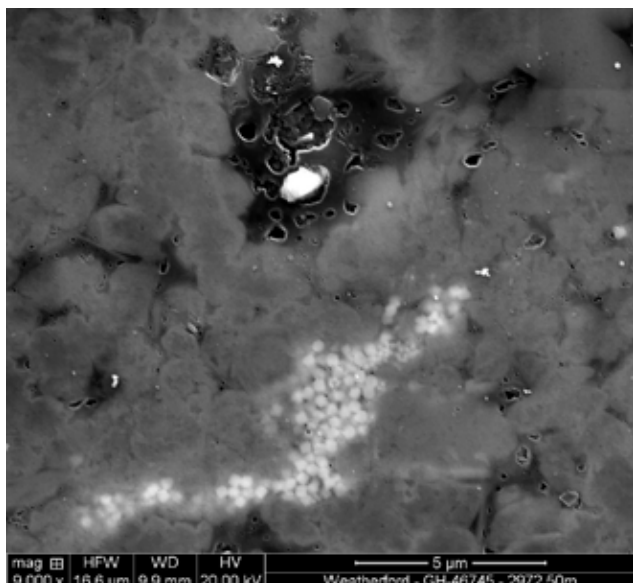
The dataset from the Komie well includes only Muskwa samples, and mineralogical analysis was carried out on a sample adjacent to the porosity-TOC sample, not the same sample, which introduces a potential source of error in attempting to identify relationships between porosity and rock composition. In this dataset, no strong correlation exists between either total or effective porosity and TOC, or between porosity and any specific mineral, which is essentially the same finding as for the Maxhamish well.

PORE CHARACTERISTICS AND DIMENSIONS

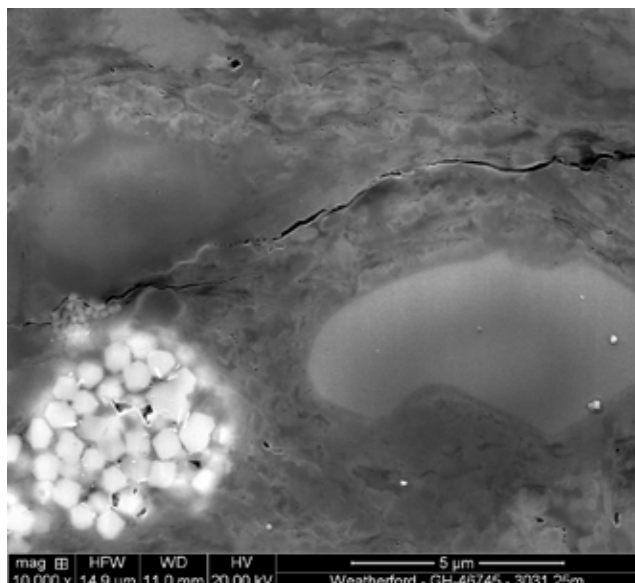
Pore dimensions and the location of pore spaces are important because of their influence on water saturation, gas storage capacity, permeability and adsorption effects. As noted above, however, characterizing shale porosity is remarkably challenging because of the small pore sizes, thus requiring analytical techniques not needed for coarser-grained reservoirs.

Scanning electron microscope (SEM) images can be used to characterize pore shapes and sizes. Under some circumstances it is possible to image 20 nm pores, but in many cases the resolution of SEM images is coarser. Figure 5 illustrates different modes of porosity occurrence: in organic matter (Fig. 5a), in the interstices between pyrite crystals in framboids (Fig. 5b), between clay flakes (Fig. 5c) and in dolomite crystals (Fig. 5d). Pores are resolved down to

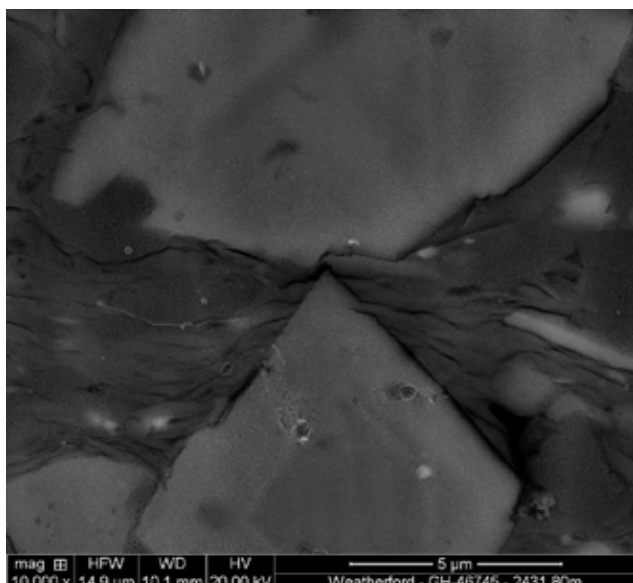
approximately 20 nm in these images. Pores vary in shape depending on the mode of occurrence, notably flattened in pores between clay flakes and rounded in the other settings. Three-dimensional aspect ratios cannot be determined from these photos, but it is reasonable to expect that pore networks associated with framboids are isolated and roughly spherical because of the shape of the framboids.



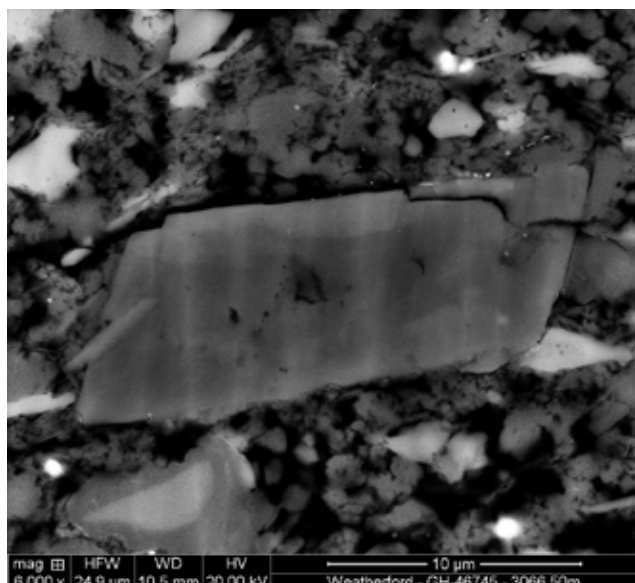
5a



5b



5c



5d

Figure 5. The SEM images of Horn River shale samples from the Nexen Komie and EOG Maxhamish wells, illustrating various modes of porosity occurrence. Images from reports by Weatherford in well files at the British Columbia Ministry of Energy, Mines and Natural Gas: a) Pores developed in organic matter (dark pore filling material in the upper part of the photo), Otter Park member, EOG Maxhamish well, 2972.49 m; b) Porosity developed in pyrite framboid (white minerals in the lower-left part of the photo), Otter Park member, EOG Maxhamish well, 3031.23 m; c) Porosity between clay flakes (especially in the middle-right part of the photo), Muskwa Formation, Nexen Komie well, 2431.83 m; d) Porosity in dolomite crystal (the middle of the photo), Evie member, EOG Maxhamish well, 3066.51 m.

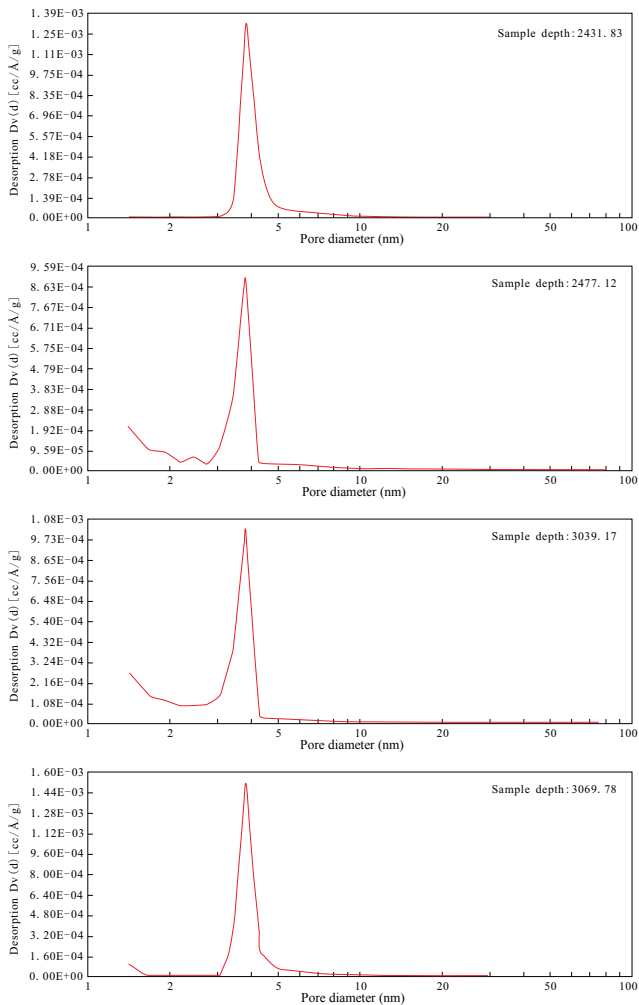


Figure 6. Representative pore-size distributions from nitrogen adsorption-desorption experiments. Height of curve is a measure of relative frequency of pore diameters. Modified after Dong and Harris (in press). Methods are described in detail in Dong and Harris (in press): a) Muskwa Formation, Nexen Komie well, 2431.83 m; b) Muskwa Formation, Nexen Komie well, 2477.12 m; c) Otter Park member, EOG Maxhamish well, 3039.17 m; d) Evie member, EOG Maxhamish well, 3069.78 m.

Porosity and pore size can be estimated by quantitative analysis of the images. These data show a range of pore diameters from 20 nm to more than 1000 nm, with modes ranging from 20 to 40 nm (Dong and Harris, in press). Image analysis also consistently underestimates He-porosity measurements reported by TerraTek and CBM solutions. This discrepancy is most likely the result of pores occurring in sizes below the resolution of the SEM.

Both nitrogen adsorption-desorption and high-pressure MICP experiments indicate substantial populations of much smaller pores. Adsorption-desorption experiments reveal a substantial population of pores with a dominant size range between 3 and 5 nm (Fig. 6). The shapes of the hysteresis loops (a comparison between the adsorption and desorption curves) suggests the pores are largely slit-shaped (Dong and Harris, in press).

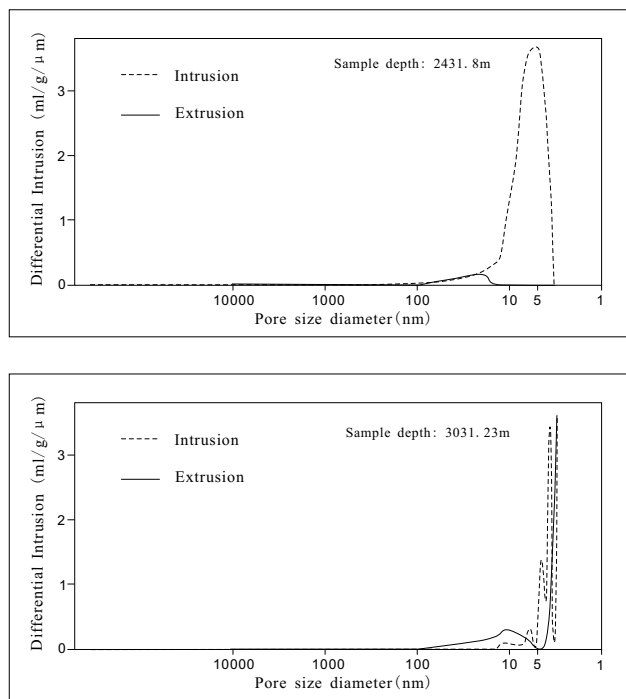


Figure 7. Pore throat sizes calculated from high-pressure MICP experiments: a) Muskwa Formation, Nexen Komie well, 2431.83 m. b) Otter Park member, EOG Maxhamish well, 3031.23 m.

The MICP data from two samples (one Muskwa and one Otter Park) provide similar information, indicating dominant pore throat sizes of 6 and 4 nm, respectively (Fig. 7). It should be noted that MICP and adsorption-desorption experiments provide somewhat different information: the former represents the size of pore throats, whereas the latter indicates the size of pore diameters. It is possible for large diameter pores to be connected by small pore throats, but the combined information from adsorption-desorption and MICP experiments indicates that in this case, pore diameters and pore throats are of similar size.

DISCUSSION

In this report, the authors have mined data contained in released reports from Horn River well files at the British Columbia Ministry of Energy, Mines and Natural Gas and combined that with the authors' analytical work on porosity systems in the Horn River shale reservoirs. The results highlight both the complexity of pore systems in these shales and the challenges of analyzing these rocks.

Pores in shale reservoirs are known to have different size characteristics, modes of occurrence, and—presumably—different controls. Good models for predicting reservoir behaviour depend on understanding these relationships. Research on the Horn River shale reveals complexities in the size, distribution and interconnectivity of pores.

Two lines of evidence suggest that a considerable fraction of porosity occurs as small pores: 1) He-porosity data is consistently higher than porosity measured by analysis of SEM images from the same sample and 2) SEM images show larger pores than are indicated by adsorption-desorption and MICP experiments. These datasets together indicate that the SEM images fail to record a significant fraction of total porosity. Similar observations have been recorded by Curtis et al. (2012) for a number of other shale reservoirs.

If SEM images are used as the primary source of information for porosity characterization, controls on some reservoir properties may be misinterpreted. Large pores undoubtedly contribute more to permeability than small pores (Dewhurst et al., 1999), so a misunderstanding of pore sizes may not affect interpretations of controls on permeability. Gas storage volume, however, does depend on total porosity, so misunderstanding where the significant volume of porosity occurs can affect models for gas storage. Moreover, gas desorption effects are surface-area dependent, which in turn depend on pore size. This affects models for gas flow during the production life of the reservoir.

The authors' Horn River database, although currently small, points to significant stratigraphic differences in reservoir properties. Data taken from TerraTek reports suggest that total porosity in the Evie and Otter Park members is associated with organic matter, based on moderately strong correlations between TOC and porosity. That relationship is not present in the Muskwa data, suggesting that there is a different mode of porosity occurrence in that unit. This topic will be a major focus in the authors' research group during the next three years.

Porosity differences in the same stratigraphic unit are also evident in a comparison between wells at different distances from the basin edge. Measured total porosity from He-pycnometry in a set of Muskwa measurements averaged 10.9% in a well near the basin margin (Nexen Komie), total porosity measurements in a set of Muskwa data averaged 5.6% in a well farther from the margin (Maxhamish) whereas average Muskwa TOC content was higher in the Maxhamish well than in the Komie well (5.8% versus 2.5%). Geographic position within a shale basin can lead to different rock compositions, either because of decreasing coarse sediment composition toward the basin margin or because of variable biogenic contributions. Interpretations here are complicated by possible interlaboratory variation in analytical results, which is suspected to be particularly problematic in porosity data.

CONCLUSIONS

Data taken from publically available well files have been combined with the experimental results to shed light on porosity controls in the Horn River shale reservoir. Three findings are highlighted:

- Significant differences in the modes of porosity occurrence are evident in the different reservoir units. Total porosity correlates moderately well with TOC in the Evie and Otter Park samples, suggesting that porosity is largely associated with organic carbon in these units. No correlation exists between total porosity and either TOC or any mineral in Muskwa data. This suggests that porosity in that unit is distributed among several phases.
- Geographic differences exist in TOC and porosity in Muskwa data, although these differences in porosity may be an artifact of different laboratories and analytical procedures. Nonetheless, differences are likely between wells in different parts of the basin due to varying contributions from sediments shed from platforms and to varying biogenic production of organic matter and silica.
- Scanning electron microscope images, while visually appealing, may fail to capture a large fraction of porosity occurring as pores less than 10 nm in diameter. The large pores readily apparent in SEM images are probably the major contributor to reservoir permeability, but small pores contribute significantly to the total gas storage of the reservoir. It is suspected that the small pores also need to be taken into account for gas desorption effects during production, given their high surface area, but such relationships have yet to be documented.

ACKNOWLEDGMENTS

The authors thank the British Columbia Ministry of Natural Gas Development for providing access to Horn River well files and for initial funding of the Horn River research study. Warren Walsh and Fil Ferri of the British Columbia Ministry of Natural Gas Development were particularly instrumental in facilitating these studies.

The authors also thank Drs. Nancy Zhang and Eric Flaim of the Integrated Nanosystems Research Facility at the University of Alberta for training and guidance in the use of the Autosorb-1 instrument and Randy Kofman for carrying out high-pressure MICP measurements in the lab of Dr. Doug Schmitt at the University of Alberta.

REFERENCES

- Bernard, S., Horsfield, B., Schulz, H.-M., Wirth, R., Schreiber, A. and Sherwood, N. (2012): Geochemical evolution of organic-rich shales with increasing maturity: A STXM and TEM study of the Posidonia Shale (Lower Toarcian, northern Germany); *Marine and Petroleum Geology*, Volume 31, pages 70–89.
- Chalmers, G.D., Bustin, R.M. and Power, I.M. (2012): Characterization of gas shale pore systems by porosimetry, pycnometry, surface area, and field emission scanning electron microscopy/transmission electron microscopy image analyses: examples from the Barnett, Woodford, Haynesville, Marcellus, and Doig units; *AAPG Bulletin*, Volume 96, pages 1099–1119.
- Curtis, M.E., Sondergeld, C.H., Ambrose, R.J. and Rai, C.S. (2012): Microstructural investigation of gas shales in two and three dimensions using nanometer-scale resolution imaging; *AAPG Bulletin*, Volume 96, pages 665–677.
- Dewhurst, D.N., Yang, Y. and Aplin, A.C. (1999): Permeability and fluid flow in natural mudstones, in *Muds and Mudstones: Physical and Fluid Flow Properties*, Aplin, A.C., Fleet, A.J. and Macquaker, J.H.S., Editors, *Geological Society of London, Special Publication* 158, pages 23–43.
- Dong, T. and Harris, N.B. (in press): Size distribution and morphology of pores in the Horn River Shale, Middle and Upper Devonian, northeastern British Columbia; in *Electron Microscopy of Hydrocarbon Shale Reservoirs*, Camp, W., Diaz, E. and Wawak, B., Editors, AAPG, Memoir 102.
- Dvorkin, J. (2009): The Kozeny-Carman equation revisited; unpublished paper, URL <http://pangea.stanford.edu/~jack/KC_2009_JD.pdf> [February 2013].
- Ferri, F., Hickin, A.S. and Huntley, D.H. (2011): Besa River Formation, western Liard Basin, British Columbia (NTS 094N): geochemistry and regional correlations; in *Geoscience Reports 2011, British Columbia Ministry of Energy, Mines and Natural Gas*, pages 1–18.
- Fishman, N.S., Lowers, H.A., Hackley, P.C., Hill, R.J. and Egenhoff, S.O. (2012): Porosity in shales of the organic-rich Kimmeridge Clay Formation (Upper Jurassic), offshore United Kingdom; *Search and Discovery Article #50620*, 56 pages.
- Loucks, R.G., Reed, R.M., Ruppel, S.C. and Jarvie, D.M. (2009): Morphology, genesis, and distribution of nanometer-scale pores in siliceous mudstones of the Mississippian Barnett Shale; *Journal of Sedimentary Research*, Volume 79, pages 848–861.
- Lucia, F.J. (1995): Rock fabric/petrophysical classification of carbonate pore space for reservoir characterization; *AAPG Bulletin*, Volume 79, pages 1275–1300.
- McPhail, S., Walsh, W., Lee, C. and Monahan, P.A. (2008): Shale units of the Horn River Formation, Horn River Basin and Cordova Embayment, northeastern British Columbia; *British Columbia Ministry of Energy, Mines and Natural Gas, Petroleum Geology Open File Report No. 2008-1*, 14 pages.
- Potma, K., Jonk, R., Davie, M. and Austin, N. (2012): A mudstone lithofacies classification of the Horn River Group: integrated stratigraphic analysis and inversion from wireline log and seismic data; Presented at the 6th BC Unconventional Gas Technical Forum, *British Columbia Ministry of Energy, Mines and Natural Gas*, URL <<http://www.empr.gov.bc.ca/OG/oilandgas/petroleumgeology/UnconventionalGas/Documents/K%20Potma.pdf>>.
- Reynolds, M.M. and Munn, D.L. (2010): Development update for an emerging shale gas giant field—Horn River Basin, British Columbia, Canada; SPE Unconventional Gas Conference, *Society of Petroleum Engineers*, paper no. 130103-MS, 17 pages.
- Ross, D.J.K. and Bustin, R.M. (2008): Characterizing the shale gas resource potential of Devonian-Mississippian strata in the Western Canada sedimentary basin: application of an integrated formation evaluation; *AAPG Bulletin*, Volume 92, pages 87–125.
- Slatt, R.M. and O'Brien, N.R. (2011): Pore types in the Barnett and Woodford gas shales: contribution to understanding gas storage and migration pathways in fine-grained rocks; *Search and Discovery Article #80166*, 18 pages.

CONVENTIONAL OIL POOLS OF BRITISH COLUMBIA

Ed Janicki¹

Janicki, E. (2013): Conventional oil pools of British Columbia; in Geoscience Reports 2013, *British Columbia Ministry of Natural Gas Development*, pages 41–44.

¹Geoscience and Strategic Initiatives, British Columbia Ministry of Natural Gas Development, Victoria, British Columbia; Ed.Janicki@gov.bc.ca

Key Words: Field, pool, pay, porosity, permeability, pressure, drive, trap, recoverable, log

INTRODUCTION

Oil exploration in the Peace River region of northeastern British Columbia began in the 1920s in conjunction with widespread settlement resulting from agricultural development. Exploration resumed (Janicki, 2008) in earnest in the late 1940s after the building of the Alaska Highway and the discovery of oil at Leduc in Alberta, which demonstrated the potential of the Western Sedimentary Basin. Production at Leduc began in 1955 with an oil well in the Boundary Lake Field along the Alberta border near Fort St. John. Throughout the 1960s, 1970s and into the early 1980s, oil companies also found and developed many oil fields¹ in northeastern British Columbia. Many of the early fields initially produced thousands of barrels per day and continue to produce most of British Columbia's oil. In recent decades, though, new discoveries of large conventional oil pools have been few and far between. Most of the more recently developed oil pools² consist of only one or two wells with considerably less than one million barrels of recoverable oil. Levels of oil production in the province peaked at around the year 2000 and have been in decline ever since, despite the relative stability and general upward trend of oil prices. Conventional oil exploration in northeastern British Columbia now presents expensive technical challenges because undiscovered accumulations are small and subtle.

At current oil prices, the economics for oil exploration in northeastern British Columbia are marginal; however, new technologies such as horizontal drilling, 3D seismic, reservoir modelling, multistage fracking and improved recovery techniques provide the possibility for greater oil production from existing conventional oil fields. Horizontal drilling has already been successful in extending the life

of many existing conventional pools in British Columbia or making marginal pools economic. Some near-depleted pools could be ideal candidates for enhanced recovery using CO₂ (Janicki, 2010) or for carbon capture and storage. As these new technologies become more established and refined, the cost for their application has decreased, which in turn may enable companies to reconsider the economics of conventional oil in northeastern British Columbia.

Conventional oil production from existing oil fields has a number of attractive advantages when compared with unconventional oil:

- Risk is relatively low because the geology can be well understood using publically available information or seismic information that can be purchased cheaply.
- Small companies can make a good economic return with relatively small investments because the capital outlays are generally far less than for unconventional oil.
- The regulatory environment is well established and straightforward.
- Farm-ins can be arranged with current mineral rights holders.
- Prospective lands around the edges of existing fields might be unleased and therefore available.
- Enhanced recovery from existing fields causes a relatively light environmental footprint because much of the necessary surface infrastructure is already in place; therefore, extensive—and often controversial—fracking is not usually necessary.
- British Columbia produces generally high gravity conventional crudes.
- Oil—particularly light oil—is likely to be valuable for decades to come because no other energy sources can match it for portability and uses beyond transportation.

¹Field: "The surface area underlaid or appearing to be underlaid by one or more pools, and the subsurface regions vertically beneath that surface area" (Government of British Columbia, 1996).

²Pool: "Underground reservoir containing an accumulation of petroleum or natural gas, or both, separated or apparently separated from another reservoir or accumulation" (Government of British Columbia, 1996).

PUBLICATION

Little new information has been published about British Columbia's conventional oil fields since production began to decline in the late 1990s. Until 1997, the British Columbia Ministry of Energy and Mines (now the Ministry of Energy, Mines and Natural Gas) regularly published updated sets of oil and gas pool maps. Although the British Columbia Oil and Gas Commission maintains a current set of pool maps and data, their maps are not available to the public in a readily accessible, consolidated format. This paper summarizes the key points of an upcoming open file publication (currently under review) that will take the Oil and Gas Commission's oil pool database and reproduce it in a format that details the main points of major oil pools and provides pertinent comments on geological characteristics.

This paper presents one example from the many pools to be profiled in an upcoming open file report. To some extent, the information provided will be patterned after Sikabonyi (1964), who put together a "reference volume helpful during their (oil companies) daily work". Although Sikabonyi stated that the purpose "was not to outline and interpret, but to collect and to compile the existing information", the open file will include some interpretational content to direct users' attention to important aspects of each pool that might not be obvious at first glance. Each pool to be profiled in the open file has been selected because it either has more than one well or some other significance. The format will allow for the addition of more pools in revisions.

OPEN FILE CONTENT

The most recent set of oil and gas pool information (from 1997) included just maps, whereas the new open file will provide additional information and updated maps. Each pool profiled will provide a map (Fig. 1), representative wireline logs (Fig. 2) and a page (Table 1) outlining reservoir parameters for the pool. The page of parameters will be divided into three categories:

- 'field parameters' will include the field code and pool code numbers assigned to each pool by the Oil and Gas Commission for ease of reference,
- 'reservoir data' will provide engineering characteristics of the pool such as porosity and oil formation volume factor, and
- 'reserves' will outline the amounts of oil produced and amounts remaining.

Notes at the bottom of the page will summarize some features of interest for a pool.

The reservoir parameters on the data sheet are those considered by the author to be the most fundamental for defining a pool's potential production performance and for

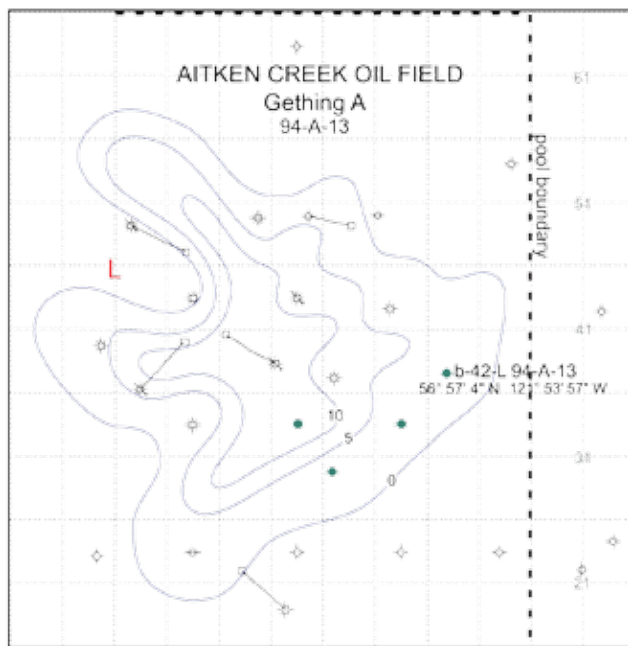


Figure 1: Example of a map provided for each pool profiled in the upcoming open file release. Contour interval is 5 m net Gething A oil pay, and the discovery well is b-42-L-94-A-13. The entire updip portion of the pool (northwest) is undrained by oil wells and gas is being injected into the updip side of the pool (contours are from the British Columbia Oil and Gas Commission).

estimating reserves. The final reservoir parameters listed in the open file may be slightly different depending on feedback received from workers who may use this publication. The author welcomes input from readers on what information should be considered for updates.

Metric versus Imperial

Many of the wells that will be profiled in the new open file were drilled prior to the widespread adoption of the metric system by the oil industry in 1978 (federal metric legislation did not come into full effect until 1980); therefore, some wells are outlined with a combination of metric and imperial units. For ease of cross-reference with original logs and well files, depths are given in feet for wells drilled prior to 1978. Pressures are given in the more familiar units of pounds per square inch (psi) and the metric equivalent of kilopascals (kPa).

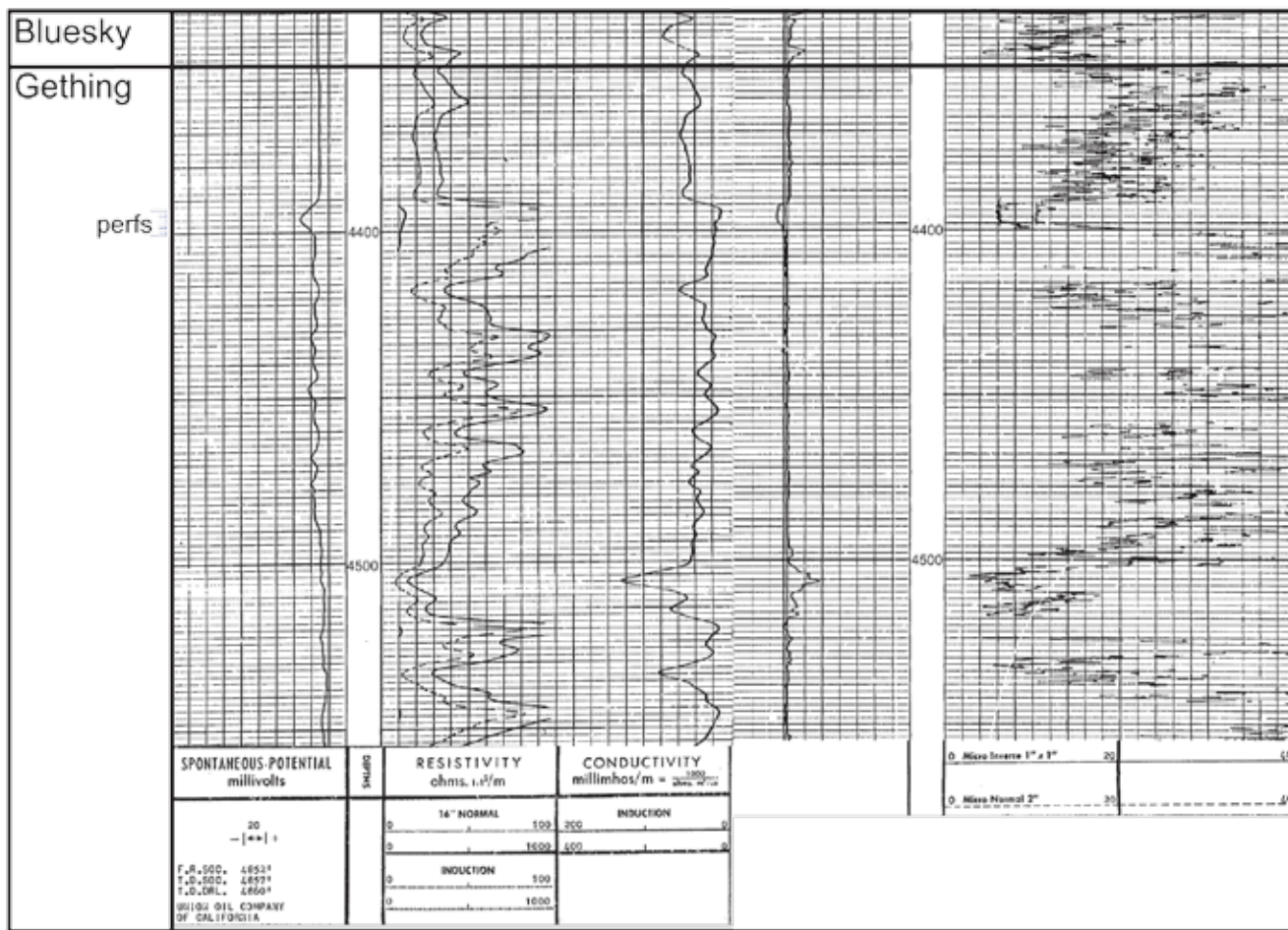


Figure 2: Example of representative wireline logs provided for each pool profiled in the upcoming open file release: elog and microlog for discovery well b-42-L-94-A-13. The microlog indicates good permeability across the perfed interval (4392'-4400').

FUTURE PUBLICATIONS

A digital format for the open file will allow for the addition of pools or the correction of inaccuracies as they are identified. Future work on oil fields and pools will build upon the foundational information in the open file. Focus will turn to the fields and pools showing the greatest promise for gains in production after the application of new technologies. Subsequent publications on oil fields and pools will contain much greater levels of detail and interpretation, similar to what can be found in field and pool studies such as those done by Rose (1990), Hogg (1998) and Janicki (2003).

TABLE 1: EXAMPLE OF THE PAGE OUTLINING RESERVOIR PARAMETERS FOR EACH POOL PROFILED IN THE UPCOMING OPEN FILE RELEASE. AITKEN CREEK OIL FIELD, GETHING A: FIELD PARAMETERS, RESERVOIR DATA AND RESERVES.

AITKEN CREEK OIL FIELD Gething A	
Field Parameters	
Field code: 0200	Pool Code: 2700A <i>These numbers are assigned by OGC to the pool</i>
Discovery well: 200/b-042-L 094-A-13/00	WA#: 00485 Rig Release: 1962/12/10
Other oil and gas shows: Gething gas	<i>This line shows other overlapping productive formations</i>
Number of producing wells (November 2012)	Oil: 4 Gas: 10 Injection: 4
Reservoir Data	
Average depth of producing zone: 4348 ft., 1325 m	<i>Depth is given in feet for older wells</i>
Lithology of reservoir rock: sandstone	
Trap type: stratigraphic	
Estimated maximum reservoir thickness: 12 m	
Area of pool: approximately 1630 acres or 660 hectares within contour limits	
Drive mechanism: gas depletion	
Average porosity (%): 12	
Average net pay: 5 m	
Average permeability: 74 millidarcies	
Average water saturation (%): 27	
Oil formation volume factor (%): 131	
Gravity (degrees API): 42	
Original pressure: 1561 psi, 10 763 kpa	
Reserves	
Estimated Original Oil in Place: 14 055 160 barrels	
Recovery Factor (%): 65 (gas injection)	
Estimated Recoverable Oil: 9 135 850 barrels	
Cumulative Oil Production: 8 547 580 barrels	
Remaining Recoverable Oil: 588 270 barrels	
Remaining Original Oil in Place (%): 39	
Cumulative Water Production: 91 090 barrels	
Notes: Recovery is very high due to gas injection. This pool is part of the Aitken Creek gas storage project and a number of the wells are gas injection.	<i>This section provides data that could be used to estimate reserves. Figures are provided by the Oil and Gas Commission.</i>
<i>Notes are observations made by the author perhaps not immediately apparent to the reader.</i>	

REFERENCES

- British Columbia Ministry of Energy, Mines and Natural Gas (1997): Geological reference book (net pay maps); *British Columbia Ministry of Energy, Mines and Natural Gas*, Stock #116C (out of print).
- Evoy, R.W. (1998): Reservoir geometry of the Doig Formation, Buick Creek Field, northeastern British Columbia; in Oil and gas pools of the western Canada sedimentary basin, Hogg, J.R., Editor, *Canadian Society of Petroleum Geologists*, Special Publication S-51, pages 127–135.
- Government of British Columbia (1996): Petroleum and natural gas act; *Government of British Columbia*, RSBC 1996, Chapter 361, Part 1—Definitions.
- Hogg, J.R., Editor (1998): Oil and gas pools of the western Canada sedimentary basin; *Canadian Society of Petroleum Geologists*, Special Publication S-51, 161 pages.
- Janicki, E.P. (2003): Hydrocarbon pools of the southwestern Great Slave Plain, Northwest Territories; *Northwest Territories Geoscience Office*, Open File 2003-05.
- Janicki, E.P. (2008): Petroleum exploration in northeastern British Columbia; in *Geoscience Reports 2008, British Columbia Ministry of Energy, Mines and Natural Gas*, pages 41–59.
- Janicki, E.P. (2010): Triassic porosity trends in northeastern British Columbia—update February 2009; in *Geoscience Reports 2010, British Columbia Ministry of Energy, Mines and Natural Gas*, pages 93–97.
- Labute, J.G., Evoy, W.R. and Clegg, M. (1998): The Middle Triassic Halfway “C” pool, northeastern British Columbia; in Oil and gas pools of the western Canada sedimentary basin, Hogg, J.R., Editor, *Canadian Society of Petroleum Geologists*, Special Publication S-51, pages 111–125.
- Rose, M.L., Editor (1990): The Canadian Society of Petroleum Geologists oil and gas pools of Canada series; *Canadian Society of Petroleum Geologists*, Volume 1, unpaginated binder.
- Sikabonyi, L.A. (1964): Oil and gas fields of northeastern British Columbia, a reference volume, 1st edition; *West Canadian Graphic Industries Ltd.*, unpaginated binder.

HELIUM IN NORTHEASTERN BRITISH COLUMBIA

Elizabeth G. Johnson¹

ABSTRACT

Global demand for helium is increasing at a time when world reserves are in decline. The price of grade A helium has quadrupled in the past 12 years. Liquefied natural gas (LNG) processing can be used to capture helium as a value-added byproduct at concentrations as low as 0.04% by volume. The Slave Point, Jean Marie (Redknife) and Wabamun formations of northeastern British Columbia preferentially have helium associated with many of their natural gas pools. The mechanism for this accumulation appears to be flow in hydrothermal brines from helium-enriched basement granitic rocks along deeply seated faults. Separately, the Evie member of the Horn River Formation also has anomalous helium accumulation in its shale gas related to uranium decay in organic-rich shales.

Johnson, E.G. (2012): Helium in northeastern British Columbia; in Geoscience Reports 2013, *British Columbia Ministry of Natural Gas Development*, pages 45–52.

¹Geoscience and Strategic Initiatives Branch, British Columbia Ministry of Natural Gas Development, Victoria, British Columbia; Elizabeth.Johnson@gov.bc.ca

Key Words: Helium, LNG, Jean Marie, Slave Point, Wabamun, Evie, Horn River Formation

INTRODUCTION

Helium is a nonrenewable resource that has developed important strategic value. Helium (atomic number of 2) exists primarily as the stable isotope, ⁴He, which is produced on the earth through alpha decay of radioactive elements such as uranium and thorium. It is a common constituent of natural gases and is believed to be present in trace amounts in all natural gases (Broadhead, 2005). Once formed, helium moves easily through the earth's crust, escapes into the atmosphere and leaves the earth's gravitational field. In larger deposits in the United States, helium is found in well-sealed natural traps within porous strata after having migrated from uranium-bearing granitic source rocks (Groat et al., 2010).

Helium is extremely light, stable and inert. Because of its low molecular mass, it has a thermal conductivity, a specific heat and a sound conduction velocity that are all greater than any other element except hydrogen. Liquid helium has the lowest boiling point of any substance. Because of this, it is used in cryogenics and to provide the low temperatures needed for superconducting magnets, such as those used in most MRI scanners in hospitals, which accounts for 28% of the global demand. It is also used to condense hydrogen and oxygen to make rocket fuel. Helium is commonly used as a shielding gas for welding, which accounts for 11% of global use. Because helium has very small atoms, it is more diffusive than air so it can be mixed with oxygen to make breathing mixtures for divers (2% of the United States consumption in 2011). Helium also has a refractive index very close to 1 so it is commonly used in

optical fibre technology (8% of global use; Peterson and Madrid, 2012; Anonymous, 2012).

In recognition of its strategic value, the United States created the Federal Helium Reserve in the Bush Dome Reservoir, Texas, in 1925. The primary source for the Federal Helium Reserve is the world-class Hugoton Reservoir in Kansas, Oklahoma and Texas. Other helium resources in the United States are contained in the Panoma Field (Kansas), the Keyes Field (Oklahoma), Panhandle West and Cliffside fields (Texas) and the Riley Ridge area (Wyoming; Peterson and Madrid, 2012). In 1996, a decision was made to phase out the Federal Helium Reserve. In 2012, the Federal Helium Reserve contained 670 million cubic metres of helium (Madrid, 2012). This reserve is expected to be substantially depleted to a mandated 16.6 million cubic metres by 2015 (Groat et al., 2010).

For many years, the United States produced more than 90% of the commercially usable helium in the world. As of 2012, the United States accounted for 34% of the world's helium reserves and resources and 76% of global annual production (Table 1). Algeria, Qatar and Russia have reserve bases comparable to that of the United States, but large-scale production has been limited (Groat et al., 2010). Qatar developed its first dedicated helium plant in 2005 and Australia's first helium plant came online in 2010. Globally, seven international helium plants are in operation in Algeria, Qatar, Australia and Russia, and more are planned in the next 5 years (Fig. 1; Groat et al., 2010; Madrid, 2012). Production from these facilities is expected to be sufficient to meet worldwide helium demand for the next five years.

After that, access to additional reserves will be required (Madrid, 2012).

The helium supply and demand market is dynamic (Groat et al., 2010). As of 2012, the United States was the largest market for helium (36%), followed by Asia (28%) and Europe (22%; Garvey, 2012). In recent years, the price of grade A helium has quadrupled (Fig. 2; Madrid, 2012). The United States government's price for crude helium has

risen from \$49.50 per thousand cubic feet gas delivered in 1999 to \$75.75 per thousand cubic feet in 2011 (\$2.73 per cubic metre; Madrid, 2012). Meanwhile, the price of grade A refined helium, a higher value product, doubled. Between 2006 and 2011, the price of grade A refined helium rose from \$80 per thousand cubic feet in 2006 to \$160 per thousand cubic feet in 2011.

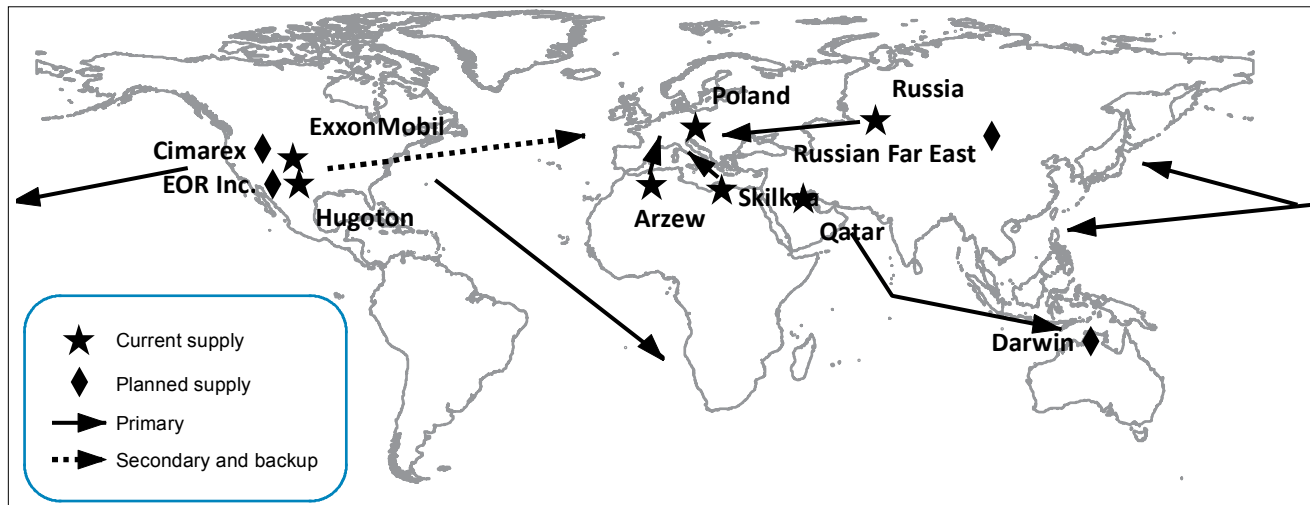


Figure 1. Origin and destination for large segments of the helium market in 2008 (the following values are the approximate amount of helium consumed in each region, in Bcf): United States, 2.8; Canada and South America, 0.3; Europe, 1.7; Asia, 1.5; Africa, Middle East, and India, 0.15. Source: CryoGas International (after Groat et al., 2010).

TABLE 1. WORLD PRODUCTION, RESERVES AND RESOURCES (MADRID, 2012).

	2011 production (million cubic metres)	Reserves (million cubic metres)	Resources (billion cubic metres)
United States (extracted from natural gas)	83	4 000	16.4
United States (from Cliffside Field Reserve)	57		4.3
Algeria	20	1 800	8.2
Canada	N/A	N/A	2
China	N/A	N/A	1.1
Poland	3	33	
Qatar	15	N/A	10.1
Russia	6	1700	6.8
other countries	N/A	N/A	
World Total	180	N/A	

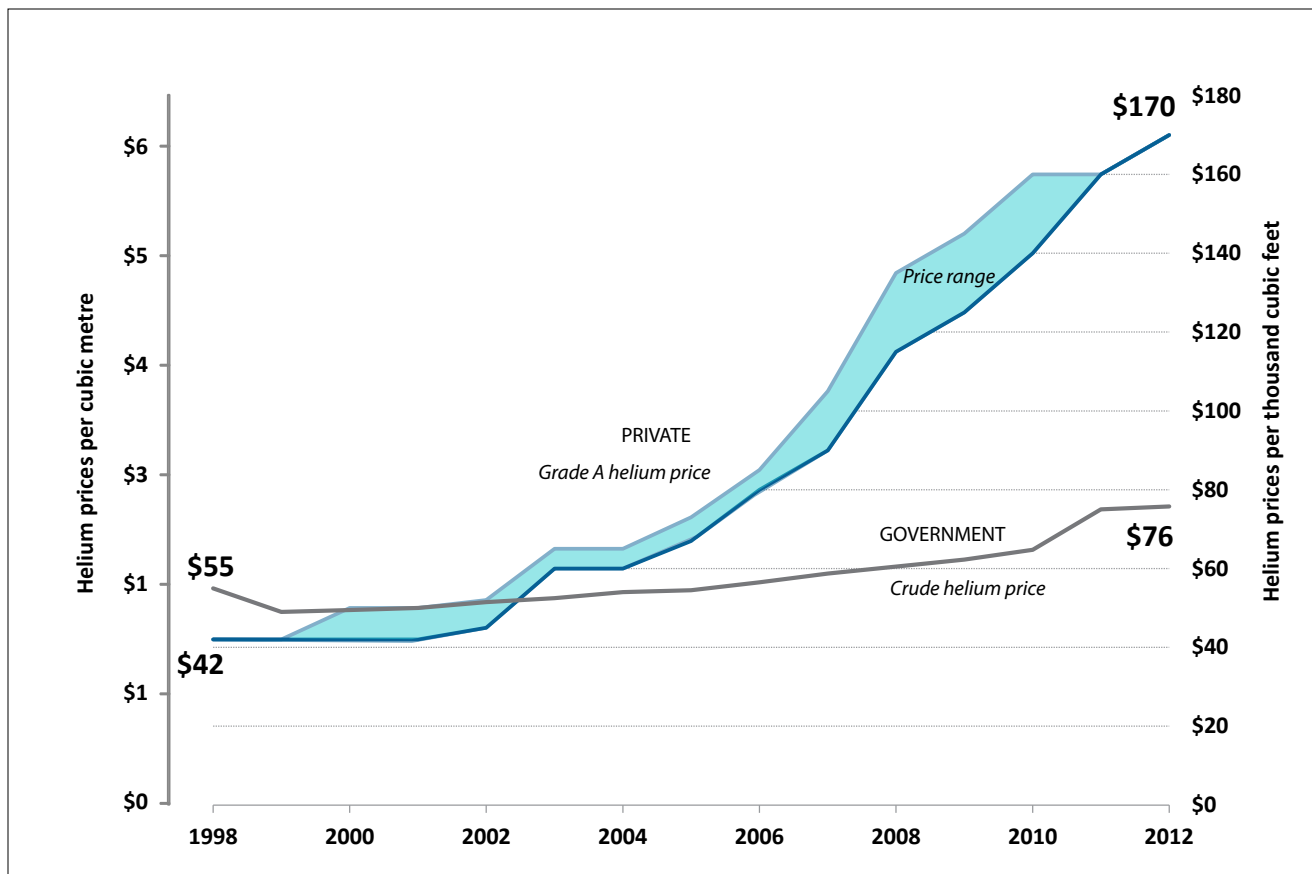


Figure 2. Price increases in grade A and crude helium between 1999 and 2011 (source: US Geological Survey; after Plumer, 2012)

Although a rising helium price has been partially driven by growth in the high-tech manufacturing sectors in China, Taiwan and South Korea (Fig. 2; Garvey, 2012), a perceived shortage in global helium supply associated with the sell-off of the United States Federal Helium Reserve has also been a factor. While there is currently sufficient helium to meet global demand, recent disruptions in helium supply (e.g., the Algerian plant explosion of 2004 and the Shute Creek Wyoming plant going offline in 2011) have been felt almost immediately by end users (Kynett, 2012). The average time between helium production by separation and delivery to the consumer is 45–60 days (Fig. 1; Kynett, 2012). Some market analysts anticipate that between 2016 and 2020, global demand will outstrip production, but in subsequent years a number of large-scale projects may be implemented (Anonymous, 2012).

Helium can be economically produced as a primary commodity or as a secondary byproduct. Primary helium reservoirs are not generally spatially associated with petroleum production. For primary helium production, concentrations in reservoirs vary over a broad range from a few parts per million to more than 7% by volume. Wells with helium concentrations of greater than 0.3% by volume can be commercialized solely for their helium content (Madrid, 2012). Most of the helium produced in the United States is

obtained from reservoirs with less than 1.5% helium in their gases (Broadhead, 2005).

There are several geological models for helium accumulation. Generally, world-class helium deposits like the Hugoton Reservoir form over granitic basement rocks connected by a fault to a porous reservoir, and are capped by a tight anhydrite seal (Broadhead, 2005). Although commercial helium is not generally associated with petroleum production, there are exceptions. Helium may migrate upward with the assistance of a carrier fluid (e.g., saline water) and become trapped in the subsurface under conditions that also trap natural gases like methane (Brown, 2010). Helium in pore water fractionates easily into migrating gas. In the case of some petroleum basins (e.g., Anadarko Basin, San Juan Basin), it is thought that helium generated in basement rocks that underlie the gas basins diffuses vertically upward to become entrained with migrating gas and then migrates updip through overlying Paleozoic sedimentary rocks until it is trapped in a reservoir (Broadhead, 2005). Alternatively, in extensional terranes, helium may migrate through deep-seated fractures and concentrate within overlying reservoir rocks (Broadhead, 2005).

In natural gas production, helium tends to exist at low concentrations and is commonly vented to the atmosphere to improve the heating value of the gas; however, in cases

where natural gas is to be liquefied for transport (i.e., LNG), helium can be effectively separated and concentrated. Natural gas reserves with helium concentrations as low as 0.04% by volume can have economic helium byproduct streams (e.g., the Las Raffan plant, from gas in Qatar's North Field; Groat et al., 2010). This process of helium recovery through LNG processing has led Qatar to become a world leader in helium production (Groat et al., 2010).

Industrial plants extract helium from natural gas by a process of fractional distillation (Fig. 3). Low temperature and high pressure are used to liquefy natural gases, but since helium has a lower boiling point than any other element, it remains a gas when other components in the gas stream have liquefied (Clarke and Van Schagen, 2010). At -193°C , most nitrogen and methane condense and can be drained. Helium can comprise up to 50–90% of the waste gas purged from a natural-gas plant after the natural gas has condensed (Andrieu et al., 2006). After initial separation, crude helium can then be further purified to generate grade A helium (99.997% by volume or better) by using either activated charcoal absorbers at very low temperature and high pressure or pressure swing adsorption processes (Beebe et al., 2000).

HELIUM ESTIMATES FOR NORTHEASTERN BRITISH COLUMBIA

British Columbia has the potential to produce helium in association with LNG. The British Columbia Oil and Gas Commission (OGC) recognizes 430 natural gas pools in northeastern British Columbia with 0.04% mole fraction or more of helium gas, the fraction required to produce helium for commercial venture. The top 22 pools account for 70% of the known helium and contain $50 \times 10^6 \text{ m}^3$ of helium (Fig. 4). This is estimated by applying the helium fraction from the representative sample gas analysis for the pool to the listed remaining raw gas reserves for each pool (Table

2). The majority of these 22 pools have an average helium mole fraction between 0.04% and 0.1%.

Collectively, the largest helium accumulations in northeastern British Columbia are in pools in the Slave Point Formation associated with the Horn River Basin and the Cordova Embayment, and the overlying Jean Marie

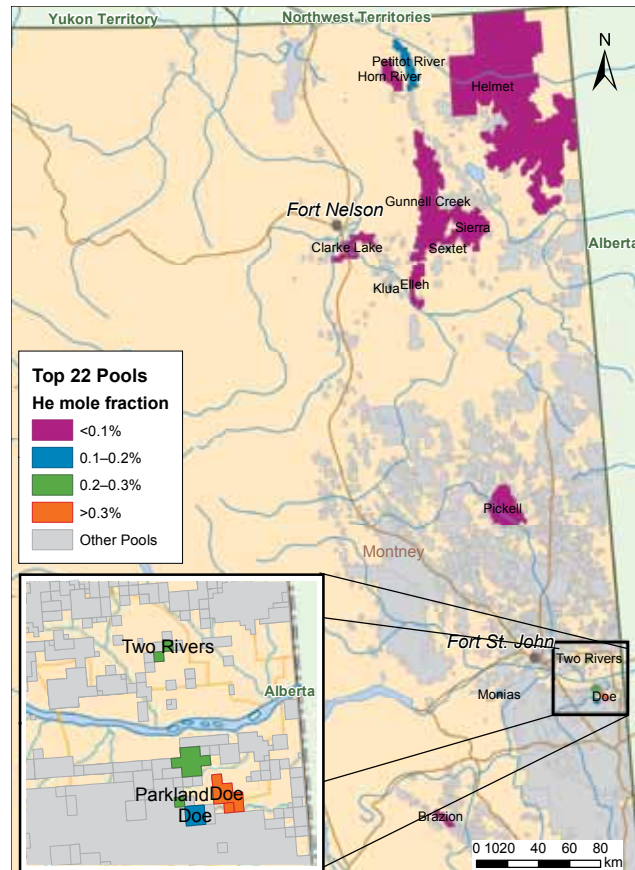


Figure 4. The 22 gas pools in northeastern British Columbia that hold the majority of helium in the province. Pools are colour coded by the helium mole fraction of the representative gas analysis for the pool.

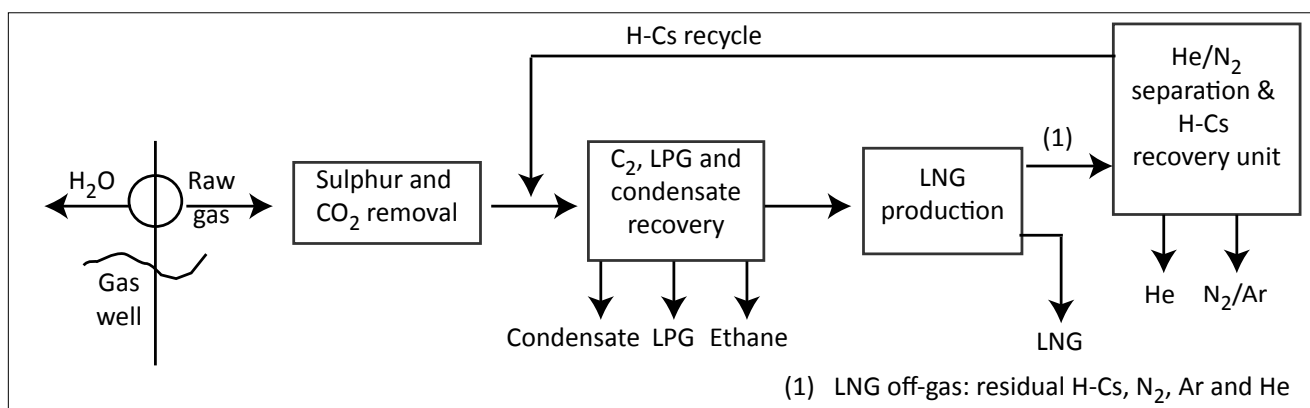


Figure 3. A liquefied natural gas (LNG) train with helium (and other byproduct) recovery (after Clarke and Van Schagen, 2010).

TABLE 2. BRITISH COLUMBIA POOLS WITH THE GREATEST HELIUM ACCUMULATIONS IN THE REMAINING RAW GAS.

Area	Formation/ member	Pool seq	Porosity	Reservoir initial pressure (kPa)	Formation temperature (°K)	Datum depth (m)	He mole fraction	OGIP He (e ³ m ³)	Remaining gas raw He (e ³ m ³)
Helmet	Jean Marie	A	6%	6 881	336	710	0.07%	44 954	17 312
Gunnell Creek	Jean Marie	A	8%	9 028	346	1 061	0.07%	17 464	6 401
Horn River	Evie	C	5%	28 700	408		0.04%	15 945	3 977
Clarke Lake	Slave Point	A	7%	20 064	383	1 524	0.09%	90 900	3 779
Sierra	Jean Marie	A	5%	9 105	339	834	0.05%	6 171	3 606
Parkland	Wabamun	A	2%	33 922	383	2 591	0.21%	13 926	1 652
Pickell	Notikewin	A	15%	4 612	315	3 687	0.05%	3 512	1 602
Monias	Halfway		15%	14 457	319	781	0.07%	15 398	1 390
Petitot River	Jean Marie	A	8%	6 731	361	1 010	0.10%	1 919	1 114
Klua	Pine Point	L	5%	17 949	393	1 696	0.11%	1 458	1 081
Doe	Wabamun	B	2%	33 503	375	2 701	0.36%	2 093	1 001
Two Rivers	Wabamun	C	3%	26 822	381	2 443	0.22%	1 031	817
Parkland	Wabamun	F	5%	50 136	388	2 868	0.21%	1 054	807
Doe	basal Kiskatinaw	A	10%	33 396	358	1 830	0.13%	1 522	803
Doe	Wabamun	A	6%	32 965	384	2 621	0.32%	6 041	791
Brazion	Belcourt-Taylor Flat	B	4%	50 650	398	3 435	0.04%	1 596	766
Brazion	Belcourt-Taylor Flat	A	3%	49 619	382	3 047	0.04%	2 266	747
Monias	Halfway	T	11%	14 662	320	821	0.10%	1 363	745
Two Rivers	Wabamun	B	8%	29 268	388	2 674	0.21%	817	735
Elleh North	Slave Point	A	8%	17 994	385	1 461	0.18%	1 131	712
Elleh	Jean Marie	B	8%	12 411	353	1 111	0.06%	1 680	691
Sextet	Slave Point	E	10%	18 189	380	1 491	0.14%	1 199	660

member of the Redknife Formation (Table 3, Fig. 5). Large helium reservoirs also occur in the Wabamun Formation near Fort St. John. The process that created these pools appears similar to that of large primary helium deposits in the United States. As with many Devonian and Mississippian reservoirs in the Western Canada Sedimentary Basin, these pools developed the porosity necessary for reservoir development through upward and lateral hydrothermal fluid flow (Petrel Robertson Consulting Ltd., 2003; Ma et al., 2006). Deep-seated faults, particularly strike-slip shear zones containing numerous small fault blocks prone to reactivation, promoted the movement of deep hydrothermal fluids, which accelerated reservoir-enhancing diagenetic processes (dolomitization) in carbonate reservoirs (Petrel Robertson Consulting Ltd., 2003).

Pools in the Slave Point Formation are associated with carbonates from reef banks that formed along the edge of the basins (Fig. 6). Faults along the Hay River fault zone linked deep hydrothermal fluids to Slave Point reservoirs and enhanced porosity through dolomitization (Madi et al., 2003; Janicki, 2006). Although the Slave Point Formation is conceptually very similar to the Keg River–Sulphur Point formations, capping shales provide better seals for Slave Point reservoirs (Petrel Robertson Consulting Ltd., 2003). Wells with anomalous measurements of helium occur in the pools and along the faults (Fig. 6).

The Jean Marie member of the Redknife Formation is, again, mainly limestone that is partially dolomitized by hydrothermal saline fluids. The parent fluids for the hydrothermal phase are interpreted to be residual evaporitic brines. During the latest Devonian to early Mississippian, heated brines flowed up through near-vertical fault-controlled conduits, bypassing approximately 850 m of overlying shale and basinal limestone, into the Jean Marie member, until the flow was impeded by the overlying impermeable shales of the unnamed upper member of the Redknife Formation. The brines then moved laterally into permeable limestone, creating a dolostone at the top of the Jean Marie member and the partial dolomitization of limestone distal to the faults (Wendte et al., 2009; Wierzbicki and Todorovic-Maranic, 2010).

TABLE 3. FORMATIONS WITH THE HIGHEST HELIUM ACCUMULATIONS. FOR THE PURPOSES OF THIS TABLE, ONLY POOLS WITH MORE THAN $100 \text{ e}^3 \text{m}^3$ ABOVE THE THRESHOLD OF 0.04% MOLE FRACTION HE ARE INCLUDED. ONLY FORMATIONS WITH A CUMULATIVE VOLUME OF MORE THAN $1000 \text{ e}^3 \text{m}^3$ HE ARE INCLUDED (OGIP: OFFICIAL GAS IN PLACE).

Formation	Pools	OGIP He ($\text{e}^3 \text{m}^3$)	Remaining raw He ($\text{e}^3 \text{m}^3$)	He (%)
Jean Marie	11	77 857	30 918	0.08
Slave Point	25	111 936	9 551	0.14
Wabamun	7	25 174	5 909	0.24
Evie	1	15 945	3 977	0.04
Pine Point	10	8 542	3 247	0.09
Halfway	4	17 309	2 523	0.12
Notike Win	3	5 086	2 214	0.05
Belcourt-Taylor Flat	2	3 862	1 513	0.04
Basal Kiskatinaw	2	1 884	1 080	0.09
Bluesky	3	1 928	1 011	0.21

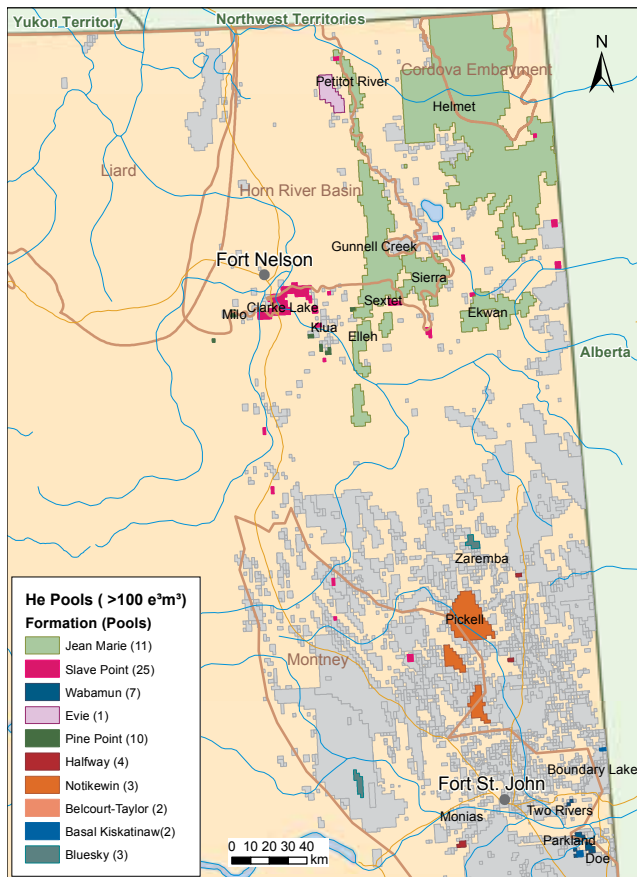


Figure 5. Pools of large helium accumulation, colour coded by formation. Only pools with greater than $100 \text{ e}^3 \text{m}^3$ were included and only formations where pools are cumulatively responsible for greater than $1000 \text{ e}^3 \text{m}^3$ were included.

Reservoirs in the Wabamun Group of the Peace River Arch area have the highest concentration of helium with large accumulations in relatively small pools. These reservoirs are proximal, and related to, deeply seated faults that connect the Precambrian granitoid basement rocks with overlying Paleozoic sedimentary rocks. The Peace River Arch is a tectonic feature that began in the Precambrian and existed until its collapse in the late Devonian to early Mississippian (Halbertsma, 1994). Wabamun Group carbonates were deposited over the pre-existing topographic high of the Peace River Arch (Halbertsma, 1994). Postdepositional tensional faults associated with the formation of the Peace River rift basin allowed hot, magnesium-rich brines to penetrate the Wabamun limestone, thereby forming a secondary more porous dolomite (Halbertsma, 1994; Ma et al., 2006). Gas fields (e.g., Doe, Parkland) are believed to have formed later from reactivation of the fault system during the Laramide orogeny of the Late Cretaceous. Fractures were cemented shut with bladed anhydrites and coarse calcites at the time of hydrocarbon generation (Mount Joy and Halim-Dihardja, 1991).

The fourth largest accumulation of helium in British Columbia is associated with the Evie member shales in the Horn River Basin. Many shale gas deposits contain little helium because helium molecules are small enough to diffuse through shale and because the helium-generating potential of the shale depends on the uranium and thorium content and the age of the shale. However, the shales in northeastern British Columbia basins (Horn River Basin, Cordova Embayment and Liard Basin) may be an exception. These shales tend to be dark grey to black, organic-rich, siliceous and (in the case of the Evie and Muskwa members of the Horn River Formation) highly radioactive (McPhail et al., 2008). The ‘hot’ zones (i.e., higher than normal uranium levels) usually correlate with the elevated organic content

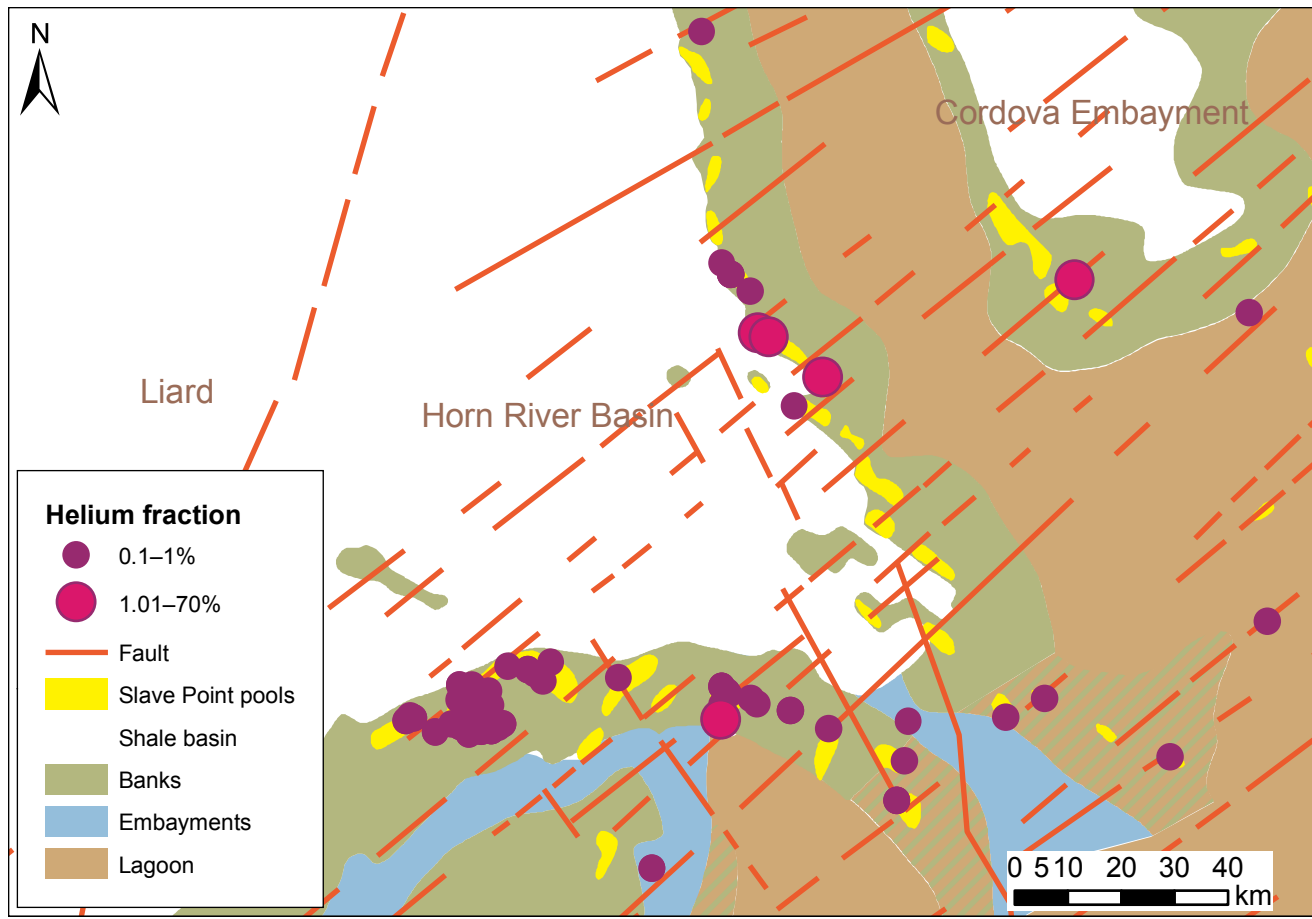


Figure 6. Slave Point paleo-environment with reef banks (green) proximal to shale basins (white). Gas pools (yellow) are thought to form from hydrothermal dolomitization associated with northwest-oriented, deep-seated faults. Faults (red) may be responsible for helium transport and accumulation. Dots represent mole fraction percent of helium in anomalous gas samples from wells.

in gas-rich horizons (Ferri et al., 2012). In the Horn River Formation, the Evie member has been measured in section as having up to 50 ppm uranium (Ferri et al., 2012). Hot shale has a helium-generating capacity eight times higher than normal shale and granite (Brown, 2010). The age of the shale (~390 m.y.) contributes to its ability to generate substantial helium over time. Additionally, Horn River Formation shales may be prospective because they are overpressured and the high basinal pressure may have countered the slow upward diffusion of helium.

SUMMARY

Many of the natural gas pools in northeastern British Columbia that are prospective targets for providing liquefied natural gas to the market may contain a value-added product that is currently not being realized. Liquefied natural gas has the potential to capture this potentially valuable byproduct. The normal processing procedure for refining of natural gas results in the release of the helium fraction of the gas to the atmosphere. The LNG process, however, facilitates the separation of helium from other natural gases. The prices of crude helium and grade A helium have risen dramatically in recent years, as United States reserves are reduced and global demand increases. Countries with high demand for grade A helium are located in Southeast Asia, where there is also a higher demand for LNG. In British Columbia, north of Fort Nelson, production from the Slave Point, Redknife (Jean Marie member) and Horn River (Evie member) formations may be enriched in helium. Near Fort St. John, gas production from the Wabamun Formation, in particular, may have added value from helium.

REFERENCES

- Andrieu, F., Tsevery, J.-M., Schmitt, N., Peyron, J.-M., Blanc, S., Pareja, T. and Cognard, M. (2006): The Ras Laffan Helium Purification Unit; *Air Liquide Advanced technologies*, URL <<http://www.airliquideadvancedtechnologies.com/en/library/publications-scientifiques-techniques/the-ras-laffan-helium-purification-unit.html>> [February 2013].
- Anonymous (2012): Innovative use of helium: Does Russia need to produce helium?; *Ernst & Young*, 17 pages.
- Beebe, R.R., Reppy, J.D., Goldman, A.M., Lander, H.R., Macaulay, M.K., Miller, M.A., Rose, A.Z., Siewert, T.A., Weisskoff, R.M., Shapero, D.C., Ehrenreich, R.M., Aylesworth, K.D. and Morgan, D.F. (2000): The Impact of Selling the Federal Helium Reserve; *The National Academies Press*, Washington, DC, 80 pages.
- Broadhead, R.F. (2005): Helium in New Mexico—geologic distribution, resource demand, and exploration possibilities; *New Mexico Geology*, Volume 27, no 4, pages 93–100.
- Brown, A. (2010): Formation of high helium gases: a guide for explorationists; *American Association of Petroleum Geologists*, AAPG Convention, April 11–14, 2010, New Orleans, LA.
- Clarke, M. and Van Schagen, F. (2010): Liquified natural gas (LNG) carbon footprints and the development of methodologies for CDM estimation and verification; *Asian Journal on Energy and Environment*, Volume 11, no 2, pages 90–95.
- Ferri, F., Hickin, A.S. and Reyes, J. (2012): Horn River basin-equivalent strata in Besa River Formation shale, northeastern British Columbia (NTS 094K/15); in *Geoscience Reports 2012*, British Columbia Ministry of Energy, Mines and Natural Gas, pages 1–15.
- Garvey, M. (2012): Waiting for the light at the end of the tunnel: the worldwide helium market; *CryoGas International*, October 2012.
- Groat, C.G., Richardson, R.C., Beebe, R.R., Campbell, J.R., Chan, M.H., Chermak, J.M., Dahl, C.A., Elam, T., Goldman, A.M., Hartness, N.E., Lee, W.J., Migliori, A., Mowery, D.C., Prats, M., Reinoehl, J.B., Sekachev, I., Siewert, T.A. and Thiemens, M.H. (2010): Selling the Nation's Helium Reserve; *The National Academies Press*, Washington, DC, 140 pages.
- Halbertsma, H.L. (1994): Chapter 13—Devonian Wabamun Group of the Western Canada Sedimentary Basin; in *Geological Atlas of the Western Canada Sedimentary Basin*, Mossop, G.D. and Shetsen, I., Editors, *Canadian Society of Petroleum Geologists and Alberta Research Council*, Calgary, Alberta, pages 203–221.
- Janicki, E.P. (2006): Distribution of Presqu'ile dolomite in the Great Slave Plain, Northwest Territories; in Potential for carbonate hosted lead-zinc Mississippi-Valley-type mineralization in northern Alberta and Southern Northwest Territories, Hannigan, P.K., Editor, *Geological Survey of Canada*, Bulletin 591, Calgary, AB, pages 179–194.
- Kynett, K. (2012): What goes up must come down: Congress deadline looms: is helium doomed?; *AAPG Explorer*, December 2012, pages 10–12.
- Ma, F., Al-Asam, I. and Yang, J. (2006): Numerical modeling of hydrothermal fluid flow coupled with mass transport: an example from the Devonian Wabamun Group, northeast British Columbia, Canada; *Journal of Geochemical Exploration*, Volume 90, no 3, page 216.
- Madi, A.J., Damte, A. and Hayes, M. (2003): Fault-associated hydrothermally-dolomitized reservoirs (HTD) in Devonian strata of northeastern British Columbia—a large-scale geological exploration concept; 2003 CSPG/CSEG Joint Convention: Partners in a New Environment, *Canadian Society of Petroleum Geologists*, Calgary, Alberta.
- Madrid, P.J. (2012): Mineral commodity summaries: Helium; *US Geological Survey*, Amarillo, Texas, URL <<http://minerals.usgs.gov/minerals/pubs/commodity/helium/mcs-2012-heliu.pdf>>.
- McPhail, S., Walsh, W., Lee, C. and Monahan, P.A. (2008): Shale units of the Horn River Formation, Horn River Basin and Cordova Embayment, northeastern British Columbia; *Petroleum Geology Open File 2008-1*, *British Columbia Ministry of Energy, Mines and Natural Gas*, page 14.
- Mount Joy, E.W. and Halim-Dihardja, M.K. (1991): Multiple phase fracture and fault-controlled burial dolomitization, Upper Devonian Wabamun Group, Alberta; *Journal of Sedimentary Petrology*, Volume 61, no 4, pages 590–612.
- Peterson, J. and Madrid, P. (2012): 2010 Minerals Yearbook: Helium; *US Geological Survey*, Amarillo, Texas, URL <<http://minerals.usgs.gov/minerals/pubs/commodity/helium/myb1-2010-heliu.pdf>>.
- Petrel Robertson Consulting Ltd. (2003): Exploration assessment of deep Devonian gas plays, northeastern British Columbia; *British Columbia Ministry of Energy, Mines and Natural Gas*, *Petroleum Geology Open File 2003-4*.
- Plumer, B. (2012): Congress turns its attention to... America's helium crisis; *The Washington Post*, Washington, DC, May 13, 2012.
- Wendte, J., Chi, G., Al-Asam, I. and Sargent, D. (2009): Fault/fracture controlled hydrothermal dolomitization and associated diagenesis of the Upper Devonian Jean Marie member (Redknife Formation) in the July Lake area of northeastern British Columbia; *Bulletin of Canadian Petroleum Geology*, Volume 57, no 3, pages 275–322.
- Wierzbicki, R. and Todorovic-Maranic, D. (2010): Exploiting natural fracture and fault fairways in the Jean Marie Carbonate Platform, N.E. British Columbia; Canadian Unconventional Resources and International Petroleum Conference, 19–21 October 2010, *Society of Petroleum Engineers*, Calgary, Alberta.

